GEORGIA DOT RESEARCH PROJECT 24-07

Final Report

A COMPREHENSIVE GUIDELINE FOR GDOT BRIDGES FIRE HAZARD ASSESSMENT

Office of Performance-based Management and Research
600 West Peachtree Street NW | Atlanta, GA 30308

February 2026

TECHNICAL REPORT DOCUMENTATION PAGE

1. Report No. FHWA-GA-26-2407	2. Government Accession No. N/A	3. Recipient's Catalog No. N/A
4. Title and Subtitle A Comprehensive Guideline for GDOT Bridges Fire Hazard Assessment		5. Report Date February 2026
		6. Performing Organization Code N/A
7. Author(s) Mohammad Jonaidi, Tien Yee, Metin Oguzmert, Dale Goff, and Matthew Henry		8. Performing Organization Report No. 24-07
9. Performing Organization Name and Address Kennesaw State University Southern Polytechnic College of Engineering and Engineering Technology Department of Civil and Environmental Engineering 655 Arnston Drive Room L 155, MD 9055 Marietta, GA 30060 Phone: (470) 578-5076, Email: mjonaidi@kennesaw.edu		10. Work Unit No. N/A
		11. Contract or Grant No. PI# 0020307
12. Sponsoring Agency Name and Address Georgia Department of Transportation (SPR) Office of Performance-based Management and Research 600 West Peachtree St. NW Atlanta, GA 30308		13. Type of Report and Period Covered Final Report (December 2024–February 2026)
		14. Sponsoring Agency Code N/A
15. Supplementary Notes Prepared in cooperation with the U.S. Department of Transportation, Federal Highway Administration.		

16. Abstract

Bridge fires can cause rapid and severe loss of structural capacity. This loss of capacity often leads to major safety risks, network disruptions, and high economic impacts. A curated history of U.S. bridge fires in the 20th and 21st centuries is presented. This history identifies recurring ignition sources, contributing factors, and damage patterns associated with bridge fires. The research team further synthesizes current knowledge on critical temperatures and heat-induced defects in steel and concrete. They evaluate rapid nondestructive testing (NDT) methods that can be used for a post-fire triage inspection. Integrating the historical case studies, common trends found in the historical record of bridge fires, material behavior, and NDT information, the team presents practical guidance to support post-fire triage of highway bridges. In addition, they propose a methodology that may be implemented to develop a single, easy-to-use universal model to determine the residual structural capacity of fire damaged concrete. Laboratory burn testing of concrete samples was conducted to quantify residual compressive strength as a function of changes in rebound hammer values and ultrasonic pulse velocity. During testing, the model produced a standard error of 8 percent for estimating residual compressive strength. This indicates promise for refinement with further testing. A three-factor model that incorporated visual cues was also developed. The three-factor model improved overall fit but raised concerns about robustness and practical reliability. The report concludes with recommendations for post-fire inspection procedures, expanded training for bridge and maintenance personnel, and wider availability of NDT equipment to support timely, consistent, and defensible triage decision following bridge fires.

17. Key Words Bridge Fire, Bridge Fires, Post-fire Assessment, Post-fire Inspection, Fire Damage, Nondestructive Testing, Triage Procedures, Steel Fire Performance, Concrete Fire Performance, Bridge Fire History, Bridge Fire Trends	18. Distribution Statement No Restrictions

19. Security Classification (of this report) Unclassified	20. Security Classification (of this page) Unclassified	21. No. of Pages 182	22. Price Free

Form DOT F 1700.7 (8-72) Reproduction of completed page authorized.

GDOT Research Project 24-07
Final Report

A COMPREHENSIVE GUIDELINE FOR GDOT BRIDGES FIRE HAZARD ASSESSMENT

By

Mohammad Jonaidi, Ph.D.,
Associate Professor of Civil Engineering

Tien Yee, Ph.D.
Assistant Chair of the Department of Civil and Environmental Engineering

Metin Oguzmert, Ph.D., P.E., S.E.
Professor of Civil Engineering

Dale Goff
Graduate Research Assistant

Matthew Henry
Graduate Research Assistant

Kennesaw State University Research and Service Foundation, Inc.

Contract with
Georgia Department of Transportation

In cooperation with
U.S. Department of Transportation, Federal Highway Administration

February 2026

DISCLAIMER STATEMENT

This document is disseminated under the sponsorship of the Georgia Department of Transportation and the United States Department of Transportation in the interest of information exchange. The State of Georgia and the United States Government assume no liability of its contents or use thereof.

The contents of this report reflect the views of the authors, who are responsible for the facts and accuracy of the data presented herein. The contents do not necessarily reflect the official policies of the Georgia Department of Transportation or the United States Department of Transportation.

The State of Georgia and the United States Government do not endorse products of manufacturers. Trademarks or manufacturers' names appear herein only because they are considered essential to the object of this document.

AI STATEMENT

The authors hereby declare that the work presented in this report is our own original research. We confirm that this work was conducted entirely during the term of this research project. Throughout the writing process, we have utilized artificial intelligence (AI) tools to assist with grammar and sentence structure; however, we confirm that the content of this report is entirely our own work and does not include any text, quotations, or ideas from other authors without proper attribution. We take full responsibility for the originality and integrity of the research presented in this report.

SI* (MODERN METRIC) CONVERSION FACTORS

APPROXIMATE CONVERSIONS TO SI UNITS

Symbol	When You Know	Multiply By	To Find	Symbol
		LENGTH		
in	inches	25.4	millimeters	mm
ft	feet	0.305	meters	m
yd	yards	0.914	meters	m
mi	miles	1.61	kilometers	km
		AREA		
in^2	square inches	645.2	square millimeters	mm^2
ft^2	square feet	0.093	square meters	m^2
yd^2	square yard	0.836	square meters	m^2
ac	acres	0.405	hectares	ha
mi^2	square miles	2.59	square kilometers	km^2
		VOLUME		
fl oz	fluid ounces	29.57	milliliters	mL
gal	gallons	3.785	liters	L
ft^3	cubic feet	0.028	cubic meters	m^3
yd^3	cubic yards	0.765	cubic meters	m^3
		NOTE: volumes greater than 1000 L shall be shown in m^3		
		MASS		
oz	ounces	28.35	grams	g
lb	pounds	0.454	kilograms	kg
T	short tons (2000 lb)	0.907	megagrams (or "metric ton")	Mg (or "t")
		TEMPERATURE (exact degrees)		
°F	Fahrenheit	5 (F-32)/9 or (F-32)/1.8	Celsius	°C
		ILLUMINATION		
fc	foot-candles	10.76	lux	lx
fl	foot-Lamberts	3.426	$candela/m^2$	cd/m^2
		FORCE and PRESSURE or STRESS		
lbf	poundforce	4.45	newtons	N
lbf/in^2	poundforce per square inch	6.89	kilopascals	kPa

APPROXIMATE CONVERSIONS FROM SI UNITS

Symbol	When You Know	Multiply By	To Find	Symbol
		LENGTH		
mm	millimeters	0.039	inches	in
m	meters	3.28	feet	ft
m	meters	1.09	yards	yd
km	kilometers	0.621	miles	mi
		AREA		
mm^2	square millimeters	0.0016	square inches	in^2
m^2	square meters	10.764	square feet	ft^2
m^2	square meters	1.195	square yards	yd^2
ha	hectares	2.47	acres	ac
km^2	square kilometers	0.386	square miles	mi^2
		VOLUME		
mL	milliliters	0.034	fluid ounces	fl oz
L	liters	0.264	gallons	gal
m^3	cubic meters	35.314	cubic feet	ft^3
m^3	cubic meters	1.307	cubic yards	yd^3
		MASS		
g	grams	0.035	ounces	oz
kg	kilograms	2.202	pounds	lb
Mg (or "t")	megagrams (or "metric ton")	1.103	short tons (2000 lb)	T
		TEMPERATURE (exact degrees)		
°C	Celsius	1.8C+32	Fahrenheit	°F
		ILLUMINATION		
lx	lux	0.0929	foot-candles	fc
cd/m^2	$candela/m^2$	0.2919	foot-Lamberts	fl
		FORCE and PRESSURE or STRESS		
N	newtons	0.225	poundforce	lbf
kPa	kilopascals	0.145	poundforce per square inch	lbf/in^2

* SI is the symbol for the International System of Units. Appropriate rounding should be made to comply with Section 4 of ASTM E380. (Revised March 2003)

TABLE OF CONTENTS

LIST OF FIGURES

LIST OF TABLES

LIST OF ABBREVIATIONS AND SYMBOLS

ASTM	American Society for Testing and Materials
CalTrans	California Department of Transportation
DAQ	Data Acquisition System
E	Elastic Modulus
F	F-statistic
FHWA	Federal Highway Administration
GDOT	Georgia Department of Transportation
GPR	Ground Penetrating Radar
HRR	Heat Release Rate
IE	Impact Echo Test
LH	Leeb Hardness Test
LH	Leeb Hardness Value
LNG	Liquefied Natural Gas
MT	Magnetic Particle Test
MW	Megawatt
NDT	Nondestructive Testing
NFPA	National Fire Protection Association
OLS	Ordinary Least Squares
PT	Dye Penetrant Test
$\dot{Q}_{f,max}$	Peak heat-release rate
R	Distance from modified point source and the closest girder surface
RH	Rebound Hammer
RH	Rebound Hammer value

RH_{pre}	Rebound Hammer value pre-burn
RH_{post}	Rebound Hammer post-burn
Significance F	*p*-value for F
SS	Sum of Squares
T	Temperature
$T_{surface}$	Surface temperature of concrete
UPV	Ultrasonic Pulse Velocity device
UPV	Ultrasonic Pulse Velocity value
UPV_{post}	Ultrasonic Pulse Velocity post-burn
UPV_{pre}	Ultrasonic Pulse Velocity pre-burn
UT	Ultrasonic Testing

df	Degrees of Freedom
$f'c$	Compressive strength of concrete
$f'c_{control}$	Compressive strength of control sample
$f'c_{post}$	Compressive strength of test sample post-burn
ft/s	Feet per Second
kW	Kilowatt
m^2	Meters squared
mm	Millimeter
n	Exponent used to calculate incident radiative heat flux
psi	Pounds per Square Inch
p-value	Probability of obtaining a result at least as extreme as what was observed by random chance
$\dot{q}''$	Incident radiative heat flux

t	Time
$w_{c,max}$	Maximum crack width attributed to elevated temperatures
β_0	Y-intercept in multifactor model
β_1	Coefficient for %RH in multifactor model
β_2	Coefficient for %UPV in multifactor model
β_3	Coefficient for $w_{c,max}$ in multifactor
$\chi_{r,max}$	Radiative fraction
ν	Poisson's ratio
ρ	Density
°C	Degrees Celsius
%f'c	Percent remaining compressive strength
%RH	Percent change in rebound hammer mean between pre-burn and post-burn readings
%UPV	Percent change in ultrasonic pulse velocity

EXECUTIVE SUMMARY

This report presents a practical, field-ready framework for the development of post-fire triage of highway bridges. It combines (1) a structured literature review and historical summary of bridge fires; (2) a discussion of common trends found among bridge fires; (3) a review of critical temperatures for steel and concrete; (4) a review of factors that affect critical temperatures for steel and concrete; (5) a summary of rapid, easily deployable nondestructive testing (NDT) methods for fire-damaged elements; and (6) a proposed means to develop a simple statistical model to translate measured changes in NDT readings into a residual capacity percentage in concrete.

The report also synthesizes visible and measurable indicators for rapid triage following a fire. It details how bridge inspection teams and maintenance personnel examine color change, spalling, paint damage, distortion in steel elements, and other observable clues to assess a bridge structure. Further, the report proposes basic inspection techniques to systematically review the damaged bridge.

The proposed method of calculating residual compressive strength makes use of changes in rebound hammer and ultrasonic pulse devices pre- and post-heating. These changes in readings are statistically linked to the percentage of residual compressive strength. An ordinary least squares two-factor model using these factors is presented as providing the strongest performance in the test dataset. The model produced a standard error of approximately 8 percent, making it suitable for further development.

The research further developed a three-factor model that added maximum crack width as a third factor. This model was influenced the most by changes in the ultrasonic pulse device readings, followed by crack width; the change in rebound hammer readings offered negligible

support. This method provided a better fit than the two-factor model, although there were lingering questions about its efficacy. The authors concluded that more research is needed to develop this model into a usable product.

Recommendations prioritize periodic training on post-fire triage inspections. This includes the use of NDT devices to aid in this investigation. The authors further recommend that Georgia Department of Transportation (GDOT) maintenance and bridge inspection personnel have access to these devices should the need arise. Further investigation into the development of a model to determine residual strength following a bridge fire is also recommended.

CHAPTER 1. INTRODUCTION AND BACKGROUND

American bridge owners face various difficulties due to fires that occur at bridge structures. Fire often spreads rapidly across bridge elements [1], [2], [3], [4], [5], [6], [7], [8], [9]. The elements experience extreme thermal loading that can lead to local or widespread damage [1], [2], [3], [4], [5], [6], [7]. The damage associated with fire often includes the yielding of steel elements [10], [11], [12], [13], [14]. Additionally, steel will frequently lose its protective coating [15], [16], [17]. In concrete, inspectors often see cracking, delamination, and spalling in response to extreme heat [11], [18], [19], [20], [21], [22]. Additionally, the relaxation of prestressing strands or reduced bond strength between the mild steel reinforcement and concrete is possible [23], [24], [25], [26], [27], [28]. Traditional degradation occurs throughout the life of a bridge; however, fire can cause a bridge's structural elements to lose capacity in a matter of minutes [4], [29], [30], [31], [32], [33], [34], [35]. For this reason, there is an urgent need for engineers and inspectors to make a strong initial assessment of a fire-damaged bridge.

The first, and most time-sensitive, part of post-fire bridge assessments occurs during the initial assessment phase, or the post-fire triage inspection [36], [37]. This inspection should begin as soon as the fire is out and the site is safe for inspection [16], [37], [38], [39], [40]. During the inspection, bridge inspectors work with structural engineers to determine the extent of the damage [16], [37], [38], [39]. This initial assessment will guide the next course of action [16], [37], [38], [39]. The information gathered during this phase will help transportation officials answer a variety of questions [1], [11], [37]: What is the extent of the damage? Can this bridge stay open? Does it need load restrictions? What sort of repair actions should be taken? Should we simply replace the bridge? Accurately finding the information to answer these

questions will have a direct impact on public safety. The information gathered during the triage inspection may also mandate a more in-depth investigation [1], [11], [37], [41].

Bridge inspectors can use a variety of inspection techniques to examine the structure. A hands-on visual inspection is essential to identify telltale indicators of critical fire-related defects and to focus subsequent nondestructive testing (NDT) on the location of greatest concern [16], [37], [38]. Inspectors can also make use of NDT methods [1]. NDT methods include rebound hammers (RHs), ultrasonic pulse velocity (UPV), ground penetrating radar (GPR), ultrasonic testing (UT) for steel, and hardness tests [1], [42], [43], [44], [45], [46]. These tools allow inspection teams to examine damage that is difficult to observe visually. In this way, the use of NDT and visual inspection methods aids inspectors in quickly and accurately determining the extent of damage to a bridge element [47], [48], [49].

Often, post-fire triage inspections are difficult because inspection teams lack important information. The team may not have information about peak temperature, burn duration, fuel source, or fuel quantity [41]. In these cases, the bridge inspection team functions as a group of detectives searching for clues. These clues include changes in aggregate color, blistering of paint, steel deformation, and spalling patterns [16], [50], [51], [52]. The team must also inspect geometric alignment, joint displacement, and bearing conditions for additional telltale signs of structural damage [53], [54], [55], [56], [57]. The clues gathered here provide valuable information about the nature of the fire and the extent of the damage to the bridge. Inspectors and engineers can use reference charts with their experience-based heuristics to understand these visible clues [58]. The clues found during the inspection should be thoroughly documented in inspection reports.

The main purpose of the triage inspection is to ensure structural and public safety. Accurately completing the inspection of a bridge after a fire depends on a combination of structural understanding, in-field experience, and engineering judgment. Inspection personnel must work under public scrutiny with a limited amount of time. Nevertheless, the triage inspection can help determine the scope of planned rehabilitation projects and/or emergency repair activities [16], [37], [38], [39]. This ensures transportation networks remain safe for all users.

America's bridges are aging and degrading. An aging transportation network faces additional risk from fire; therefore, in addition to understanding age-related degradation, bridge inspectors should understand how fire affects and degrades bridge construction materials. This additional knowledge serves as an add-on to the impact of efficient and repeatable inspection procedures [1], [8], [35], [59]. In this way, bridge inspectors, armed with knowledge and protocols, serve as the first line of defense for the recovery efforts following a bridge fire. This text is offered as a primer to help develop bridge inspectors and post-fire inspection procedures.

CHAPTER 2. OBJECTIVES

The objectives of this report are as follows:

1. *Conduct a historical review of bridge fires in the 20th and 21st centuries to identify common trends.* A summary of the historical record is provided in chapter 3 of this report. A discussion of common trends, including primary causes of bridge fires, factors that influence the severity of bridge fires, and where bridge fires fit into the larger picture of bridge failures is presented in chapter 4.
2. *Review the technical literature on post-fire materials testing to identify the commonly used testing methods for common construction materials.* These methods are summarized in chapter 5 and chapter 6. They are further evaluated to determine the most appropriate techniques for use following a bridge fire.
3. *Develop a proposed methodology for a universal calibration curve to estimate residual compressive strength of concrete after fire exposure.* The proposed procedure and supporting analysis is presented in chapter 7.
4. *Recommend guidelines for initial post-fire bridge inspection.* The recommended guidelines and supporting rationale are provided in chapter 5 through chapter 8.
5. *Develop training materials for bridge inspection personnel based on the research findings documented in this report.* This training is a synthesis of the material presented in this report as well as in existing inspection curricula and guidance.

CHAPTER 3. A BRIEF HISTORY OF BRIDGE FIRES IN THE UNITED STATES

Bridge fires occur infrequently. That said, they can cause significant damage to transportation infrastructure when they occur [4], [60], [61]. Common bridge fire causes include automobile accidents, arson, electrical faults, wildfires, and flammable material storage. In some cases, a bridge may partially or completely fail, resulting in disruption of the local transportation networks [1], [9], [60], [61], [62]. The recorded bridge fires in the 20th and 21st centuries demonstrate the vulnerability of bridge structures to fire-related damage [4], [9], [60], [61], [62]. Studying these incidents can aid transportation officials in improving fire resilience, emergency response, and future bridge design standards. The purpose of this chapter is not to present an exhaustive history of bridge fires in the United States. Rather, the authors present a curated set of case studies, drawn from the historical record, to illustrate recurring patterns in ignition sources, contributing factors, damage severity, and community impact. The intent is to illustrate common trends that inform contemporary assessment, response, and mitigation practices.

DEKALB STREET BRIDGE FIRE, BRIDGEPORT, PA (1924)

On April 14, 1924, at approximately 3:40 in the afternoon, a fire erupted on the DeKalb Street Bridge, which spanned the Schuylkill River between Norristown and Bridgeport, Pennsylvania. Originally constructed in 1830, photographic evidence suggests the structure featured four wooden arches on stone piers [63]. More contemporaneous photographs show the addition of intermediate timber supports for the structure [64].

The exact ignition source remains unclear; some accounts suggest a car backfire on the wooden structure may have sparked the blaze [63], [64], [65]. Within 10 min, the fire had consumed the entire length of the structure, turning its arches into a smoldering inferno [63],

[64]. Later sources indicate that the fire resulted from petroleum products from automobiles that soaked into the timbers of the superstructure. Once the fire started, it was impossible to stop [63], [64]. The fire completely destroyed the timber superstructure (see figure 1).

Because the structure was a vital connector for travelers between Norristown and Bridgeport, the fire resulted in a major disruption of local traffic. To remedy this, local officials opened a temporary structure a few months later [64]. Eventually, a concrete structure replaced this temporary solution; the concrete structure is still in service today [63].

Figure 1. Photo. DeKalb Street Bridge post-fire [66].

BELLBANK COVERED BRIDGE FIRE, LANCASTER COUNTY, PA (1979)

The Bellbank Covered Bridge, constructed in 1850 (reconstructed in 1861), was a timber structure that carried Street Road across Octorara Creek, connecting Oxford Township to Colerain Township in Pennsylvania [67], [68], [69]. The bridge was an example of 19th-century timber-covered bridge construction that used a multiple kingpost truss system that was common

to the region (see figure 2). It measured approximately 112 ft in length and served as a functional and cultural landmark during its lifetime [68], [69].

Prior to reconstruction, the structure sustained fire damage due to a lightning strike [67], [69]. Despite its age, the structure remained in service into the late 20th century, surviving public proposals for its demolition in the 1960s [67]. However, on March 19, 1979, the bridge was destroyed by a deliberate act of arson. Early investigations by local fire officials confirmed that a gasoline can was recovered amid the debris [70]. Efforts to rebuild the structure failed, and a steel beam structure was built in its place [69], [70].

This case highlights the vulnerability of timber bridge structures to fires that occur both naturally and by arson. Furthermore, the Bellbank incident also exemplifies the challenges of preserving historic structures in the face of limited resources and evolving infrastructure standards.

Figure 2. Photo. Bellbank Covered Bridge [71]; Photographed by Mr. John H. Ramsey, Jr.

BIG FOUR BRIDGE FIRES, LOUISVILLE, KY (1987, 2008)

In December 1987, a significant fire broke out on Louisville's Big Four Bridge after Christmas lights short-circuited and ignited the timber deck [72], [73]. The blaze burned for hours, with firefighters from both Louisville, Kentucky, and Jeffersonville, Indiana, battling the flames [72], [73]. After the fire, the steel truss was largely undamaged. This fire provides an example of the hazard electrical installations can provide to combustible bridge elements.

This point was underscored when another electrical fire struck the Big Four Bridge on May 7, 2008 (see figure 3) [72], [73], [74]. An electrical fault in a lighting system sparked a fire above the Ohio River [74]. Construction workers were attempting to replace the beacon lights on the bridge [75]. Once again, the fire spread along timber elements of the span that eventually fell into the Ohio River, causing a stop of all river traffic [73], [75]. Once again, only minor structural damage was reported to the steel truss, but many of the timbers were burned away according to photographic evidence [74].

The fact that no steel members needed replacement after either fire indicates that the Big Four Bridge's trusses had sufficient thermal mass and redundancy to avoid catastrophic failure in these events. Both incidents point to a broader hazard of electrical failures causing bridge fires.

Figure 3. Photo. Big Four Bridge 2008 fire [76].

PLEASURE BEACH BRIDGE FIRE, BRIDGEPORT, CT (1996)

The Pleasure Beach Bridge was a swing bridge in Bridgeport, Connecticut, constructed in 1927 to connect the city to Pleasure Beach [77], [78], [79]. At the time, Pleasure Beach was home to a popular amusement park and summer cottages [79], [80]. The deck of the structure was constructed of creosote-treated timbers that were intended to prevent rot [81]. Creosote-treated timbers present an elevated fire hazard and can ignite from hot metal or sparks [82]. The structure was frequently closed for repairs [81].

On June 16, 1996, the timber elements were set ablaze by a discarded lit cigarette landing between the planks [79], [81]. Witnesses saw flames destroy approximately 150 ft of decking as onlookers formed a bucket brigade to help combat the flames [80], [83]. Photographic evidence

shows that the steel truss survived but the approach spans were destroyed and impassable (see figure 4). By the time the fire was out, the connection between Pleasure Beach and the mainland was severed, creating the "state's largest ghost town" [77]. The Pleasure Beach Bridge demonstrates that relatively inconsequential ignition sources can lead to devastating results.

Figure 4. Photo. Pleasure Beach Bridge post-fire [78].

DUMBARTON RAIL BRIDGE FIRE, SAN FRANCISCO BAY (1998)

Constructed in 1910, the Dumbarton Rail Bridge was the first bridge structure to span San Francisco Bay, shortening the route by 26 miles [84], [85]. At the time of its construction, it was the costliest bridge in California [84]. It carried a single railroad track with timber trestle approaches on both ends and a steel swing span in the middle to allow ship traffic [85], [86]. By

1998, the bridge had been out of service for 16 years [84], [85]. The timber elements remained in place, soaked in creosote [84].

At approximately 7 p.m. on January 3, 1998, locals in Menlo Park, California, reported flames on the abandoned western trestle of the Dumbarton Rail Bridge [85], [87]. A fire crew from Menlo Park responded in the middle of a rainstorm, arriving to discover a 1,750-ft section of the western portion of the bridge engulfed in flames [84], [85], [87]. Winds carried the toxic smoke from the fire, severely reducing visibility near the structure and closing a nearby highway for approximately 6 h [84], [85], [87]. The intense blaze destroyed the creosote-soaked timber structure despite the storm (see figure 5) [84], [85]. It took nearly 18 h before the fire department declared the fire under control [85]. Even then, pockets of fire smoldered in the collapsed piles and had to be removed later [85]. Large sections of the abandoned structure fell into the bay during the fire, and charred railroad ties were seen floating on the water [87]. Although arson was suspected, an official cause of the fire was never determined [84], [87].

The Dumbarton Rail Bridge fire is a notable example of how vulnerable timber structures are to fire. It also points to the impact that fires on decommissioned structures can have on transportation infrastructure when not properly cared for.

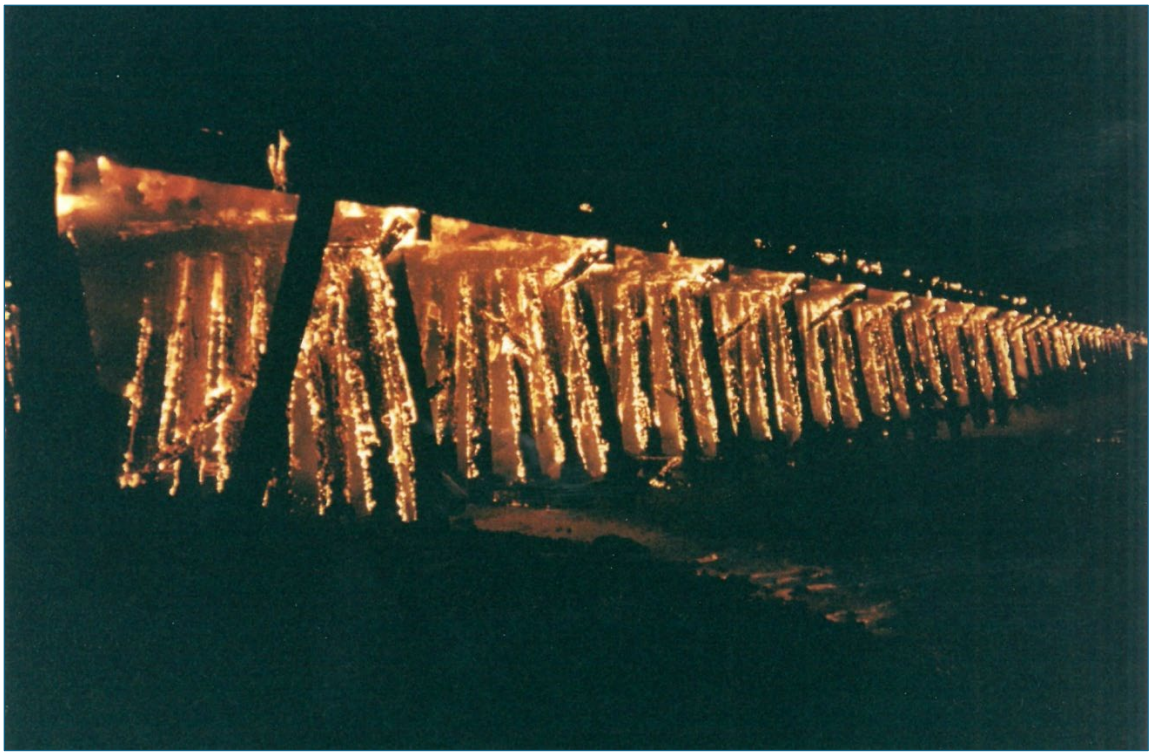

Figure 5. Photo. Dumbarton Rail Bridge fire [84].

FIRST MALFUNCTION JUNCTION FIRE, BIRMINGHAM, AL (2002)

Malfunction Junction is a notorious interchange of three interstates in Birmingham, Alabama, connecting I-65, I-20, and I-59 [88], [89]. The ramps, opened in 1970, eventually saw traffic far exceeding their design capacity [88]. It gained the name Malfunction Junction because of its frequent accidents [90].

On January 5, 2002, a tanker truck carrying gasoline collided with a car at the interchange [90], [91], [92]. The crash caused the tanker to overturn and burst into flames, sparking an explosion and fire that led to a partial failure of an overpass at one of Alabama's busiest highway interchanges [90], [92]. The explosion resulted in the death of the truck driver, and smoke was seen across the city [90], [92].

The burning fuel compromised the steel superstructure of the overpass, causing the girders to experience up to 10 ft of deflection, threatening the stability of the whole structure (see

figure 6) [34], [91]. Authorities immediately closed the interchange. In the days that followed, crews demolished the ramp and hauled away about 5,000 yd^3 of debris, along with 200 tons of steel [91]. Engineers fast-tracked a replacement bridge; the interchange was reopened to traffic in only 37 days [93]. The swift reconstruction was hailed for its fast pace [92].

The 2002 fire at Malfunction Junction demonstrates the danger that tanker trucks and the broader transportation of flammable and combustible materials present to bridge structures. It further demonstrates the vulnerability of steel structures to elevated temperatures.

Figure 6. Photo. Malfunction Junction 2002 post-fire [94].

SECOND MALFUNCTION JUNCTION FIRE, BIRMINGHAM, AL (2004)

On October 21, 2004, Malfunction Junction was once again the site of a tanker truck fire [34], [89], [92], [93]. A Kenworth tanker, reported to be carrying 9,000 gallons (gal) of diesel

fuel, crashed on the I-65 North connector and ignited [95]. As the fuel burned, witnesses reported a large column of black smoke rising from the interchange [95]. Unlike in 2002, city officials allowed I-65 to remain open, but they closed I-20/I-59 through the interchange [95]. An aide to the mayor said the bridge was charred with large pieces of concrete falling from the structure [95]. The ramp remained out of service for 6 weeks as the structure was once again reconstructed [92], [93].

As a site of multiple bridge fires, Malfunction Junction provides an interesting data point. Research in 2013 noted that these two recorded tanker truck fire events resulted in complete collapse at this structure [89]. These incidents serve as examples of how bridge fires not only pose a danger to public safety but also to local economies. Political and economic interests are often involved in repair and recovery decisions, as the Malfunction Junction fires demonstrate.

PORTAL BRIDGE FIRE, KEARNY, NJ (2005)

The Portal Bridge was built in 1910 [96]. It was a 961-ft-long steel swing-span bridge that spanned the Hackensack River between Kearny and Secaucus, New Jersey [96], [97]. The bridge carried two tracks for Amtrak [96]. The bridge's deck and fender system were constructed of creosote-treated timber [98].

On May 12, 2005, an improperly installed circuit breaker sent more than 12,000 V of electricity into the Portal Bridge [98], [99]. This sudden jolt of electricity caused the timber elements to ignite. The fire snarled train traffic between New York and New Jersey for nearly 10 h [99], [100]. The fire burned for approximately 2 h, but the bridge did not collapse [99], [100]. Repair costs were estimated to be about $5 million [101]. The incident underscores the potential for electrical failures to ignite fires, particularly in the presence of highly combustible materials.

MACARTHUR MAZE COLLAPSE, OAKLAND, CA (2007)

On April 29, 2007, a tanker truck carrying gasoline was traveling on I-880 in Oakland, California [102], [103]. The truck overturned at the MacArthur Maze interchange and started to burn. Approximately 8,600 gal of gasoline leaked from the wrecked truck and caught fire [4], [74], [102]. The fire spread along portions of I-880 and began to heat the steel girders of the overpass above [102], [104]. After approximately 20 min of intense heat, the steel girders gave way [4], [74], [105]. A 165-ft section of I-580 fell onto I-880 [103] (see figure 7).

Investigators found that temperatures reached over 1,000°C [102]. The extreme heat caused the girders to yield, which led to the failure of the structure [105]. Investigators found bolted angle connectors pulled out of place by the intensity of the heat [105]. The failure of the girders created a domino effect that damaged the bent caps [105]. In this case, the heat weakened the steel, leading to the failure of the bridge itself.

The California Department of Transportation (CalTrans) worked quickly to close the damaged structures [103]. Inspectors found that there was minimal damage to the lower I-880 structure, and they were able to reopen it relatively quickly [106]. However, the collapsed spans of I-580 required full replacement [106]. Contractors worked around the clock, and the bridge was rebuilt in 25 days [106]. Repair costs were estimated at $9 million; however, economic losses were estimated to be approximately $156 million [107].

The MacArthur Maze fire clearly shows that bridges can suffer catastrophic consequences of hydrocarbon fuel fires. It further demonstrates that in fires with multiple structures involved, there can be uneven impact of the blaze on structures, leading to the need for a varied response in recovery and rebuilding efforts.

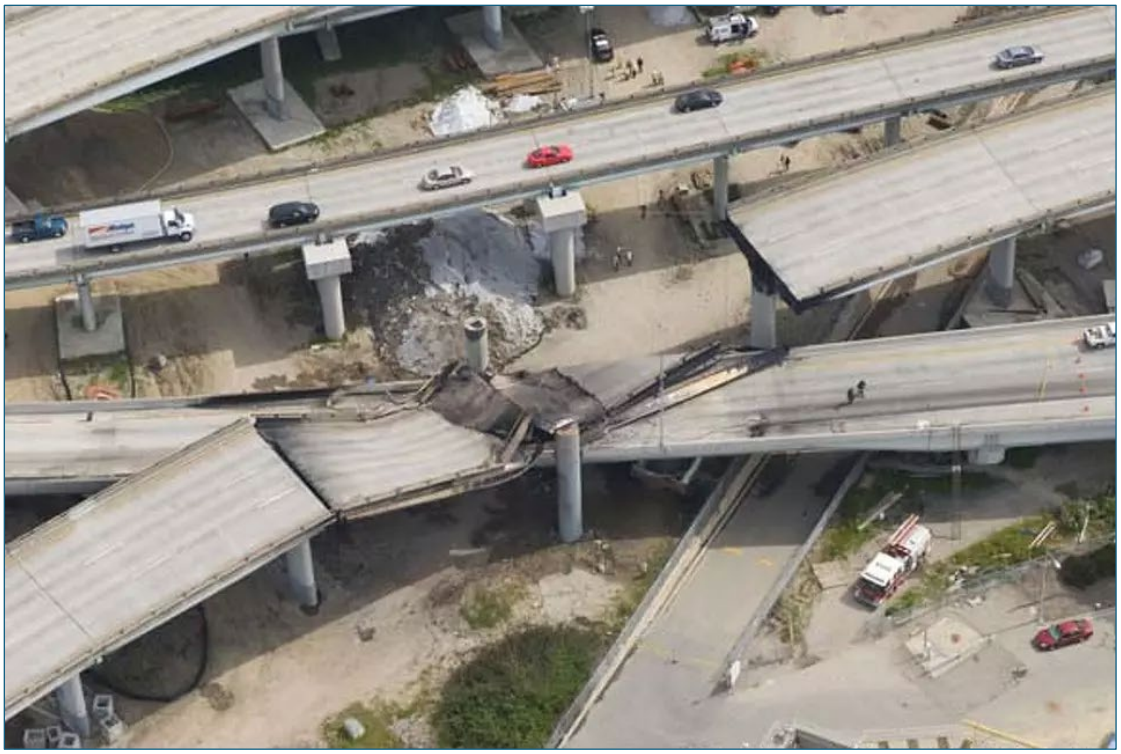

Figure 7. Photo. MacArthur Maze post-fire [108].

PARAMOUNT BOULEVARD BRIDGE, MONTEBELLO, CA (2011)

The Paramount Boulevard bridge in Montebello, California, was constructed in 1967 and crossed over the Pomona Freeway [109]. The bridge was constructed using reinforced concrete [110], [111].

On December 14, 2011, a double tanker truck carrying about 8,800 gal of gasoline was traveling eastbound on State Route (SR) 60 [112]. While driving, the driver noticed that his truck was on fire and stopped the vehicle under the Paramount Boulevard overpass [112]. While stopped under the bridge, the cargo of the truck exploded [113]. The heat from the fire forced the driver to abandon his truck for safety; the truck then burned for hours, damaging critical members of the structure (see figure 8) [110]. Initial investigations indicated that the cause of the fire was overheated brakes, but it was later discovered that the truck's transmission snapped and then punctured its fuel tank [109], [112], [113].

After the fire was extinguished, inspectors found damage to the concrete girders and deck, particularly significant spalling [110], [111]. One report indicated that the heat was sufficient to burst the concrete deck [110]. In the aftermath of the fire, CalTrans restored 1,000 ft^2 of roadway; in contrast, the affected bridge was removed by demolition because the damage was deemed irreparable [110], [111], [112].

Figure 8. Photo. Paramount Boulevard bridge fire [113].

I-85 BRIDGE FIRE AND COLLAPSE, ATLANTA, GA (2017)

On March 30, 2017, a fire was started under the I-85 overpass near Piedmont Road in Atlanta, Georgia [4]. The fire resulted in a 92-ft span of the bridge failing [114], [115]. No one

was injured in the fire, but the collapse created a transportation crisis because over 200,000 vehicles per day had to be rerouted to alternate routes [116].

Several years before the fire, the Georgia Department of Transportation (GDOT) placed 76 reels of high-density polyethylene conduit and 9 racks of fiberglass conduit under the structure [114]. This material was highly flammable [4], [114], [117]. The police reported that the fire was started when a man ignited a shopping cart chair under the bridge [117]. This fire spread to the stored materials [117]. Once the conduit was ignited, the material melted, creating an even larger flame [114]. The extreme heat caused the span to deflect and fail (see figure 9) [4], [114], [115]. This was primarily caused by the loss of prestressing in the concrete girders [114].

The fire also caused secondary damage. In addition to the span that failed, five additional spans had significant fire-related defects [114], [115]. These spans had to be removed [114], [115]. This meant that a significant portion of the overpass needed to be replaced [114].

As part of the emergency response, GDOT closed both northbound and southbound I-85 [116], [117]. Days later, the state awarded contracts to rebuild the damaged portion of the overpass. A bonus of $3.1 million would be given if the project was completed early [116]. In 43 days, the contractor completed the rebuild early, at a cost of $15 million [116].

The collapse of Atlanta's I-85 overpass changed the way transportation officials think. In the wake of the fire, GDOT enlisted the help of the state fire safety commissioner [117]. Together, they reviewed GDOT's policy on storing materials under bridge structures [114], [117]. Other states and the federal government also took notice. The Federal Highway Administration (FHWA) issued guidance that said storing combustible materials under bridges was not allowed [114], [118]. In 2023, FHWA reminded states of this rule following a similar

fire that occurred in Los Angeles [118]. It was determined that space under bridge structures should remain minimally used. This fire illustrates that human-caused ignitions can severely disrupt public safety and mobility.

Figure 9. Photo. Atlanta Interstate bridge failure [119].

HONEY RUN COVERED BRIDGE, PARADISE, CA (2018)

The Honey Run Covered Bridge was constructed in the late 1880s in Butte County, California [120], [121], [122]. The three-span Pratt truss spanned 238 ft across Butte Creek [120], [122]. In 1988, the bridge was added to the National Register of Historic Places [120], [122]. At the time of its destruction, the Honey Run Covered Bridge was considered the last of its kind (see figure 10, right photo) [122].

Early in the morning on November 8, 2018, a 911 call reported a fire beneath a Pacific Gas & Electric Company (PG&E) transmission tower [123], [124], [125]. This fire encountered a dry and windy California environment that allowed the fire to spread rapidly [125], [126]. In just over an hour from initial reports, the fire, known as the Camp Fire, spread to the town of Paradise and the Honey Run Covered Bridge [127]. The timber bridge was soon engulfed in flames and destroyed (see figure 10, left photo) [120], [122].

The fire burned much more than the bridge; over 153,000 acres were burned, nearly 19,000 homes and buildings were destroyed, 85 people lost their lives, and 2 people are still missing (as of 2025) [128]. The Honey Run Covered Bridge demonstrates that bridge structures, especially timber structures, are vulnerable to wildfires, underscoring the need for targeted prevention and response planning.

Figure 10. Photos. Honey Run Covered Bridge post-fire (left) and pre-fire (right) [122].

MANNING-RYE COVERED BRIDGE, COLFAX, WA (2020)

In 1918, a unique timber bridge structure was erected over the Palouse River in Colfax, Washington [129]. The structure was originally called the Harpole Bridge but was later renamed

the Manning-Rye Bridge [130]. The bridge consisted of an encased timber Howe truss that left the timber cross bracings and top exposed to the air [130]. The bridge was constructed to carry rail lines [130], [131]. However, by the 1970s, the railroad abandoned the lines carried by the through truss. Eventually, a property owner took ownership of the bridge and converted the rail line and bridge into a driveway [130], [131].

On September 7, 2020, several wildfires broke out in Washington [132], [133], [134]. Similar to the Camp Fire discussed above, high winds and dry conditions allowed fires to spread rapidly throughout Cascadia [132], [134]. These fires destroyed 181 homes and laid waste to over 600,000 acres of land [135]. One child died in these fires [135], [136]. The fire also caused the loss of the Manning-Rye Covered Bridge [129], [130], [131]. The Manning-Rye Covered Bridge fire and the Honey Run Covered Bridge fire display the vulnerability of bridges, especially timber structures, to wildfires. Wildfires will be addressed in more detail in chapter 4.

FAIRFIELD AVENUE OVERPASS – I-95, NORWALK, CT (2024)

On May 2, 2024, the Fairfield Avenue Overpass in Norwalk, Connecticut, was less than 10 years old [137]. At 5:30 a.m., a collision occurred between a tractor trailer, a tanker truck, and a passenger car [137], [138]. The tanker truck, carrying 8,500 gal of gasoline, came to a stop under the overpass [139]. The tanker split open as a result of the impact and spilled gasoline that ignited [137], [138], [139]. One report said that the flames were hot enough to melt steel [138]. The girders deflected as they were heated [138]. Following the fire, Connecticut decided to remove and replace the fire-damaged structure [137], [138], [139]. This fire further highlights the vulnerability of steel structures to hydrocarbon pool fires.

DANIEL CARTER BEARD "BIG MAC" BRIDGE, CINCINNATI, OH (2024)

The Big Mac Bridge consists of twin tied-arch structures that carry I-471 across the Ohio River between Ohio and Kentucky [140]. The arches are 760 ft long and 160 ft tall [140]. Although the official name of the structure is the Daniel Carter Beard Bridge, locals chose to name it after the hamburger from McDonald's based on its appearance [141]. The total length of the structure is 2,100 ft [142].

On November 1, 2024, a fire started under the southbound approach at the 1000 Hands Playground [143], [144]. Early reports said the fire was caused by an encampment of unhoused persons; however, these claims later proved to be unfounded [143], [144]. Instead, early that morning, three individuals were riding around Cincinnati looking for scooters to steal [143], [144]. At 2:28 a.m., they arrived at the playground, where two of the three individuals collected brush and other debris and started a fire for pyromaniacal joy [143], [144].

Initial inspection of the bridge post-fire found significant damage to three of the beams and the deck [145]. These elements needed to be removed, along with a damaged highway sign [145], [146]. The repair efforts for this structure cost $10 million and took 100 days to complete [144]. This incident, like the 2017 Atlanta fire, reinforces that human carelessness can have wide-ranging consequences to the U.S. bridge inventory.

CHAPTER 4. DISCUSSION OF BRIDGE FIRES

In chapter 3, this report reviewed a history of bridge fire events from across the United States. Often, each of these events is treated as a random, stand-alone occurrence. However, upon examination of the history, certain trends become apparent. The stories of these fires are not only tales of destruction. Each bridge fire serves as a critical data point that aids in understanding structural vulnerabilities, human error, material behavior under thermal stress, and the evolving challenges of fire safety in transportation.

Chapter 3 did not provide an exhaustive history, but it did reflect a wide range of ignition sources. Bridge fire history demonstrates how wildfires, tanker truck fires, arson, and electrical faults can lead to a bridge fire. Within each of these stories, consistencies in the types of damage were found. Certain bridge designs, construction materials, and locations appear repeatedly in the stories of individual bridge fires. These commonalities provide a basis for further exploration.

An analysis of these stories follows, which will identify and evaluate common trends across the various bridge fires. This chapter examines (1) which fire scenarios are most associated with severe structural loss, (2) how construction materials influence expected damage severity, and (3) whether specific bridge types or locations exhibit elevated susceptibility. These questions speak directly to the heart of risk mitigation, inspection planning, and design resilience. The goal of this report is to make this knowledge actionable. Inspectors should be able to employ this knowledge when they are called upon to perform a post-fire triage inspection on a bridge structure. Additionally, such information may be used to help prevent future fires by influencing design principles. This knowledge is vital as the American infrastructure network ages, climate risks continue to increase, and fire hazards become more frequent.

Bridge fires are a major threat to bridge structures and other transportation infrastructure because they can cause severe structural damage, economic loss, and loss of life [4], [6], [9], [35], [38], [62], [69], [110]. However, bridge design codes often ignore this risk [4], [38], [110]. Bridge fires are often started by vehicular accidents (especially those that involve tanker trucks), arson, accidental ignition, and wildfires [4], [62], [147], [148]. Various factors contribute to the severity of bridge fires. The source of fuel, bridge construction materials, bridge design, fire duration, and environmental conditions all affect the level of damage a bridge can suffer from a fire [2], [6], [10], [149], [150], [151], [152], [153], [154], [155].

The literature has identified hydrocarbon fuels, such as gasoline or diesel, as the most severe fuel source. Fires caused by hydrocarbon fuels often lead to failure of structural members. This is particularly true among steel and composite bridge structures [2], [6], [10], [149], [150], [151], [152], [153], [154], [155]. Smaller vehicle fires and fires from electrical sources tend to cause less severe, localized damage [2], [6], [149], [151], [156], [157]. Compared to other bridge failure modes, failures due to fire are less frequent but can be more severe in their immediate impact and recovery requirements [9], [35], [38], [110], [158]. The next few sections of this chapter will synthesize the historical context, primary causes, severity patterns, and comparative risks of bridge fires.

HISTORICAL OVERVIEW AND FREQUENCY OF BRIDGE FIRES

Bridge fires are more rare than building fires, but they have caused notable failures in the United States. A survey of over 1,000 bridge failures that occurred between 1980 and 2012 found that about 3.2 percent of failures due to external causes were from fire, exceeding bridge failures caused by wind or earthquakes [4], [159]. Quiel and Pessiki reinforce this point by noting that fire produced a failure rate comparable to, or exceeding, that of other hazards, such as

earthquakes or construction defects [160]. Recent literature highlights the rising vulnerability of bridges to fire [9].

Historically, fire was not explicitly considered in bridge design because of perceived low probability. A series of high-profile incidents in the 21st century shifted that view. For example, the 2007 MacArthur Maze collapse and the 2009 Hazel Park, Michigan, collapse show the vulnerability of bridge structures to tanker truck fires [4], [74], [105], [161], [162]. Since 2000, many bridge fires have been caused by tanker truck fires [4]. However, human-caused ignition has become a growing concern, as highlighted by the 2017 Atlanta and the 2024 Big Mac fires. Refer to chapter 3 for case studies from U.S. bridge fires.

In the United States, vehicle accidents are the primary driver of bridge fires, especially automobile accidents that involve hydrocarbon fuels, which produce rapid heating and severe damage even with a prompt response [4], [34], [102], [163]. Bridges with unprotected steel girders are particularly susceptible to elevated temperatures [4], [163]. In addition to automobile accidents, arson, wildfires, and electrical fires have been the cause of multiple bridge fires [62], [114], [160], [164]. Compounding the fire are factors that affect the severity of the fire. These factors are addressed later in this chapter (see Factors That Affect Damage Severity).

Unlike wind loading or earthquake loading, bridge design standards do not address fire loading [4], [35], [165]. In 2017, National Fire Protection Association (NFPA) 502 became the first major standard to address fire loading in bridge design by providing a standard to protect primary structural elements from extreme thermal events [160], [166]. The goal of this design policy was to allow easier firefighter access, reduce the fire's ability to damage the structure, and reduce economic loss caused by a bridge fire [166]. Overall, while the likelihood of a bridge fire remains low, the consequences are high. These consequences are driving increased public

awareness and a shift within the engineering community toward explicit consideration of fire in assessment, response, and mitigation planning [1], [4], [34].

UNDERSTANDING FIRE

For post-fire triage inspections, fire intensity is characterized by heat release rate (HRR). HRR can be defined in two ways. First, it can be defined by the rate of energy release from the fire [167], [168], [169]. The units for this measure are typically expressed as kilowatts (kW) or megawatts (MW). This method of quantifying HRR is preferred by the NFPA. The second way to quantify HRR is as the rate of energy release normalized by burning area [4], [170]. The units for this are typically expressed as kilowatts per square meter (kW/m^2). For example, the United Kingdom defines the maximum HRR for a building as 2,500 kW/m^2 [4], [170]. Regardless of convention, HRR quantifies the energy output of the fire, which governs the demand on bridge components [4], [170].

Flame spread refers to the propagation of burning across the fuel source [171], [172], [173]. This is driven by the heating and subsequent ignition of unburned material ahead of the flame front [171], [172], [173]. The flame front is the boundary between burning and unburning regions [171], [172], [173]. The rate and pattern of spread depend on fuel type and thickness, orientation, airflow, and ambient conditions [171], [174], [175], [176].

There are three distinct modes of flame spread. In *concurrent* flame spread, the fire spreads with gravity or airflow [174], [175]. Concurrent spread is typically faster due to enhanced heat transfer. *Opposed-flow* flame spread occurs when flame moves across the fuel source against airflow [173], [177]. Opposed-flow flame spread typically progresses slower than concurrent flame spread and is often easier to extinguish. *Surface* flame spread is when flame spreads over the fuel surface. It is a critical phenomenon in both wildfires and structural fires

[171], [173], [178]. Related to flame spread, flashover occurs when a fire reaches a point of intensity at which all combustible materials ignite [179], [180], [181].

Another critical parameter to understand is heat flux. Heat flux is the rate of thermal energy transfer per unit area per unit of time (W/m^2) [182], [183], [184]. For post-fire triage, heat flux represents the incident thermal load delivered from the fire to the bridge components. Heat flux governs the rate of temperature increase in materials; thus, it can govern the onset of degradation and loss of strength [58].

PRIMARY CAUSES OF BRIDGE FIRES

This section summarizes the principal sources of ignition and exposure that lead to bridge fires. They are organized into five categories: (1) tanker trucks, (2) other vehicles, (3) arson, (4) accidental ignition, and (5) wildfires. For each category, this section outlines typical heat-release rates and burn durations. Where available, case histories illustrate structural outcomes. The objective is to provide a clear basis for triage inspection and risk prioritization by linking common ignition scenarios to expected demands on bridge components.

Tanker Trucks

Chapter 3 reviewed a brief history of bridge fires in the United States and showed that tanker trucks carrying hydrocarbon fuels present a worst-case scenario as an ignition source [4], [34]. Tanker truck fires result in intense blazes that can result in severe damage to the bridge's structural elements [4]. These fires often lead to expensive repair or replacement costs and economic losses [4]. The MacArthur Maze fire (see MacArthur Maze Collapse, Oakland, CA (2007)) stands as a great example of the cost of tanker truck fires on bridge infrastructure. The economic losses were estimated at approximately $6 million/day with a total economic loss of

$156 million [4], [105], [107]. In 2011, the Paramount Boulevard Bridge fire in Montebello, California (see Paramount Boulevard Bridge, Montebello, CA (2011)) resulted in a $40 million replacement cost following a tanker fire [4], [185]. Because of the large-scale impact of these fires, they often have outsized economic impacts compared to bridge fires from other sources.

Historical tanker-truck–caused bridge fires also point to the high rate of failure for bridges involved in this type of incident. In addition to the MacArthur Maze fire and Paramount Boulevard fire, the bridge failures at Malfunction Junction (see First Malfunction Junction Fire, Birmingham, AL (2002) and Second Malfunction Junction Fire, Birmingham, AL (2004)) are further example of these issues [4], [74]. Where severe damage occurs due to tanker truck fires, two primary factors affect the outcome of the fire. The first factor is the quantity of fuel carried by the tanker leading to longer burn durations [34], [89]. The second is the location of the fire relative to the bridge structure [34]. These factors are discussed later in this chapter (see Factors That Affect Damage Severity).

Accidents involving tanker trucks often produce a large pool of burning fuel that can lead to severe damage to a bridge structure [58], [186], [187], [188]. These fires often exhibit extremely high HRR [189], [186], [187], [190], [191]. Research shows that tanker truck fires can have an HRR of up to 300 MW of energy [4], [89], [166]. This stands in stark contrast to the energy released from a passenger vehicle fire, which is only up to 10 MW [4], [166]. In addition, the time to reach peak HRR happens almost instantly in tanker truck fires [4], [166].

The primary mode of heat flux from a tanker truck fire is thermal radiation [4], [192], [193], [194]. Because of the high HRR, heat flux causes the temperature of the structural elements to rise rapidly [10], [153], [192], [195], [196]. The intense heat that is transferred to the structural elements can result in material degradation [153], [195], [196]. This degradation can

often continue even after the fire is extinguished [153], [195], [196]. A point source model will estimate heat flux using the HRR, fire duration, flame height, and fire location relative to the bridge [58]. This is discussed in more detail in Assessing the Risk.

Peak temperatures during a hydrocarbon fire are extremely high and are dependent upon the ignition fuel source. Tanker truck fires typically burn between 800° and 1,000°C. Some estimates place these fires at more than 1,000°C, but this is met with some skepticism by fire researchers [4]. Nevertheless, an inspection team can estimate the peak temperatures by the fuel being carried.

Gasoline typically burns at 1,100°–1,300°C [186], [187], [197]. Gasoline's high volatility contributes to an increased burn rate compared to heavier fuels, such as diesel [198], [199]. The HRR for gasoline is 2,400 kW/m^2 [34]. The burn rate of gasoline is typically 0.04–0.06 kg/m^{2}s (2–3 min per 100 gal of gasoline) [198], [199], [200]. Wind can increase the burn rate by increasing the oxygen supply to the fire. However, the burn rate will level off as winds increase in speed [199], [200]. Larger pools of gasoline will burn at higher rates [200]. In general, gasoline fires tend to burn hotter and may spread more rapidly compared to diesel [186], [187], [197]. It should be noted that aviation fuels tend to burn at 1,000°C [201] with similar burn rates (and burn rate factors), 0.04–0.07 kg/m^{2}s, to that of gasoline [198], [200].

Diesel fires typically peak between 900° and 1,200°C [186], [197]. Diesel tends to burn at lower temperatures than gasoline but for longer periods of time [186], [187], [197]. Diesel also has a lower HRR (1,950 kW/m^2) compared to gasoline [34]. The typical burn rate for diesel is 0.03–0.05 kg/m^{2}s (2.8–4.6 min per 100 gal), with influences similar to that of gasoline [198], [199], [200].

In addition to traditional automobile fuels, tanker trucks can carry highly flammable alcohols [34]. Ethanol fires can reach peak temperatures similar to gasoline. However, methanol fires burn at similar temperatures to diesel [189], [197]. The burn rates for both alcohols are in the 0.03–0.06 kg/m^{2}s (2.2–4.4 min per 100 gal) range, with ethanol having a slightly higher burn rate [202], [203]. Like the other fuel sources, pool size and wind play a major role in the speed of the burn rate [202]. Alcohol-fueled fires pose a threat to bridge structures similar to gasoline-fueled fires [189], [197].

Liquefied natural gas (LNG)–fueled fires burn at a peak temperature of 900°–1,100°C [197]. This is similar to the temperature exhibited by diesel-fueled fires. LNG fires experience rapid vaporization, which leads to an intense fire that is often short-lived [197]. LNG fires have the fastest burn rates of the fires discussed in this section. Their burn rate is 0.18–0.19 kg/m^{2}s (about 25 s per 100 gal) [204], [205]. Similar to the other fuels, pool size and wind affect the burn rate [204] [205].

Total burn times are highly dependent upon fuel type, fuel quantity, spill geometry, substrate type, how quickly the fuel was ignited, and heat transfer mechanisms [206], [207], [208], [209], [210], [211], [212]. Burn times, however, have varied from 30 to 150 min [4], [34]. During this time, structural collapse could occur [4], [34]. This trend is often reflected in the many hydrocarbon fuel fire curves that have been developed [58], [166].

Numerous bridges in recent history have failed due to the damage caused by tanker truck fires. They serve as the most destructive initial ignition source for bridge structures. When the battle is between a bridge and a tanker truck, the bridge has a strong possibility of losing. Any report of a tanker truck fire should be taken seriously and investigated as soon as possible.

Other Automobiles

Tanker trucks are not the only vehicles on the road that can cause fire. Light vehicles, buses, and other semi-trucks cause more frequent fires than tanker trucks, yet these fires are less severe [4], [34], [89]. This is because of the lower quantity of fuel burn compared to tanker truck fires [34]. These vehicles tend to release far less energy for shorter durations [34], [89]. This means that generally other vehicles cause less severe damage to bridge structures [34], [89]. Additionally, unlike with tanker truck fires, other vehicle fires tend to develop slower, allowing firefighters time to respond [4].

The HRRs of these vehicles tend to be lower than those of trucks hauling hydrocarbon fuels. Passenger cars, both electric and internal combustion, have HRR up to 10 MW, reaching their peak quickly [58], [165], [213]. If more than one passenger car is on fire, the HRR can be up to 20 MW within 10 min [58], [165], [213]. These fires can reach over 1,000°C inside the vehicles [214], [215]. The smoke temperature can reach up to 285°C at 1.5 m above the flame [214]. These temperatures can cause damage to the bridge, but the risk is lower than that of tanker truck fires [4], [34]. Passenger vehicle fires can burn up to 80 min, with a flashover time in as little as 2.5 min [215], [216], [217], [218].

Bus fires produce higher HRR than that of passenger cars. Their peak HRR can be up to 34 MW, reaching this peak in as little as 7 min and with temperatures in excess of 1,000°C [58], [165], [213], [219], [220]. Buses have longer burn times due to their size. They will reach flashover within approximately 8 min [218], [219], [221]. Total burn times can be longer than 60 min [219].

Tractor trailer trucks carrying general goods have a wide range of peak HRR values. They can range from 20–200 MW, depending upon the goods they are carrying [58], [165],

[213]. Similar to buses, these peak HRRs can be reached in as little as 7 min [58]. Burn times for these large trucks are difficult to narrow down due to cargo they may be carrying [222]. Like the other vehicles, peak temperatures can exceed 1,000°C [219], [223].

Arson

Arson also plays a role in the bridge fire landscape [224]. For example, the New York Department of Transportation reports that 8 percent of bridge fires are caused by arson [89], [225]. Compared to vehicle accidents, arson is more likely to occur in remote areas on timber structures [89], [225].

Historically, timber bridges, especially covered bridges, are particularly vulnerable to arson [4], [74], [110], [148], [226]. In 2013, the U.S. Department of Agriculture estimated that 700–900 covered bridges remain in the United States and that these bridges are "susceptible to arson and vandalism" [226]. The National Society for the Preservation of Covered Bridges estimates that about three covered bridges a year are lost due to arson [227]. The Ponn Humpback Bridge in Ohio, for example, was burned by an arsonist in 2013. Fire officials indicated that its remote location and lack of lighting made it an easy target for arson [228].

While rural timber structures are most vulnerable to arson, bridges with stored materials or debris are also susceptible to arson [89], [114], [118], [229]. In Atlanta, a portion of an I-85 overpass collapsed and required replacement, as discussed in I-85 Bridge Fire and Collapse, Atlanta, GA (2017). In Los Angeles, a portion of the I-10 overpass was severely damaged when stored materials were set ablaze. The structure was stabilized with temporary shoring and reopened in relatively quick order [230], [231]. In Cincinnati, arsonists used debris gathered under the Big Mac bridge to start a fire (see Daniel Carter Beard "Big Mac" Bridge, Cincinnati, OH (2024)). This resulted in the bridge being closed for 100 days [229].

Accidental Ignition

In some circumstances, accidents cause fires to start. One source of accidental ignition is from construction-related activities, such as cutting or welding [4], [34], [232]. History shows that construction activities have caused fires on bridge structures [4], [34]. For example, in 2024, construction workers in Hesperia, California, accidentally ignited wooden formwork while using metal-cutting tools [4], [233], [234]. In another case, a New York construction crew set a pile of construction waste on fire, which spread to nearby scaffolding [3], [4]. Both incidents exemplify the risk posed due to poor work site maintenance coupled with spark-producing maintenance activities.

Other times, things that seem insignificant become more impactful, especially when timber is involved. A 2002 fire on a Kansas railroad bridge was caused by an overheated wheel bearing that dropped onto railroad ties and destroyed the entire timber structure [4]. The Metro-North Railroad bridge over Harlem River in New York was temporarily closed in 2010 when a transformer blew and ignited the timber piles [235]. Internationally, in 2011, children playing with fire accidentally completely destroyed the Yuquig Bridge, a woven timber arch, in China [4], [236].

Wildfires

As the climate changes, the United States is experiencing an increase in wildfires [237], [238], [239]. These high-intensity fire events are not just an environmental issue [237]; they can also be disastrous to the public infrastructure [164], [240], [241]. A wildfire near a bridge can ignite combustible components and damage structural elements of the bridge [164], [241]. Wright et al. further warn that timber structures are far more susceptible to failure during a wildfire compared to steel or concrete bridge structures [89]. Their conclusion was supported by

the work of Refai [238]. Overall, it should be noted that there is limited research concerning bridges damaged by wildfires [238].

Extreme wildfire events are 2.2 times more common since 2003 [239]. These events exhibit extremely high HRR, often in excess of 1,000 MW [239], [242], [243]. Peak temperatures of wildfires can exceed 1,000°C, with surface temperatures strongly dependent upon the fuel source [244], [245]. Elevated HRR, high temperatures, and access to fuel can lead to a flashover event [243], [246], [247]. These events lead to rapid uncontrolled fire spread [243], [246], [247]. Whereas the burn time at any one location is relatively short, under these circumstances, rapid ignition of timber elements is possible [238], [246], [248]. Further, large amounts of debris collected under the structure can ignite, causing damage similar to the arson discussed above.

FACTORS THAT AFFECT DAMAGE SEVERITY

Fire causes are related to, but unique from, the various factors that impact the severity of fires on bridge structures. Four main factors should be considered relative to bridge fire severity: (1) fuel type and quantity, which determine how hot and how long a fire can burn; (2) location (on, under, or near the bridge) of the fire and the vertical clearance; (3) presence of additional combustible materials; and (4) bridge type and usage.

Fuel Quantity and Type

Fire load is the amount of heat energy released by burning all combustible materials in a given area [249], [250], [251]. Fire load is calculated by multiplying the mass of each fuel item per unit area (fuel load) by its calorific value [249], [250], [251], [252], [253]. This calculation helps to identify the potential severity of the fire [249], [250], [254]. An increase in fire load can

lead to an increase in peak HRR, peak temperatures, and heat flux [255], [256]. It is important to remember that this relationship assumes that an area is well ventilated [255].

The calorific value represents the amount of heat energy that is released when the fuel is burned [257], [258]. This value is highly dependent upon the chemical makeup of the fuel. Fuel sources with higher concentrations of carbon and hydrogen tend to have higher calorific values [257], [258]. Fuel sources such as gasoline have a calorific value of 44-47 MJ/kg [259], [260]. This is opposed to biomass materials, such as wood, drift, and vegetation, that have a value of 5–41 MJ/kg [261], [262].

To summarize, fire load shows two factors related to fuel that play a role in determining how severe a fire can be. First, the pure quantity of fuel over a given area, quantified as fuel load, will lead to an increase in fire load. Second, fuels with greater calorific values can increase fire load. Ultimately, an increase in fire load can lead to an increase in the severity of the fire and the damage to the bridge structure.

Fire Location and Vertical Clearance

The location of a fire changes the level of damage severity [34], [58]. Quiel et al. examined 31 different bridge fires and found that fires under a structure were far more likely to produce severe damage compared to fires on or beside a bridge structure [58]. Approximately two-thirds of the structures with fires under them experienced heavy damage or collapse [58]. Peris-Sayol et al. echoed these data in their 2017 research paper [34]. They found that fires under a bridge result in a higher damage level [34]. However, it should be noted that a tanker truck spill of a hydrocarbon fuel on a structure could result in similar damage levels compared to fires under a structure [34], [58].

Fires located under a structure tend to cause the most damage due to buoyancy. Buoyancy is the upward force that causes hot gases and flames to rise toward structural elements (see figure 11) [263], [264]. This occurs as the heated air becomes less dense and rises relative to the surrounding cooler air [264], [265], [266]. Buoyancy will concentrate smoke and heat to structural elements above the fire, increasing heat flux [264], [265], [266], [267].

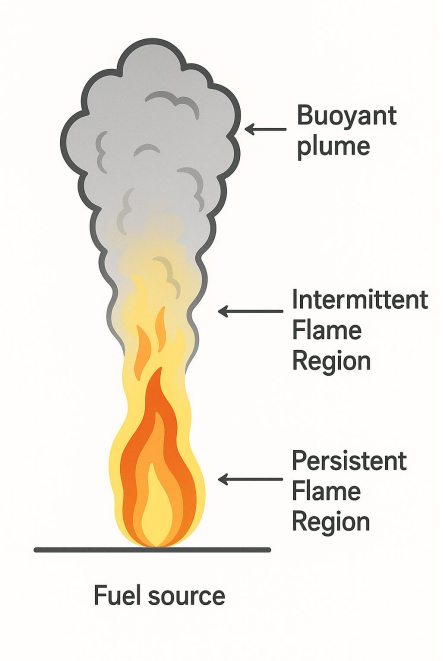

Figure 11. Diagram. Fire plume.

Fire modeling and experiments demonstrate that the highest rate of heat flux takes place where the fire plume directly contacts the structure [268], [269], [270], [271]. A fire plume is the column of hot gases, flames, and combustion products that rise above the source of the fire due to buoyancy [272], [273], [274]. The fire plume consists of three parts. First is the area of continuous visible flames directly above the fuel source, known as the persistent flame region (see figure 11) [272], [273], [274]. The intermittent flame region is the area of the fire where flames appear and disappear and generally becomes less stable [272], [273], [274]. Finally, the

area above the flame where hot gases mix with the cooler surrounding air (known as "air entrainment") and the flame is no longer visible is known as the buoyant plume region [272], [273], [274]. The size and shape of the fire plume are dependent upon the HRR of the fire, the size of the fuel source, and other environmental factors [274], [275], [276].

Presence of Additional Combustibles

The presence of additional combustibles has the potential to increase the severity of the bridge fire. This is accomplished by increasing HRR, extending burn durations, or elevating peak temperatures [2], [4], [9], [62], [151], [277]. Additional combustible material, such as debris or construction materials, can transition the fire into a more sustained thermal event [2], [4], [277], [278]. The additional materials add to the total fuel load and can prolong the combustion period [2], [4], [9], [62], [151]. In addition to an increased fire load, additional materials under a structure may entrap heat [4], [277], [278], [279]. This entrapped heat can present a danger to vulnerable bridge structural elements [6], [150], [151], [280].

Bridge Type and Usage

Bridge type can have a major impact on susceptibility to bridge fires. Timber bridge elements are the most susceptible to fire [34]. Approximately 79 percent of timber structures collapse during fire events [34]. Timber elements, compared to steel or concrete, will ignite easily [147], [148], [164], [281]. These structures have a unique quality in which the bridge itself serves as a source of fuel for the fire [4]. Timber elements should be examined closely during the initial assessment following a bridge fire due to their susceptibility to damage at even low temperatures.

Steel will lose strength as temperatures elevate [282], [283], [284]. Significant strength loss will begin around 500°C, with continued degradation at higher temperatures [282], [283], [284]. The elastic modulus of steel will also decrease, thus causing the steel to lose stiffness as it heats [282], [283]. Welds and high-strength steel may lose strength more rapidly than mild steel [284], [285], [286]. Unprotected steel exhibits poor fire performance during intense heating [4]. Despite being subject to damage during bridge fires, steel tends to suffer, on average, less severe damage compared to concrete or timber [34]. The inspector may see discoloration, paint blistering, paint cracking, paint delamination, steel deformations, or the development of surface rust [15], [16], [17].

Reinforced concrete and prestressed concrete elements provide better fire performance compared to steel and timber [4], [34], [58], [110]. Although concrete damage levels are higher than that of steel, concrete structures have historically been less likely to collapse following a fire [4], [34], [58]. Inspectors may see various defects that were due to fire damage, including change in aggregate color, cracking, delamination, surface roughness, spalling, and exposed reinforcement [18], [287], [288], [289], [290].

In addition to bridge material, the bridge's structural system also affects the amount of damage a structure may see from a fire. I-shaped girders are particularly prone to damage due to their thin webs and flanges [6], [9], [34], [291], [292]. Bridges that use these types of girders account for approximately 77 percent of bridge structures with heavy to severe damage [34]; however, this may be due to their popularity. Suspension bridge cables can be vulnerable to direct heating [153], [293], [294].

There is limited research into whether bridge location is a factor in the severity of bridge fires [2], [34]; however, some locations may limit the activity of firefighters, thus increasing the

likelihood of more severe damage [4]. Further, an increase in traffic volume also increases the likelihood of fires at bridge structures due to the potential increase for hazardous goods being transported [2], [295].

ASSESSING THE RISK

This section presents Lehigh University research and adapts it into an operational screening method to be used as a tool for bridge fire events. Using a small set of readily obtainable inputs, the method supports rapid, defensible pre-mobilization judgments of likely damage severity. Damage classes are assigned by comparing incident heat flux with established temperature thresholds for steel and concrete. The resulting tool is intended to support triage, resource mobilization, and temporary risk control rather than replace detailed analysis. It guides inspection prioritization, the imposition of temporary restrictions pending review, and the selection of follow-up actions. The subsequent sections summarize the research and provide recommendations for tool development.

Summary of Quiel et al. [58]

Quiel et al.[1] have defined temperature-based damage states and built practical damage-classification graphs for steel and concrete girders subject to fire. Their research provides an important framework for rapid classification of bridge fires. Figure 12 shows the classification of damage for steel I-shaped girders (p. 38). Figure 13 visualizes the classification of damage for concrete girders (p. 38). In both figures, blue circles represent heating without potential damage to the structure. Green squares represent areas of potential damage to the structure. Finally, red triangles represent areas of critical damage to the structure. The specifics of these classifications

[1] Page numbers within Quiel et al. [58] are cited in parentheses in this section.

are drawn from various codes and will be discussed in more detail in chapter 5 and chapter 6. These limits present a unique opportunity to rapidly assess how critical a fire can be to a structure.

Quiel et al. performed a two-dimensional (2D) thermal finite element analysis across numerous combinations of incident heat flux ($\dot{q}''$) and exposure duration (pp. 36–39). Each simulation outcome is plotted per established temperature thresholds and is shown on the graphs in figure 12 and figure 13. The graphs show a clear distinction between areas of potentially no damage, potential damage, and critical damage.

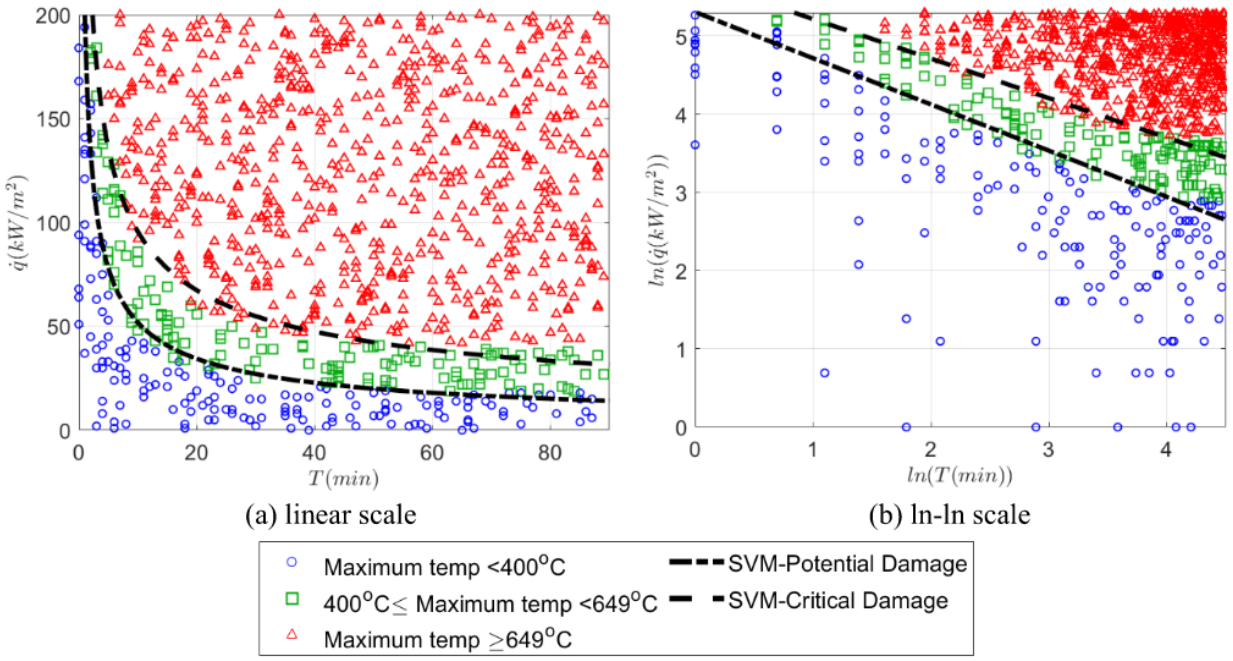

Figure 12. Graphs. Damage classification graphs for steel girders [58]
SVM = support vector machine.

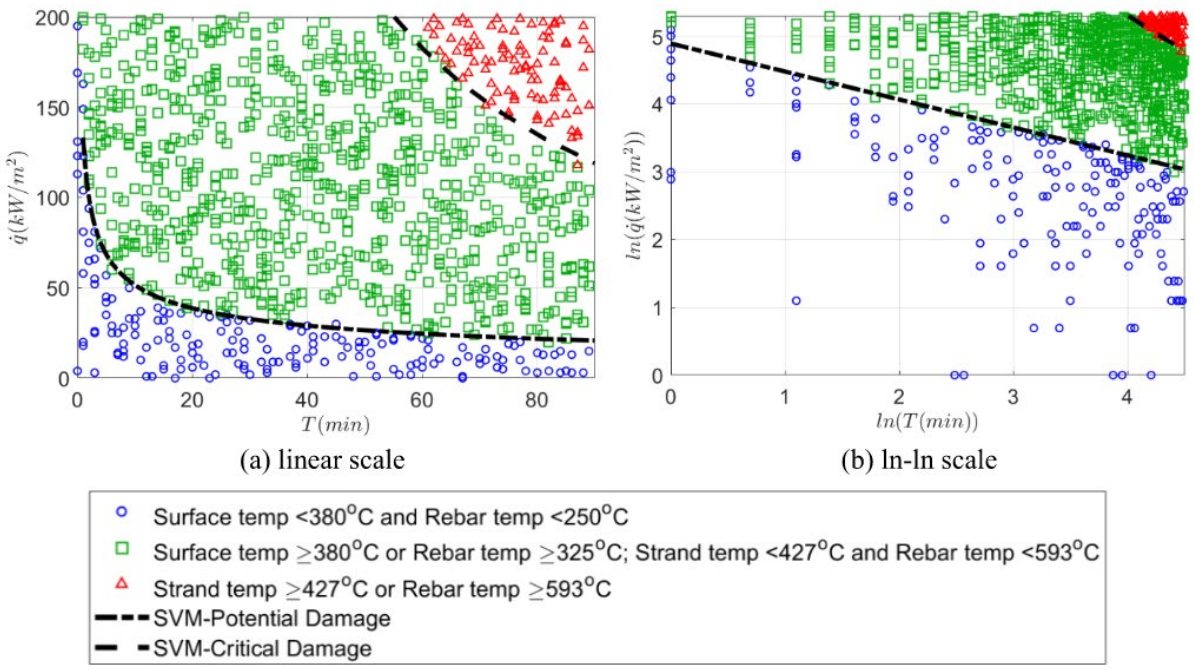

Figure 13. Graphs. Damage classification graph for concrete girders [58]. SVM = support vector machine.

To place a fire on the graph, Quiel et al. obtained the peak incident heat flux at the girder using a modified point source model (pp. 36–39). This model is shown in equation 1 (pp. 22–24). In the equation, $\chi_{r,mps}$ is the radiative fraction, $\dot{Q}_{f,max}$ is the peak heat-release rate of the fire, θ is the angle between the line of sight and the closest bridge element, R is the distance from the modified point source to the target, and n is an exponent calibrated to 2.2. Once $\dot{q}''$ is obtained, this can be plotted against the exposure time.

$$\dot{q}'' = \frac{\chi_{r,mps}\dot{Q}_{f,max}\cos\theta}{4\pi R^n} \qquad \text{Equation 1}$$

Practical Implications for Rapid Assessment of Bridge Fires

The research summarized in the previous section (see Summary of Quiel et al.) provides a practical basis for the development of an assessment tool in the form of an Excel worksheet to classify the criticality of a bridge fire. This tool can enable GDOT's initial, defensible assessment using readily available incident information. The results may be suitable for guiding the dispatch of personnel or making temporary decisions to close the fire-damaged structure.

To apply the framework, GDOT engineers should gather data, much of which may be obtained from the emergency incident command prior to mobilization of department forces. Where the information is uncertain, the tool in Excel should allow for conservative assumptions. This tool is intended to be used for screening and prioritization of GDOT's resources; further evaluation may be required to arrive at a final determination. Engineers will need the following data for input into the tool:

1. *Structural system or member type*: To answer this question, engineers need to determine if the element in question is steel or concrete.
2. *Key geometry of the exposed member*: The calculation will require input of the horizontal distance from the fire centerline to the face of the nearest structural element (i.e., the horizontal offset). Associated with this, engineers must obtain the elevation difference between the fire source and the nearest structural element (i.e., the vertical offset).
3. *Fire scenario*: Engineers should obtain information on the principal fuel source and the estimated duration of peak fire intensity.

COMPARISON WITH OTHER BRIDGE FAILURE MODES

A bridge structure may fail in various ways. This section reviews common failure modes and assesses how failure due to fire fits into the broader picture. In the United States, hydraulic events, such as flooding and scour, are the leading cause of collapse [159]. The second leading cause comes from vehicle impacts or overload [159] s. Less common, but still relevant to the discussion, are failures due to deterioration, wind, seismic activity, fire, and structural deficiencies [4], [74], [34], [159].

Scour is the erosion of soil from around bridge foundations by flowing water [89], [296], [297], [298], [299]. It is the leading cause of failure for bridges in the United States [296], [297], [298], [299]. Various studies have demonstrated that scour has been the cause of 47.1–60 percent of bridge failures in the United States [159], [298], [300], [301], [302].

The second most common cause of failure for bridge structures is overload [89], [159], [300]. Structural overload accounts for approximately 20–28 percent of bridge failures [159], [300]. Overload takes on two forms: direct overload and impact load. Direct overload is caused by crossing vehicles exceeding the bridge's design limits, resulting in structural failure [303], [304]. An impact load is when a vehicle, ship, train, or aircraft strikes a bridge, resulting in structural failure [300], [302], [305].

The third major cause of bridge failure in the United States is deterioration [89], [159]. Deterioration is the gradual decline in the condition of a bridge over its life [29], [30], [31], [32], [33]. The natural degradation of a bridge leads to 6.8 percent of bridge failures [159]. Various factors, such as chemical changes, material properties, and traffic loading, lead to the degradation of structural elements [29], [306]. The presence of cracks, spalls, corrosion, and section loss are all signs that a bridge is deteriorating [307].

Fire ranks as the fourth leading cause of bridge failures [89], [159]. Fire accounts for approximately 3 percent of bridge failures, which exceeds the totals for wind and earthquake [4], [159]. Yet, unlike wind and earthquake, fires are not accounted for in bridge design [4], [58]. As discussed previously, fires can lead to rapid degradation and damage of structural members [4], [34], [74].

Next in the list are bridge failures due to construction and design flaws [300], [308]. These causes account for approximately 2.5 percent of bridge failures [159]. Internationally, the failure of the Lamgadi Bridge in Nepal shows how inadequate design, improper load calculations, poor detailing, or failure to account for specific load cases can result in the collapse of a bridge structure [309]. These types of failure only make up a small percentage of bridge failures, but they do receive outsized attention when they occur [310], [311], [312]. The hope is that these closer examinations will reduce human error and prevent future collapses [310], [311], [312].

Earthquakes account for about 2 percent of bridge collapses in the United States [4], [159]. The rarity of collapses due to earthquakes is the result of rigorous design standards [4], [313]. The design codes direct engineers to account for seismic loading [313]. Bridges constructed prior to modern seismic standards face higher earthquake vulnerability, reflecting the absent or minimal seismic design and detailing [314], [315].

The final primary cause of failure is wind, which accounts for approximately 1.8 percent of bridge failures in the United States [4], [159]. One popular example of a wind-related bridge failure is the Tacoma Narrows Bridge collapse in 1940 [316]. Winds, regardless of the source, can cause structures to vibrate, flutter, or gallop, resulting in fatigue of the structural members [316], [317], [318]. This is especially true for suspension and cable-stayed bridges [316], [317],

[318]. Similar to earthquakes, as discussed above, modern design helps account for the effects of wind on bridge structures [313], [316], [319].

When examining the broader picture, bridge fires are more rare than flood or scour events, but they are not freak accidents that bridge owners can discount. When a bridge does collapse due to fire, the consequences are often severe. Fires tend to occur on busy corridors; thus, a fire-related collapse could result in the disruption of the flow of people and goods around urban areas as well as potentially having broader economic impacts. These consequences merit serious attention from transportation officials.

CHAPTER 5. STEEL BRIDGES

This chapter consolidates guidance for evaluating steel bridge components following fire exposure. The researcher team first defines critical temperature as the temperature at which reduced strength and stiffness threaten load-bearing capacity. Then, they summarize typical critical ranges and their dependence on in-service demand, temperature distribution, boundary conditions, steel grade, and section geometry. Finally, this information is translated into inspection practices by outlining common indicators of distress and the appropriate use of NDT to corroborate findings and localize concerns. The objective of this chapter is to present field-ready triage processes that can lead to informed decision-making following extreme thermal events.

CRITICAL STEEL TEMPERATURES

This section reviews how elevated temperatures reduce the load-bearing capacity of steel bridge components and then identifies the key factors that determine when a temperature becomes critical. As temperature rises, steel experiences progressive loss in yield strength. This leads to a reduced margin against instability and could lead to failure. There is no single temperature level at which steel will enter critical condition; critical temperature levels depend on various factors. Understanding these interactions provides a defensible basis for post-fire assessment. These ranges help the agencies understand when to dispatch inspectors, implement load restrictions, or request deeper engineering analysis.

How Differing Temperatures Affect Steel

The critical temperature for steel bridge components is the approximate temperature at which the member's residual strength is reduced sufficiently to threaten load-bearing capacity. Many standards cite a lower-bound critical temperature of about 550°C. However, the typical critical range is 500–700°C [320], [321], [322]. Table 1 summarizes representative residual capacity versus temperature. The precise curves may vary by product or in situ conditions, but the overall trend is broadly similar across steel grades [320], [322]. In addition to the degradation of yield strength, steel experiences a reduction in elastic modulus at increased temperatures. However, in structural fire assessments, the loss of strength is typically the governing property for determining critical temperature and evaluating risk of failure [285], [323], [324], [325]. Table 2 provides retention factors for steel [323].

Table 1. Critical temperatures for steel.

Temperature (°C)	Residual Capacity (%)	Notes on Capacity Reduction
20	100	Baseline
200	90–95	Minimal loss
400	70–80	Noticeable reduction
500	60–70	Rapid decline begins
600	40–50	Significant loss
700	20–30	Severe loss
800+	<20	Most structural capacity lost

Quiel et al. provide practical guidance for temperature-based screening thresholds [58]. Their report concludes that when any location along a steel I-girder exceeds 400°C, there is potential for structural damage [58], [323]. Further, when steel temperature at any location on the girder exceeds 649°C, structurally critical damage could occur [58], [326]. Quiel et al.

developed these temperatures explicitly for steel I-girders as representative sections [58]. The researchers note in their report that similar criteria could be applied to other steel elements. However, as the report does not provide member-specific limits for other steel elements, agencies may wish to develop member-specific criteria following similar methods.

Table 2. Retention factors for steel properties.

Temperature °F (°C)	Elasticity Factor	Proportional Limit Factor	Yield Factor
68 (20)	1.00	1.00	1.00
200 (93)	1.00	1.00	1.00
400 (200)	0.90	0.80	1.00
600 (320)	0.78	0.58	1.00
750 (400)	0.70	0.42	1.00
800 (430)	0.67	0.40	0.94
1,000 (540)	0.49	0.29	0.66
1,200 (650)	0.22	0.13	0.35
1,400 (760)	0.11	0.06	0.16
1,600 (870)	0.07	0.04	0.07
1,800 (980)	0.05	0.03	0.04
2,000 (1,100)	0.02	0.01	0.02
2,200 (1,200)	0.00	0.00	0.00

Factors that Affect Critical Temperatures

Field performance during a thermal event is governed by more than a single temperature threshold. Multiple factors can improve or diminish a member's capacity under thermal exposure. Higher load ratios reduce the temperature at which failure occurs, and nonuniform heating can concentrate damage to critical zones. Rotation restraint of steel members generally improves performance by enhancing stability. However, axial restraint can lower critical temperatures by inducing compressive forces. Steel grades also matter. High-strength steel

typically exhibits lower critical temperatures than mild steels. Finally, section geometry affects susceptibility to local and global instability. The subsections that follow address each factor in more detail and provide guidance for post-fire assessments.

Load Ratio

Critical steel temperatures are load ratio–dependent [322], [320]. Load ratio is defined as the ratio of the applied load on a structural member to the ultimate load-carrying capacity at room temperature. As the load ratio increases, the critical temperature decreases. For example, one study found that raising the load ratio from 0.2 to 0.8 reduced the critical temperature from 670°C to 565°C [322]. For reference, load ratio may be expressed as in equation 2.

Engineers should account for in-service demands of steel members during and after fire events. Higher load ratios may warrant more conservative temperature thresholds, thereby making the bridge structure a higher priority. Higher load ratios may necessitate immediate inspection, the addition of temporary support, or the application of load restrictions.

$$Load\ Ratio = \frac{Applied\ Load}{Ultimate\ Capacity\ at\ Room\ Temperature} \qquad \text{Equation 2}$$

Temperature Distribution

Temperature distribution refers to the nonuniform heating of steel bridge elements during a fire [322], [327]. This effect is frequently not represented in laboratory settings. In the laboratory, samples are exposed to uniform furnace temperatures that do not necessarily capture spatiotemporal gradients observed in the field [284], [328], [329]. Recognizing that real-world fires seldom heat members evenly is essential for post-fire assessment. Inspectors should

prioritize zones of likely peak temperature for the common heat-related damage mechanisms described in Common Heat-Related Defects in Steel.

Restraint Conditions

Rotation and axial restraint materially influence the critical temperature at which steel loses its load-bearing capacity [328], [330]. Increasing the rotational restraint at member ends raises stability and can increase the critical temperature. Thus, this added stability allows a member to withstand higher thermal exposure before failure. This effect is particularly pronounced in steel columns. In columns with greater end fixity, the effective length is reduced. This allows for delayed buckling and can lead to significantly larger increases in critical temperatures [328], [331], [332], [333].

By contrast, axial restraint generally lowers the critical temperature. When thermal expansion is restrained, compressive forces accumulate as the steel heats. This increases the risk of yielding and instability at lower temperatures. Reported reductions in critical temperature due to axial restraint can be approximately 200°C [330], [333], [334], [335], [336]. For assessment purposes, engineers should document and consider in situ boundary conditions when conducting post-fire assessments.

Steel Grade

The grade of steel can influence the critical temperature at which a member loses load-bearing capacity during a fire. In general, high-strength and ultra-high-strength steels exhibit greater sensitivity to elevated temperatures than mild-strength steels at comparable load ratios [337], [338], [339]. Under similar demand, ultra-high-strength steel showed an approximately 10 percent reduction in critical temperature compared to high-strength steel [337]. Capacity loss

can initiate at temperatures as low as 300°C for certain ultra-high-strength products [338], [339]. There are variations in critical temperature within the high-strength steel groupings, but as a general rule, the higher the initial strength of the steel, the more pronounced the deterioration at high temperatures [337], [338], [339]. For post-fire assessments, engineers should identify the steel grade and use grade-appropriate temperature–strength data for the analysis.

Section Geometry

The cross-sectional geometry of a steel member influences critical temperatures for loss of bearing capacity in a fire. Key factors include slenderness, compactness, and shape. Members with lower slenderness generally tolerate higher temperatures before instability. This is reflected in reduced susceptibility to thermal buckling [340], [341], [342]. Conversely, slender members and thin-walled elements tend to reach instability at lower temperatures. Localized buckling has been reported at temperatures as low as 400°C [342], [343], [344], [345], [346]. The presence of stiffeners can raise critical temperature by increasing buckling resistance [347]. Hollow structures often retain higher critical temperatures compared to open structures. This effect is due to improved resistance to local buckling and more favorable heat-transfer characteristics [342], [348], [349].

For post-fire assessment, engineers should coordinate with inspection teams to help identify and document section classification (i.e., compact, slender, etc.), unbraced lengths, stiffener configurations, and section type (i.e., open or hollow).

COMMON HEAT-RELATED DEFECTS IN STEEL

Fire exposure can produce a characteristic set of defects in steel bridge elements. Common defects include global or localized distortion, local buckling, waviness in flanges or

web, and the formation of plastic hinges. In addition to base-metal damage, connections (such as welds and bolts) can also be damaged due to increased temperatures. These defects can reconfigure load paths, leading to progressive failures and, in severe cases, collapse. Therefore, post-fire inspections should document the location, extent, and asymmetry of distortion and buckling. Further, inspectors should note areas of potential microstructural changes. Engineers can map these changes and help evaluate restraint conditions to establish the need for further investigation, load restrictions, repair recommendations, or closure.

Loss of Strength and Stiffness

As the temperature of steel increases, yield strength, ultimate strength, and elastic modulus decrease in a predictable manner [17], [350], [351], [352]. In general, the progression of strength loss follows the trend summarized in table 1. Ductility also decreases as temperature increases. Decreased ductility can lead to increased risk of fracture [17], [352]. However, the temperature at which these reductions become critical depends on the factors outlined previously in Factors that Affect Critical Temperatures. Assessment thresholds and follow-up actions should be set with these influencing conditions in mind.

Permanent Deformation

As steel temperatures rise and sections enter the inelastic range, permanent deformations can develop. Common deformations include bending, buckling, and warping [353], [354], [355]. These shape changes reflect the loss of stiffness and strength as described above. Inspectors should document evidence of these deformations, detailing location and extent.

Further, inspectors should examine steel elements for the development of plastic hinges. Plastic hinges are zones where a member has fully yielded in bending while moment remains

near constant [356], [357]. The presence of plastic hinges in columns or girders or the buckling of columns are significant indicators of impending instability or collapse [353], [358]. These deformations warrant immediate load restrictions, temporary shoring, or bridge closure pending further evaluation.

Connection Failures

In addition to damage in steel girders, columns, or piles, bolted and welded connections can degrade under fire exposure. This degradation alters structural behavior and increases the risk of progressive collapse [355], [359]. Elevated temperatures reduce strength, stiffness, and ductility of connection components and the adjoining base metals. This can lead to bolt shear and weld cracking; it can also cause the connected steel to deform or fracture [355], [360], [361], [362].

As these connections weaken, the structure's intended load paths can be compromised. Forces redistribute to adjacent members, which may become overstressed [355], [360], [361]. Damage can become visible in these members that are away from the primary burn location. This reconfiguration of load effects can initiate a chain reaction of secondary failures [355], [360], [361]. Post-fire assessments should also examine connection details such as bolts and welds. Inspection reports of the post-fire triage inspection should document distress patterns that indicate redistribution of loads. These signs may necessitate load restrictions, temporary shoring, repair, or closure.

Brittle Fracture Risk

Fire exposure can induce microstructural changes in steel that degrade toughness and increase the likelihood of brittle fracture [352], [363]. These changes may begin at temperatures

as low as about 300°C. Significant grain growth typically occurs above 700°C [364], [365], [366], [367], [368]. These microstructural changes develop as fracture toughness declines, raising the possibility of crack initiation. Crack initiation is significantly more likely if fire temperatures exceed 600°C [369], [370]. These alterations can persist after cooling, leaving steel more brittle than its pre-fire condition [369], [370].

When examining a steel member post-fire, inspectors should consider the potential for reduced toughness in zones that experienced elevated temperatures. Where temperatures are suspected of exceeding the 600°C threshold, agencies should consider targeted material evaluations to confirm microstructural condition and fracture resistance before returning the structure to service.

INSPECTION TECHNIQUES FOR STEEL

This section summarizes practical methods for post-fire assessment of steel bridge components. Triage inspections should begin with a visual inspection to identify immediate hazards and document damage patterns. If necessary, inspectors can deploy portable NDT tools to corroborate and localize concerns. The Leeb hardness test (LH) can screen for heat-softened zones. UT can be used to check for changes in thickness and internal flaws. The dye penetrant test (PT) and magnetic particle test (MP) can be used to evaluate steel members or welds for discontinuities. Each method has its capabilities and limitations, but used in combination, they support defensible judgments about a structure's post-fire condition. The objective is field-ready triage while reserving destructive testing and detailed analysis for cases where risk and uncertainty warrant further review.

Visual Inspection

Visual inspection is the first line of assessment for steel structures following a fire [371]. These inspections can identify immediate hazards and help target areas that require additional testing. Key indicators associated with loss of strength and stability include changes to surface appearance, member deformation, and evidence of structural compromise [16], [351], [372], [373]. Systematic documentation of these indicators supports triage decisions and prioritizes NDT and further analytical evaluation.

Damage to protective coating systems can provide qualitative clues to elevated temperature exposure. Manifestations may include discoloration, blistering, cracking, and localized coating loss [16], [374]. However, it should be noted that corroborating research is limited. The diagnostic value may be restricted to paint systems that were previously intact and undamaged. Pre-existing degradation, surface contamination, and product variability can skew interpretation of this indicator.

Where coatings are absent, oxide color and thickness can provide a qualitative clue to thermal exposure [375]. Progressive darkening and thickening of oxides generally correlate with higher peak temperatures and longer durations of heating [375]. The presence of iron oxide may become evident at temperatures over 750°C [375]. Because oxide appearance is also dependent on atmospheric oxygen and post-fire weathering, these cues should be recorded as supporting evidence, particularly if previous inspections did not note the presence of rust or corrosion. However, this should be viewed as supporting evidence and not the sole determinant of damage state.

Fire-induced oxidation may be accompanied by surface roughness and pitting. These defects are often visible and palpable by touch. Such surface degradation often begins at

temperatures above 600°C and is associated with reduced mechanical performance of the steel [338], [376]. These changes indicate that the steel may be susceptible to fatigue or fracture [376], [377]. Following a fire, inspectors should document the location, extent, and severity of roughness and pitting in the steel member. They should note if this damage is near structural details with high-stress demands and flag these areas for targeted NDT methods and possible material testing before being returned to service.

Inspectors should document evidence of permanent deformation following fire exposure. Elevated temperatures reduce steel strength and stiffness, leading to increased instability [16], [351]. Observable manifestations include local plate buckling, global distortion, and the warping or twisting of steel elements [353], [373], [378]. Additionally, the development of plastic hinges is a critical indicator of inelastic demand [353], [379]. Similar deformation modes have been observed in concrete-filled steel tubes [379]. These deformations in a structural member may warrant additional investigations and analysis following the initial inspection.

Cracking, fractures, and connection failures are critical indicators of structural compromise after a fire. Inspectors should closely examine welds, bolts, rivets, pins, and other high-stress areas. Brittle cracking at connections is a significant red flag for reduced integrity [373]. In addition, missing, loose, or damaged fasteners constitute potential failure points and should be documented with location, extent, and orientation. Areas showing signs of structural compromise should be flagged for shoring and repairs.

Leeb Hardness Test

LH is a portable NDT method that supports post-fire initial assessments of steel bridge components [378], [380], [381]. The device propels a small impact body against a steel surface and records the ratio of rebound to impact velocity. This ratio is called the LH value (*LH*). *LH* is

correlated to the steel's hardness and, by extension, strength [378], [380], [381]. Because the test is inexpensive, rapid, and does not require section removal, it can be useful in screening and mapping areas of potential heat damage [378], [380]. This test does require some surface preparation and can be influenced by surface roughness, test location, and steel grade [378], [380], [381], [382]. Further, this test only assesses the hardness of the steel. LH tells inspectors nothing about ductility or deformation capacity without calibration [378], [380], [381], [382].

Ultrasonic Test

UT is an NDT method that uses high-frequency sound waves to interrogate steel and detect discontinuities [383], [384], [385], [386]. Following fire exposure, UT can be applied to verify the remaining thickness and to screen for cracks or voids [383], [384], [385], [386]. These findings can support judgments about residual capacity and the need for corrective action. When applied systematically, UT provides objective evidence of internal damage and reduced thickness that may not be apparent by visual inspection alone [383], [385].

Effective UT requires trained operators and adequate surface access. Additionally, the surface must be properly prepared for testing [383], [384], [385], [386]. Accuracy can be reduced by the presence of paint systems or rough surfaces [383], [384], [385], [386]. This test should be performed after the steel has cooled and should be interpreted in conjunction with visual findings and other NDT to develop a consistent post-fire evaluation.

Dye Penetrant Test

PT is a surface inspection NDT method used to detect fine surface-breaking discontinuities in steel elements and welds [387], [388], [389]. After cleaning the test area, a low-surface-tension penetrant is applied. During the dwell period, the penetrant can wick into the

open flaws by capillary action. After sufficient time has passed, the excess penetrant is removed, and a developer is applied. The developer draws penetrant out of the cracks, producing a visible indication of their location and extent [387], [388], [389]. PT is well suited for detecting the cracks in steel and welds that result from increased brittleness following a fire.

PT is highly sensitive to surface irregularities, simple to use, low cost, and versatile [390], [391], [396]. However, it is limited to surface-breaking defects after careful surface preparation [391], [392], [393]. Rough, heavily oxidized, or porous surfaces reduce the reliability of the test [391], [392], [393]. If the surface is too damaged to use PT, the inspector may wish to seek out alternative means of detecting fine, brittle cracking in structural steel members, such as magnetic particle testing.

Magnetic Particle Test

MT is an NDT method for detecting surface or near-surface discontinuities in ferromagnetic materials, such as the structural steel elements of bridges [394], [395], [396]. The test is conducted using an electric current to magnetize the yoke. Once magnetized, fine magnetic particles are applied to the surface of the steel member. Leakage fields generated by discontinuities attract the particles, which then form visible indicators that reveal the location, length, and orientation of the defect [394], [395], [396]. MT is valued for its high sensitivity, rapid execution, relative simplicity, and cost-effectiveness [394], [396], [397], [398]. Although MT is fast and sensitive in detecting defects in steel, it is limited by material type, defect depth, surface condition, and operator subjectivity [394], [399], [400].

CHAPTER 6. CONCRETE BRIDGES

This chapter synthesizes how fire affects concrete bridge elements and outlines a practical approach for post-fire triage. First, this chapter defines critical temperature ranges at which concrete begins to undergo physical and chemical changes that result in a loss of structural capacity. It then explains that the temperature at which damage becomes critical is not a single value but is dependent on various factors that govern both rate of heating and the severity of capacity loss. Finally, it translates these principles into inspection guidelines by which concrete members can be evaluated following a thermal event.

CRITICAL CONCRETE TEMPERATURES

This section summarizes how elevated temperatures degrade the load-bearing capacity of concrete bridge members. As temperatures increase, concrete begins to degrade and experiences reductions in compressive strength. The temperature at which the loss of capacity becomes critical is not a single value; it can vary with material composition, concrete cover, or extent of damage.

Temperature's Effect on Concrete

Most studies identify a critical range of approximately 300°–400°C at which the compressive strength of concrete will begin to rapidly decline [401], [402], [403], [404], [405]. Below this range, the compressive strength remains relatively stable. In some cases, there was a modest apparent increase in strength in the subcritical temperature range due to moisture loss [401], [402], [403], [405]. Above 400°C, microstructural degradation accelerates as cement paste dehydrates and aggregates expand [405], [406], [407]. As these structural changes take place,

inspectors may see surface cracking, spalling, or color changes in aggregates [1], [408], [409], [410]. By 600°C, the compressive concrete strength has typically weakened by half compared to its ambient temperature compressive strength [401], [402], [403], [405], [411]. At temperatures of approximately 800°C and above, concrete has experienced a near total loss of compressive strength [401], [402], [403], [411], [412]. These trends are summarized in table 3. Table 4 provides factors for analysis recommended by the American Institute of Steel Construction (AISC) [323].

Quiel et al. established a surface temperature of 380°C as the dividing line between no damage and potential damage [58], [166]. Internal temperatures at prestressing strands of greater than 427°C and greater than 593°C for mild steel are viewed as critical for concrete structures [58], [326].

Table 3. Common residual strength percentages.

Temperature (°C)	Residual Strength (%)	Notes
20	100	Baseline
100	90–100	Minor losses; sometimes slight increases
150	90–105	Some mixes show peak strength at this temperature
200	80–95	Gradual decline begins
300	60–90	Noticeable loss; microcracking increases
400	50–80	Strength loss accelerates
500	40–70	Major microstructural damage
600	30–50	Severe degradation; most codes use 40% reduction as reference
800	10–30	Near-complete loss of structural integrity
1,000	<10	Residual strength minimal

Limited empirical data exist on fire-induced damage to concrete structures [34], [58]. This makes the establishment of critical temperatures uncertain. The uncertainty is further compounded by the lack of consensus on temperature-based spalling prediction [58], [413]. Temperatures at mild steel reinforcement or prestressing can reach critical levels in a reduced amount of time due to the loss of cover caused by spalling [58], [414], [415], [416].

Table 4. Retention factors for concrete.[2]

Temperature °F (°C)	Compression Retention Factor		Elasticity Retention Factor	Strain at Given Temperature
	Normal Weight Concrete	Lightweight Concrete		Normal Weight Concrete
68 (20)	1.00	1.00	1.00	0.0025
200 (93)	0.95	1.00	0.93	0.0034
400 (200)	0.90	1.00	0.75	0.0046
550 (290)	0.86	1.00	0.61	0.0058
600 (320)	0.83	0.98	0.57	0.0062
800 (430)	0.71	0.85	0.38	0.0080
1,000 (540)	0.54	0.71	0.20	0.0106
1,200 (650)	0.38	0.58	0.092	0.0132
1,400 (760)	0.21	0.45	0.073	0.0143
1,600 (870)	0.10	0.31	0.055	0.0149
1,800 (980)	0.05	0.18	0.036	0.0150
2,000 (1,100)	0.01	0.05	0.018	0.0150
2,200 (1,200)	0.00	0.00	0.000	0.0000

Where spalling is observed, the screening model presented in Assessing the Risk should not be used as a governing assessment [58]. Post-fire spalling should be treated as a potential critical find pending the outcome of the complete investigation. Inspectors should document spalling location, extent, and depth. It is further recommended that inspectors make use of NDT

[2] The tensile strength of concrete at elevated temperatures can be assumed to be zero; however, it should not be any greater than 10 percent of the compressive strength at the corresponding temperature [323].

methods, such as RHs or UPV, to further ascertain the extent of the damaged area. Once this information is obtained, a new analysis using the Quiel et al. method with the reduced concrete cover can be conducted to determine the critical nature of the as-found condition [58]. This procedure provides a more conservative and defensible check on member safety.

Factors that Affect Critical Temperatures

As with steel, the temperature at which concrete reaches critical condition is not governed by a single factor. Material composition affects how the concrete responds to fire by controlling thermal expansion, moisture migration, and crack progression. Additionally, section detailing, particularly the thickness of concrete cover over reinforcement, influences heat transmission and bond retention. Greater concrete cover does not change reinforcing steel's performance at elevated temperatures, but it does delay the time for reinforcement to reach critical temperatures. Taken together, these parameters influence the rate at which damage develops and the severity of capacity loss.

Material Composition

Concrete is a composite of cement, water, aggregates, and, where specified, admixtures [417]. The constituent ingredients and their proportions influence the temperature at which fire exposure becomes critical. Water–cement ratio is a key factor in estimating a particular mix's thermal resilience [418], [419]. High water–cement ratios produce greater porosity due to excess water [420], [421]. As this excess water evaporates, it leaves voids and capillary pathways in the concrete. The resulting lower-density, more permeable mix is more susceptible to microcracking and strength loss under heating. The increased porosity provides pathways for expanding water vapor, elevating the risk of cracking and spalling at elevated temperatures [418], [421]. Notably,

while higher porosity tends to lower the temperature at which performance degrades, it can also reduce the likelihood of explosive spalling by offering additional vent paths to relieve pore pressure [422], [423].

Aggregate type also has a significant influence on concrete behavior at elevated temperatures [424], [425]. Calcareous aggregates, like limestone or dolomite, generally perform better than siliceous aggregate under fire exposure [424], [425]. They tend to remain more chemically stable at temperatures up to approximately 600°C [426], [427], [428], [429]. In addition, calcareous aggregates exhibit lower thermal expansion compared to siliceous aggregate [427], [429], [430]. As a result, concretes made with calcareous aggregates typically show greater residual compressive strength above 300°C and lower strength loss up to 600°C [426], [429], [431]. However, at temperatures in excess of 700°C, decarbonation of the aggregate can occur, leading to mass loss and concrete degradation [427], [429].

Siliceous aggregates, such as quartz or granite, undergo a phase transformation at approximately 573°C [426], [427], [429], [431], [432]. During this phase transformation, siliceous aggregates exhibit a sudden volumetric increase, raising internal stress within the concrete [426], [427], [429], [431]. The associated thermal expansion mismatch at the aggregate-paste interface promotes microcracking, thus accelerating the degradation of the concrete [426], [427], [431]. As a result, concrete made from siliceous aggregates often shows a rapid decline in compressive strength above 300°C [426], [429], [431]. Critical damage can often occur in concretes made with this aggregate at temperatures lower than 600°C [426], [429], [431].

Structural Factors

As detailed in Temperature's Effect on Concrete, increased concrete cover delays heat transmission to embedded reinforcement. Intact concrete cover extends the time before steel reaches critical temperature [433], [434], [435]. For example, increasing the cover from 20 mm to 60 mm can more than double the time it takes for internal reinforcement to reach its critical temperature [433]. Greater cover provides not only improved thermal insulation but also helps maintain the critical steel–concrete bond under heating [414], [434], [436], [437]. Preserving this bond reduces the risk of slipping and maintains composite action. While cover thickness does not change the critical temperature of the reinforcement, it improves member fire resistance by slowing internal temperature rise and sustaining the bond between the concrete and internal reinforcement.

COMMON HEAT-RELATED DEFECTS IN CONCRETE

This section summarizes common defects observed in concrete bridge elements following thermal events. The most common defects include: (1) cracking, (2) color changes, (3) spalling, and (4) carbonation. The purpose of this section is to define each defect, identify visual indicators, and provide practical guidance for systematic documentation to support post-fire triage and follow-up actions.

Cracking

Cracking is among the most commonly observed defects during post-fire initial inspection of concrete bridge elements [1], [438], [439]. Cracks manifest as either microcracks or macrocracks [440], [441]. Microcracks are very fine discontinuities in the concrete matrix that typically measure less than 0.1 mm in width [442], [443]. They are often barely visible and

may require special techniques to detect. They can originate from the normal curing process, the natural freeze/thaw cycle, or elevated temperatures [1], [444], [445]. Under fire exposure, mismatched thermal expansion between aggregates and cement pastes promotes microcrack formation [432], [441]. With continued thermal demand, microcracks can coalesce into larger, visible macrocracks [442], [446], [447].

Post-fire cracking can be a visible indicator of strength loss [442], [448]. In addition to the loss of strength, cracks facilitate deeper ingress of water and carbon dioxide (CO_2) [442], [448], [449], [450]. The increase of these substances can accelerate carbonation, which can reduce durability over time [451].

Color Changes

One visible indicator of fire exposure in concrete is aggregate-driven color change (see figure 14) [1], [452], [453]. For concrete mixes that contain siliceous aggregates, the aggregates may shift from pink to red between the temperatures of 300° and 600°C due to the presence of iron [1], [452], [453], [454]. Between 600° and 900°C, the color change will be whitish gray [1], [452], [453]. A yellowish-beige tone will appear in the concrete between 900° and 1,000°C [1], [452], [453]. These changes are associated with the gradual dehydration and decarbonation as the concrete is heated [452], [454], [455], [456]. Calcareous aggregate tends to turn whitish gray at elevated temperatures [456].

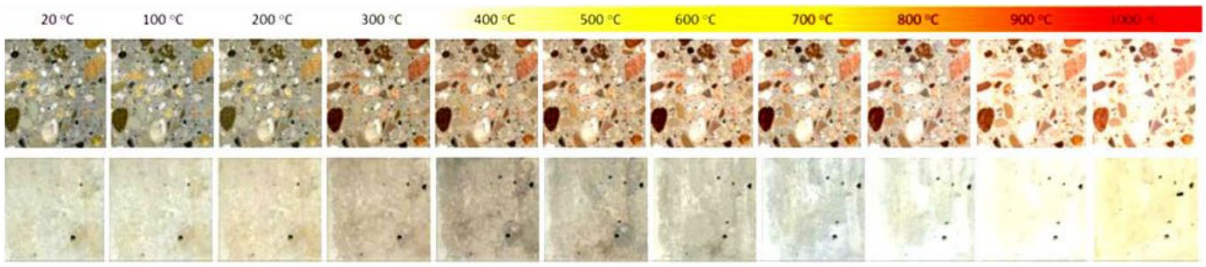

Figure 14. Photos. Color changes in concrete by temperature [452].

Recognizing these color transitions during post-fire triage can provide evidence of the potential temperature of the concrete when it was burning [454], [456], [457]. This temperature estimate can be correlated then to strength loss, as described in Critical Concrete Temperatures. Color cues should be treated as supporting evidence, however, and not a stand-alone criterion. Inspectors should document color observations with photographs and locations. These colors should be compared to undamaged portions of a similar concrete member to eliminate other possible sources of the color change.

Spalling

Spalling is a common fire-related defect in concrete bridge elements [1], [34], [58]. Concrete spalling can be defined as the localized breaking, cracking, and detachment of surface concrete, often in chunks, when tensile forces exceed the tensile strength of the material [458], [459]. Broadly speaking, fire-related spalling can occur explosively or gradually [52], [460], [461]. Explosive spalling is influenced by moisture content, heating rates, and restraint condition [460], [461], [462], [463]. It is common to categorize thermally induced spalling into three categories: thermo-hygral, thermo-mechanical, or thermo-chemical [52]. Thermo-hygral spalling arises when rapid heating vaporizes pore water, resulting in pore pressure buildup [52], [461], [464], [465]. When this pressure exceeds the concrete's tensile capacity, sudden, often

explosive, spalling can occur [52], [461], [464], [465]. Thermo-mechanical spalling results from temperature gradients that drive differential thermal expansion [52], [461], [465], [466], [467]. In locations where this expansion is restrained, tensile forces increase beyond the capacity of the concrete, resulting in spalling [52], [461], [465], [466], [467]. Thermo-mechanical spalling often progresses gradually, although abrupt failures are possible. Thermo-chemical spalling is associated with temperature-induced chemical changes that weaken the concrete matrix, leading to the gradual spalling of surface material under continuous heating [52], [461], [467].

As stated above, any observed spalling should be treated as a potentially critical finding. Inspectors should document the location, extent, and depth of spalling. These spalls should be correlated with other visual defects, and additional NDT methods should be used to ascertain the complete picture of the fire-related damage.

Carbonation

Carbonation is the process by which atmospheric CO_2 diffuses into concrete's pore system. Upon entering the pore system, CO_2 dissolves in pore water (H_2O) to form carbonic acid (H_2CO_3). Then, H_2CO_3 reacts with calcium hydroxide ($Ca(OH)_2$) to form calcium carbonate ($CaCO_3$) [450], [468], [469], [470]. The atmosphere is the primary source of CO_2, but fire events can also increase CO_2 levels [471], [472].

Several factors govern how rapidly carbonation advances in concrete. Relative humidity is a significant driver of carbonation because CO_2 must dissolve in pore water to form H_2CO_3 [473], [474], [470], [475]. If the concrete is too dry, there is insufficient pore water to sustain the reaction. If the concrete is too wet, the water-filled pores hinder the diffusion of CO_2. Relative humidities between 55 and 70 percent are the most conducive environment for carbonation progress [473], [474], [470], [475].

Temperature can also influence the rate of carbonation in concrete [474], [476], [477]. Higher temperatures generally accelerate CO_2 diffusion, resulting in greater depths of carbonation over time [474], [476], [477]. A positive, linear relationship exists between carbonation depth and temperature [474], [476], [477]. In practice, relative humidity and temperature work together to create an environment that can result in an increased rate of carbonation in concrete.

Concrete quality is a third driver of the rate of carbonation of concrete [473], [478], [479]. Lower water–cement ratios can reduce porosity of concrete and thereby decrease the rate of CO_2 ingress and lower the rate of carbonation (see figure 15) [473], [478]. Conversely, some supplementary cementitious materials can refine pore structure, which may increase carbonation depth [473], [478].

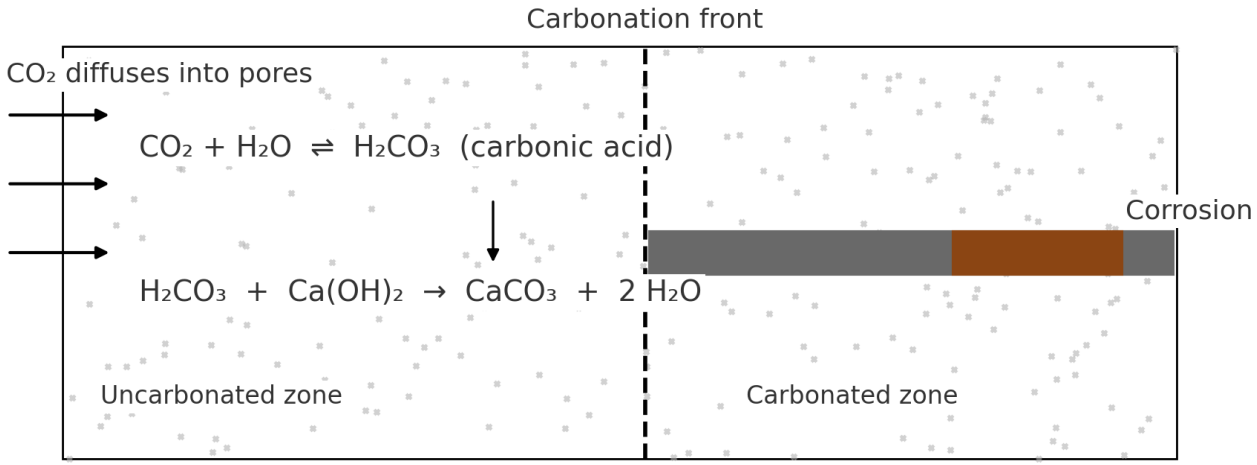

Figure 15. Diagram. Carbonation process.

Fresh concrete is strongly alkaline, with pH levels of 12.5–13 [451], [480]. As concrete ages, carbonation progresses inward from the surface, resulting in the lowering of pH levels

toward 9–11 (see figure 16) [451], [480].[3] This loss of alkalinity can depassivate reinforcing steel, which increases the possibility of corrosion [451], [481], [482]. In the presence of moisture and oxygen, the steel will corrode and expand, leading to cracking and spalling of the concrete cover [451], [481], [482], [483]. Notably, pH reduction alone is not sufficient to guarantee corrosion. Environmental exposure and detailing govern whether and how rapidly reinforcing steel will corrode [483].

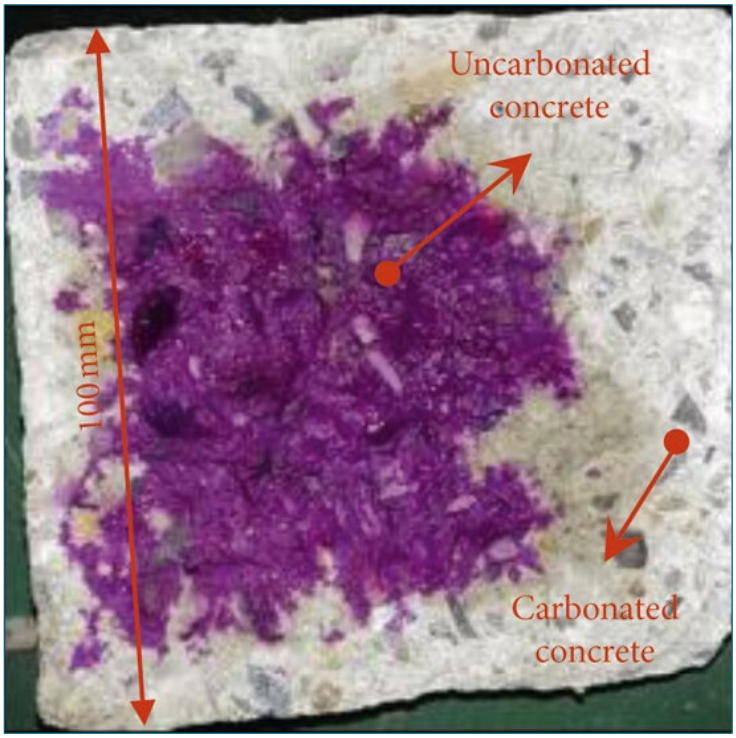

Figure 16. Photo. Example of carbon depth [471].

Fires can decompose cement hydrates, increase porosity, and facilitate deeper CO_2 penetration [408], [484]. This change in concrete structure suggests a potential increase in

[3] GDOT has documented corrosion at concrete cap-steel pile interfaces. Carbonation of the concrete at this interface is a plausible contributing mechanism. Given moisture coming from leaking joints, the presence of oxygen, and relatively wide cracking in the concrete, the loss of alkalinity from carbonation could have produced an environment that promotes the corrosion and section loss. GDOT may wish to investigate the role of carbonation in these areas. This may aid in producing a means to prevent significant steel corrosion in the future.

long-term carbonation susceptibility, thus lowering the durability of the concrete member [473], [478]. Limited evidence is available to indicate an immediate, or near immediate, increase in carbonation post-fire [472], [485]. Laboratory results indicate that rapid cooling scenarios can accelerate carbonation, but slow cooling may not show the same effect [485].[4] Practically, carbonation should be treated as a long-term durability concern post-fire.

To anticipate durability needs after a thermal event, bridge owners should establish a baseline carbonation-depth map of affected concrete members. These baseline data will enable trend monitoring at future inspections and support early, targeted maintenance before reinforcement depassivation advances. Carbonation testing kits are available for purchase and can be used for this mapping procedure [1], [486]. Alternatively, once structural integrity is confirmed, owners may limit the rate of new carbonation by sealing damaged and porous surfaces to reduce water ingress.

INSPECTION TECHNIQUES FOR CONCRETE

This section summarizes practical tools for the post-fire triage of concrete bridge elements. Following a structured visual inspection to locate hazards and map observable damage, inspection teams can develop an inspection plan to deploy NDT devices, including: (1) RHs, (2) UPV, (3) GPR, and (4) impact echo tests (IEs). These NDT devices can aid inspectors and engineers in corroborating data and localizing areas of concern. Each method has specific

[4] The research team attempted to detect post-fire increases in carbonation depth on laboratory burn samples. The results did not show an immediate, measurable increase, consistent with the findings reported by Oliveria et al. [485]. The absence of a marked change may be the result of insufficient pore water during heating to sustain rapid CO_2 dissolution, the inability of the electric furnace to create a carbon-rich environment, and/or an insufficient interval between heating and testing for carbonation fronts to advance detectably. These observations support treating carbonation as a longer-term durability concern following a fire.

strengths and weaknesses. It is best to use these methods in combination to better assess the health of a structure following a fire.

Visual Inspection

The first phase of a post-fire triage inspection of concrete bridge elements is a visual inspection [1], [487]. Inspectors should begin a visual inspection by determining the location and extent of the fire [487], [488]. They should take note of soot and plume patterning, any debris or burned materials left behind after the fire, and localized charring of items attached to the bridge structure. Inspectors should pay special attention to any visible damage patterns. If not established by emergency services prior to mobilization, inspectors should attempt to ascertain the likely heat source and duration of the fire [487], [488].

After establishing the fire's location and extent, inspectors should conduct a methodical survey of the affected concrete members, recording color (see Color Changes) and surface changes to the concrete members. Next, they should document locations of new cracking and the extent of the damage, as detailed in Cracking. Hammer tapping may be used to identify delaminated areas [1]. Any delamination found should be documented and marked. Inspectors should identify and describe spalling, as detailed in Spalling, recording any spalling that may have exposed reinforcing steel. This steel should be examined for any fire-related defects (see Common Heat-Related Defects in Steel). Inspectors should also document the extent of the steel exposure and any defects found during the inspection. Documentation can include sketches, photographs, and detailed notes. The visual inspection is concluded by translating observations into a targeted NDT plan [487], [488]. Areas showing signs of damage or distress should be prioritized for closer inspection.

Rebound Hammer

An RH is a spring-loaded NDT device. It impacts the concrete surface and reports a rebound number (*RH*). *RH* is proportional to the near surface hardness of the concrete [489], [490]. Multiple readings should be taken and obvious outliers discarded [490]. The average of the rebound number dataset should be recorded as the concrete's official *RH* [490]. The method is field deployable, portable, inexpensive, and well suited to mapping damage zones over large areas [1], [489]. However, the results are sensitive to surface condition and test setup, and, further, the accuracy depends on appropriate calibration to the specific concrete [489], [491].

Ultrasonic Pulse Velocity

UPV is a nondestructive test that transmits a high-frequency stress wave through concrete and computes its velocity from the measured travel time between a transmitter and a receiver [1], [492], [493], [494]. In a homogeneous medium, this velocity is a function of the material's elastic modulus (E), Poisson's ratio (ν), and density (ρ) [1], [492], [493], [494]. This relationship is expressed in equation 3. Longer transit times between transducers indicate potential loss of soundness from cracking, voids, delamination, or other discontinuities [493]. Because the UPV relies on elastic modulus and density, measurements can be correlated to the compressive strength of concrete; however, such correlations are specific to the concrete mix [493].

$$V_p = \sqrt{\frac{E(1-\nu)}{\rho(1+\nu)(1-2\nu)}} \qquad \text{Equation 3}$$

UPV can be used to map fire-affected zones of damage in concrete bridge members by conducting a grid survey [1], [493]. The instrument may be deployed in three configurations:

direct, semi-direct, and indirect (see figure 17) [493]. The deployment selection should be based on access. Direct transmission provides the highest sensitivity and should be the method used whenever feasible. Indirect measurements should be reserved for cases with single-face access.

UPV enables rapid screening and localization of damage, especially cracking, and delamination [493], [494]. UPV can even be deployed under constrained field conditions. Notably, UPV can be used to enhance the work of other NDT devices. For example, it can complement RH results to strengthen screening conclusions [1], [495]. However, uncalibrated strength correlations can be biased. Relationships between UPV and compressive strength are not universal and must be established for specific concrete mix designs [493]. Results are also sensitive to multiple variables, including moisture, surface irregularities, and internal reinforcement. Table 5 provides typical concrete quality based on UPV readings.

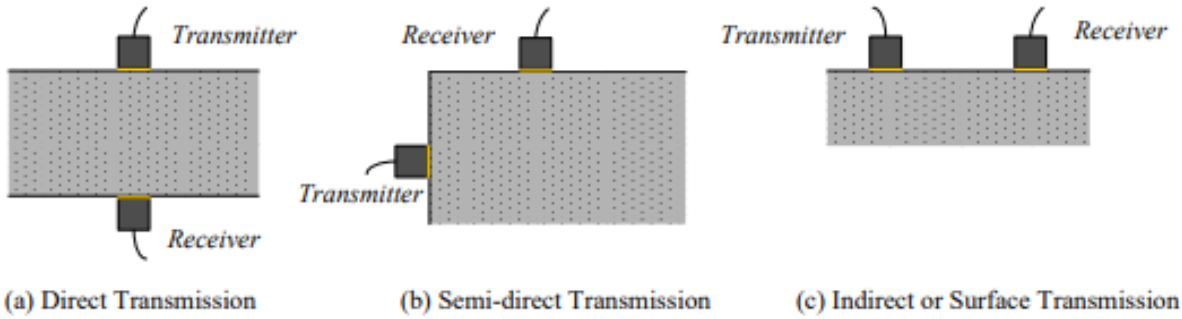

Figure 17. Diagrams. Possible transducer arrangements [489].

Table 5. General UPV ranges for concrete condition [489].

Pulse Velocity (ft/s)	Concrete Quality
>15,000	Excellent
12,000–14,999	Good, minor porosity may exist
10,000–11,999	Satisfactory, possible loss of integrity
7,000–9,999	Generally poor, likely significant defects
<7,000	Very poor

Ground Penetrating Radar

GPR is a widely used NDT method to assess concrete degradation. GPR works by transmitting radiofrequency pulses into concrete and analyzing the arrival time and amplitude of reflected signals [1], [496]. Variations in the reflection signal can indicate cracks, voids, and corrosion. Studies show an agreement between GPR results and traditional inspection and testing methods [1], [497]. Further, laboratory work has shown GPR's ability to detect grout voids in posttensioning systems, although real-world research is limited [1]. Operationally, GPR enables rapid data collection and can be deployed manually or on a vehicle [1]. Notably, the use of GPR, due to its size and mode of testing, could require traffic control to ensure safe and consistent operation [1]. For GPR to transmit a clear signal, the material being tested must be uniform and dry [1]; the performance of the device may be limited in wet or saturated areas because this condition reduces signal penetration [1]. Highly reinforced or heterogeneous sections can produce overlapping reflections, which can make an inherently subjective interpretation challenging [1]. This challenge to interpretation requires technicians to be properly trained in its use.

Impact Echo

IEs evaluate concrete by imparting a short, mechanical tap and recording the acoustic response with a transducer and data acquisition system (DAQ) (see figure 18) [1], [498], [499]. The signal is transformed into a frequency domain, which is then related to the thickness of the concrete. Deviations from the expected thickness indicate potential internal flaws [1], [498], [499]. When performed in a dense grid pattern, the data can be processed into three-dimensional (3D) representations of bridge decks [1], [497]. These 3D representations offer insights into the subsurface condition of concrete structures. However, comprehensive IE surveys require

numerous test points and often traffic control [1]. Interpretation relies on specialized software and highly trained personnel [1]. These factors limit the suitability of IE for rapid post-fire triage of a bridge structure.

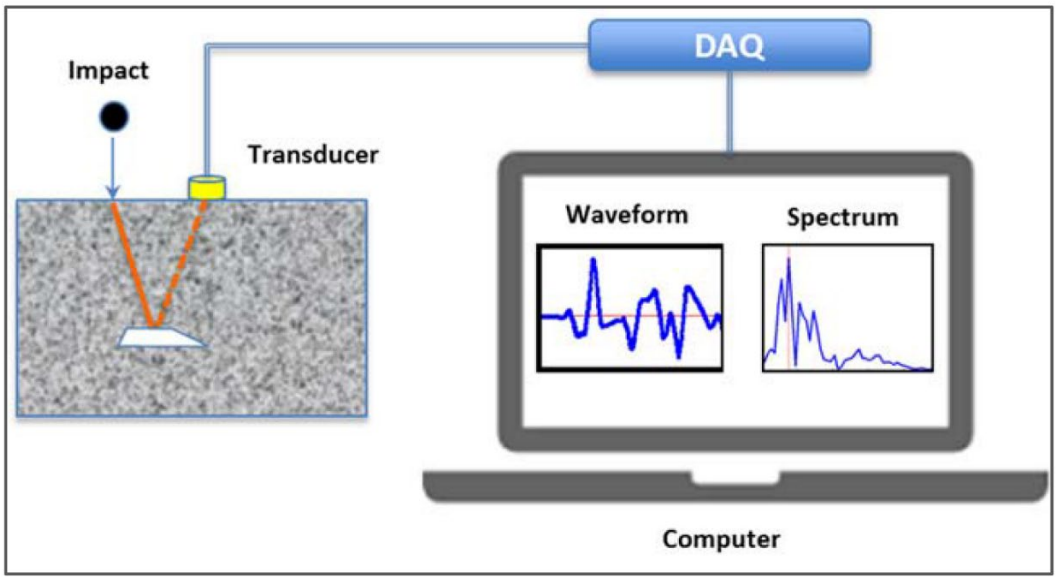

Figure 18. Schematic. Impact echo schematic [494].

CHAPTER 7. METHODS

This chapter describes the experimental procedures, materials, equipment, and analysis methods used to evaluate residual compressive strength of fire-damaged concrete in the laboratory. The purpose of this laboratory testing is to explore a practical way to develop a universal model for predicting residual concrete compressive strength following a fire. Existing models for RH and UPV are highly dependent on specific concrete design calibration and test conditions. Rather than attempting to predict absolute compressive strength for a given concrete, this study focuses on estimating the percentage of remaining compressive strength relative to the undamaged condition. This approach assumes that while individual concretes may vary when estimating specific compressive strengths, concrete as a class of construction material exhibits broadly similar trends in strength loss when subjected to elevated temperatures.

PROCEDURES

This section provides a concise narrative of the procedures followed to generate and evaluate post-fire indicators on concrete samples. The methods used in this research align with established testing standards and are adapted only where necessary. Emphasis is placed on consistent test conditions, traceable sample identification, and basic quality assurance practices to support reliable results. The following sections present the procedures in the order performed, noting any project-specific modifications to established testing standards.

General Procedures

The study began with a targeted literature review. The review covered the topics of the history of bridge fires in the United States, common trends among bridge fires, a review of how

steel and concrete react during a fire, and common inspection techniques for steel and concrete after a fire. Based on the review of available literature, the authors identified that RH and UPV are the best choices for primary, field-deployable NDTs for concrete. The test method proposed for RH is a modified version of American Society for Testing and Materials (ASTM) C805, as described in Modified ASTM C805. The test method for UPV is ASTM C597.

Concrete was then batched and cast into 4 × 8-inch cylinders for use as laboratory samples (see Materials and Samples for batching details). All cylinders were labeled according to batch and sample numbers for traceability. These samples were cured for a minimum of 28 days. Total cure time for any one sample was variable beyond the minimum cure duration based on when the test was conducted. Within each batch, samples were designated as a control sample or a test sample. The samples were maintained under consistent identification protocols to support pairing and later comparison.

Using the RH and UPV devices, pre-burn measurements were obtained and recorded on the control samples. Then, a compressive strength test was performed according to ASTM C39. The results of the compression test were recorded to establish reference properties of the concrete batches.

For the test samples, the *RH* and *UPV* were collected and documented prior to heating. Thermal exposure was then applied to the test samples using a prescribed temperature–time matrix that covered the representative bridge fire severities. Tests were conducted at 400°C for 30 and 60 min; 600°C for 30, 60, and 120 min; 800°C for 30 and 60 min; and 1,000°C for 30 min. Due to the significant degradation of the concrete following 1,000°C for 30 min, the researchers opted to not conduct further 60-min tests. The purpose of these tests was to simulate a fire at a bridge structure; therefore, ramp rate was set to the maximum achievable rate. After

heating, the samples were allowed to cool to ambient conditions before any further handling or testing.

Post-burn measurements were obtained using the RH and UPV devices on all test samples. Additionally, a maximum crack width measurement was obtained using a standard crack gauge card. Then, a compressive strength test was performed according to ASTM C39. The results of the compressive test were recorded and compared to the compressive strength of the batch control. For each specimen, the team quantified the percentage of change in the NDT indicators using the methods described in Variables and Analysis Methods.

Modified ASTM C805

The RH layout followed the pattern shown in figure 19. Eight impact locations were marked at equal angular spacing on a circle approximately at the mid-radius of the 4-inch cylinder face. Two additional locations placed symmetrically around the center were also tested. Each marked point received a single impact, and the *RH* was recorded and averaged. Data quality was screened by a deviation criterion. No individual reading was permitted to differ from the mean by more than six rebound numbers. If the limit was exceeded, additional impacts were taken and the mean recomputed until all readings satisfied the criterion. For each sample, the final mean rebound number was documented.

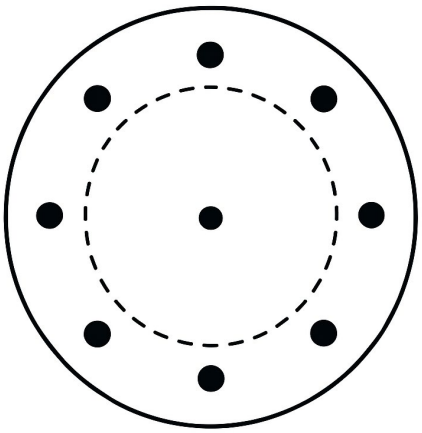

Figure 19. Diagram. Rebound hammer test pattern.

MATERIALS AND SAMPLES

Cylindrical concrete samples measuring 4 × 8 inches were fabricated in accordance with ASTM C31. To create the concrete, a 50-lb bag of Quikrete® 5000 premixed concrete was mechanically mixed with water. No additional admixtures were added to the concrete. Four batches were produced. Batch 1 used 2 bags of dry concrete with 4.0 L total water and yielded 11 samples. Batch 2 used 1 bag of dry concrete with 2.0 L of water and yielded 5 samples. Batch 3 used 1 bag of concrete mix combined with 2.0 L of water and the excess concrete from batch 2 to produce 7 samples. Batch 4 used 1 bag of concrete mix with 2.0 L of water and yielded 6 samples. In total, 29 samples were cast.

Immediately after casting, cylinders were capped and identified by batch and sample number. These samples were cured for a minimum of 28 days, as described in General Procedures.

EQUIPMENT

The following equipment was used to fabricate, condition, and test the concrete samples: 4 × 8-inch cylinder molds with caps, tamping rod, measuring tape, rubber mallet, straightedge or

float, and electric concrete mixer. A graduated 1 L cylinder was used to verify mix water. Pre- and post-thermal exposure condition indicators were obtained using a standard bridge inspection crack gauge, RH, and UPV. Thermal exposures were applied in a laboratory using an electric furnace with controlled temperature–time settings. Compressive strength testing was performed using a calibrated hydraulic press.

VARIABLES AND ANALYSIS METHODS

This section defines the procedures used to convert raw measurements into analysis-ready indicators.

Rebound Hammer Testing

This study tracked five variables related to RH testing and post-fire condition. The RH reading (*RH*) is a dimensionless index of near-surface hardness. Compressive strength ($f'c$) was measured by destructive testing of the concrete cylinders. Post-heating changes were expressed as a percentage of change in the rebound index (*%RH*) and percentage of residual compressive strength ($\%f'c$). Finally, surface temperatures ($T_{surface}$) were recorded following thermal exposure to relate measured damage indicators to heating severity.

Equation 4 can be used to calculate *%RH*. RH_{pre} and RH_{post} are the *RH* values found before and after heat exposure, respectively. Equation 5 can be used to calculate $\%f'c$.

$$\%RH = \frac{\left|RH_{post} - RH_{pre}\right|}{RH_{pre}} \times 100 \qquad \text{Equation 4}$$

$$\%f'c = \frac{f'c_{post}}{f'c_{control}} \times 100$$ Equation 5

To create an *RH* to *f'c* calibration curve, a linear regression on the two variables was conducted. The researchers treated *RH* as the independent variable and *f'c* as the dependent variable to develop an empirical relationship for estimating concrete compressive strength from the RH readings.

The second analysis compared *%RH* to *%f'c* by conducting polynomial regression. For this analysis, *%RH* served as the independent variable and *%f'c* as the dependent variable. This analysis allowed the researchers to quantify how changes in rebound response correlate to the remaining compressive strength of the heated samples.

The third analysis conducted for the RH compared *%RH* to $T_{surface}$ at temperatures in excess of 500°C. A logarithmic regression related *%RH*, the independent variable, to surface $T_{surface}$, the dependent variable. This analysis allows researchers to estimate the maximum surface temperatures of concrete samples after cooling to ambient temperature.

Each analysis supports a practical estimation task: (1) predict compressive strength from *RH*; (2) predict residual compressive strength from *%RH*; and (3) estimate peak surface temperatures from *%RH* after cooling.

Ultrasonic Pulse Velocity Testing

This study tracked four variables for UPV testing. The ultrasonic pulse velocity (*UPV*) quantifies the travel speed of the high-frequency stress wave through concrete in feet per second (ft/s). Similar to RH testing (see Rebound Hammer Testing), the compressive strength of concrete (*f'c*) was obtained using destructive testing. Post-heating changes were normalized as a

percentage of change in *UPV* (*%UPV*) to facilitate a comparison across samples and exposures. Equation 6 can be used to calculate *%UPV,* where UPV_{pre} and UPV_{post} are the *UPV* results obtained before and after heating, respectively. The percentage of residual compressive strength (*%f'c*) was used to express retained capacity relative to the corresponding batch control (see equation 5).

$$\%UPV = \frac{\left|UPV_{post} - UPV_{pre}\right|}{UPV_{pre}} \times 100 \qquad \text{Equation 6}$$

The first analysis conducted was to compare *UPV* to *f'c*. *UPV* was treated as the independent variable, and *f'c* was considered the dependent variable. A polynomial regression was conducted to develop the relationship between independent and dependent variables. The purpose of this analysis was to estimate compressive strength from the UT readings.

A second polynomial regression was conducted to compare *%UPV* and *%f'c*. For this regression, *%UPV* was treated as the independent variable and *%f'c* was considered the dependent variable. This analysis allows researchers and investigators to estimate the residual compressive strength from *%UPV*.

Crack Width

For the maximum crack-width analysis, two variables were evaluated. The first variable is maximum crack width ($w_{c,max}$) attributable to elevated temperature. This variable was measured in millimeters using a standard crack gauge. Finally, similar to the previous section (see Ultrasonic Pulse Velocity Testing), the percentage of residual compressive strength (*%f'c*) was computed according to equation 5.

A single exponential regression was conducted to determine the relationship between the maximum crack width caused by elevated temperatures and *%f'c*. This relationship allows investigators to estimate the residual compressive strength post-burn from the visible and measurable heat-related defects.

Multifactor Linear Regression Analysis

In addition to the single-factor regressions, the study developed two multivariable ordinary least squares (OLS) models. The two-factor model uses the percentage of change in *RH* as calculated in equation 4 and the percentage of change in the *UPV* as calculated in equation 6 as independent variables. The three-factor model augments these independent variables by including the maximum crack width attributed to elevated temperatures ($w_{c,max}$). For both models, the percentage of residual compressive strength, as calculated in equation 5, is the dependent variable.

The models explained in the following subsections enable an estimation of the percentage of residual compressive strength using changes in (1) surface hardness and interior condition or (2) including visible indicators to augment the changes detailed above.

Two-Factor Model

A linear regression analysis was conducted with *%RH* and *%UPV* as the independent variables and *%f'c* as the dependent variable. The purpose of this model is to estimate the residual compressive strength from combined changes in surface hardness and interior condition. The model will take the form of equation 7:

$$\%f'c = \beta_0 + \beta_1 \%RH + \beta_2 \%UPV \quad \text{Equation 7}$$

Where β_0, β_1, and β_2 are the *y*-intercept, coefficient for *%RH*, and the coefficient for *%UPV*, respectively.

Three-Factor Model

An expanded linear regression added $w_{c,max}$ as a third independent variable, measuring cracking in conjunction with surface hardness and interior condition. The updated model will take the form of equation 8:

$$\%f'c = \beta_0 + \beta_1 \%RH + \beta_2 \%UPV + \beta_3 w_{c,max} \quad \text{Equation 8}$$

Where β_3 is the coefficient for $w_{c,max}$.

CHAPTER 8. TESTING RESULTS AND DISCUSSION

This chapter presents the results of the concrete burn experiment introduced in chapter 7. The testing criteria and the raw data from each sample, along with the derived results, are presented. A summary of the analytical findings and the models consistent with the analyses concludes the chapter.

TESTING CRITERIA AND RAW DATA

Table 6 presents the thermal-exposure matrix for each of the concrete cylinder samples. Each row lists the batch number and sample number and the associated planned furnace temperature and duration of the burn for each sample. Note that samples 1-7, 2-5, 3-6, and 3-7 served as control samples and were not heated. The temperatures for the heat exposure included 400°C, 600°C, 800°C, and 1,000°C. The maximum heat exposure times are 30, 60, and 120 min. These results cover: (1) 400°C at 30- and 60-min durations, (2) 600°C at 30-, 60-, and 120-min durations, (3) 800°C at 30- and 60-min durations, and (4) 1,000°C at 30-min duration.

Table 7 reports the raw data from each sample. The table is organized by batch number and sample number. For every concrete cylinder sample, the pre-burn readings are presented. Prior to burning, the dimensionless RH_{pre} and UPV_{pre}, in feet per second, were recorded. After thermal exposure, the samples were remeasured for RH_{post} and UPV_{post}. Additionally, $w_{c,max}$ was recorded in millimeters. Cracking was not observed on any samples prior to thermal exposure.

Table 7 provides the complete set of inputs needed for subsequent analysis. Subsequent sections will delve deeper into direct comparisons between pre-burn and post-burn *RH* and *UPV* and $\%f'c$. Additionally, the recorded $w_{c,max}$ will help provide a correlation with $f'c$. These data points provide the basis for calculating the percentage of change and regression analyses.

Table 6. Concrete sample testing criteria.

Batch Number	Sample Number	Temperature (°C)	Time (min)
1	1	400	30
1	2	600	30
1	3	400	30
1	4	1,000	30
1	5	800	30
1	6	400	30
1	7	Control	
1	8	400	60
1	10	800	30
1	11	1,000	30
2	1	800	60
2	2	800	60
2	5	Control	
3	1	800	30
3	2	600	60
3	3	600	30
3	4	600	120
3	5	800	30
3	6	Control	
3	7	Control	

Table 7. Raw test results.

Batch Number	Sample Number	Pre-Burn Testing		Post-Burn Testing			
		RH Value	*UPV* (ft/s)	*RH* Value	*UPV* (ft/s)	Max Crack Width (mm)	Compressive Strength (psi)
1	1	22.0	13,660	27.4	10,972	0.025	3,760
1	2	22.9	13,509	19.9	6,850	0.100	3,620
1	3	22.6	13,668	29.0	10,847	0.025	3,710
1	4	20.7	13,732	0	0	0.450	410
1	5	24.0	13,033	16.6	1,719	0.150	1,910
1	6	25.3	13,502	26.5	10,310	0.025	4,200
1	7	23.5	14,313				4,530
1	8	23.3	13,810	29	10,137	0.025	4,220
1	10	22.6	13,732	12.7	0	0.300	990
1	11	27.1	12,808	0	0	0.450	360
2	1	24.3	13,818	16	1,129	0.250	1,400
2	2	27.5	13,482	13	1,586	0.150	1,080
2	5	25.9	13,676				4310
3	1	24.3	13,818				
3	2	25.2	13,676	19.3	2718	0.100	2540
3	3	22.1	13,537	17.9	7039	0.050	3450
3	4	35.7	13,347	21.1	3729	0.200	1830
3	5	20.2	13,761				
3	6	26.3	13,557				5470
3	7	21.8	13,704				3630

Note: Shading indicates that information could not be obtained..

A few items of interest should be pointed out from these tables. Initial review of the 400°C exposures shows an increase in the post-burn RH values when compared to the pre-burn values. This indicates surface hardening during heating. However, these samples also exhibit reductions in *UPV* and *f'c* following heating, which demonstrate a loss of internal integrity despite higher surface rebound numbers.

The 400°C burns show a divergence from the other burns and should underscore a key caution when inspecting a structure following a thermal event. An increased RH reading does not imply increased, or even preserved, compressive strength. RH is a measure of near-surface hardness, whereas UPV and compression testing capture internal condition and load bearing capacity, respectively.

Batch 3 exhibited anomalous behavior. Samples 3-1 and 3-5 were scheduled for 30 min at 800°C. However, they failed explosively as the furnace was ramping up to burn temperature. Sample 3-1 exploded when the oven was 686°C, and sample 3-5 exploded at 662°C. Such behavior is consistent with explosive spalling caused by extreme thermal events. Given the relatively small size of the samples, the failure manifested in complete fragmentation rather than localized spalling.

Literature indicates that spalling may initiate as surface temperatures reach 450°C and spall-front temperatures reach approximately 150°C [462]. The results of these failed tests highlight a practical implication for post-fire assessments. Visible evidence of explosive spalling should be noted in any inspection report and photographed. Further, the presence of explosive spalling should be treated as a potential indicator of concrete temperatures.

Both batch 3 control samples exhibited atypical compressive strengths. Sample 3-6 broke at 5,470 psi, which is significantly higher than the control sample from batches 1 and 2. Sample 3-7 broke at 3,630 psi, significantly lower than the control samples from the other batches. Both samples 3-6 and 3-7 were prepared, cured, and tested in accordance with ASTM procedure and did not exhibit any signs of defect. To normalize batch 3 results, the arithmetic mean of 4,550 psi was adopted as the batch control strength. This was done due to the lack of evidence necessary to exclude the individual results. For batch 3, researchers used 4,550 psi as $f'c_{control}$ to calculate $\%f'c$

for samples 3-2, 3-3, and 3-4; however, samples 3-6 and 3-7 will be shown with a *%f'c* of 100. This was to ensure that the test samples had a consistent batch-specific baseline while acknowledging within-batch variability.

CALCULATED RESULTS

Table 8 provides the calculated indicators used to perform regression analyses. The data are sorted by batch and sample. Column 3 presents *%RH* that was calculated using equation 4. Column 4 presents *%UPV* as calculated using equation 6. Finally, column 5 represents *%f'c*, as calculated using equation 5. The table shows a wide range of degradation. More modest degradation for samples burned at lower temperatures to near total loss of compressive strength for those samples burned at 1,000°C.

Figure 20 summarizes the residual compressive strength of the concrete samples after heating according to the testing matrix found in table 6. There is a general monotonic downward trend of compressive strength with increasing temperatures and/or durations. The average *%f'c* of concrete heated at 400°C was 87.7 percent. For the 600°C burns, the average *%f'c* drops to 62.9 percent. The average *%f'c* for the 800°C burns was 30.4 percent. Average *%f'c* is less than 10 percent for the 1,000°C burns. The steep decline beyond 400°C points to the increasing severity of internal damage at higher temperatures. This information is presented in table 9.

Table 8. Calculated results from burn tests.

Batch Number	Sample Number	*%RH*	*%UPV*	*%f'c*
1	1	24.5	19.7	83.0
1	2	13.1	49.3	79.9
1	3	28.3	20.6	81.9
1	4	100	100	9.1
1	5	30.8	86.8	42.2
1	6	4.7	23.6	92.7
1	7	0.00	0.00	100
1	8	24.5	26.6	93.2
1	10	43.8	100	21.9
1	11	100	100	7.9
2	1	34.2	91.8	32.5
2	2	52.7	88.2	25.1
2	5	0.00	0.00	100
3	2	23.4	80.1	55.8
3	3	19.0	48.0	75.8
3	4	17.9	72.1	40.2

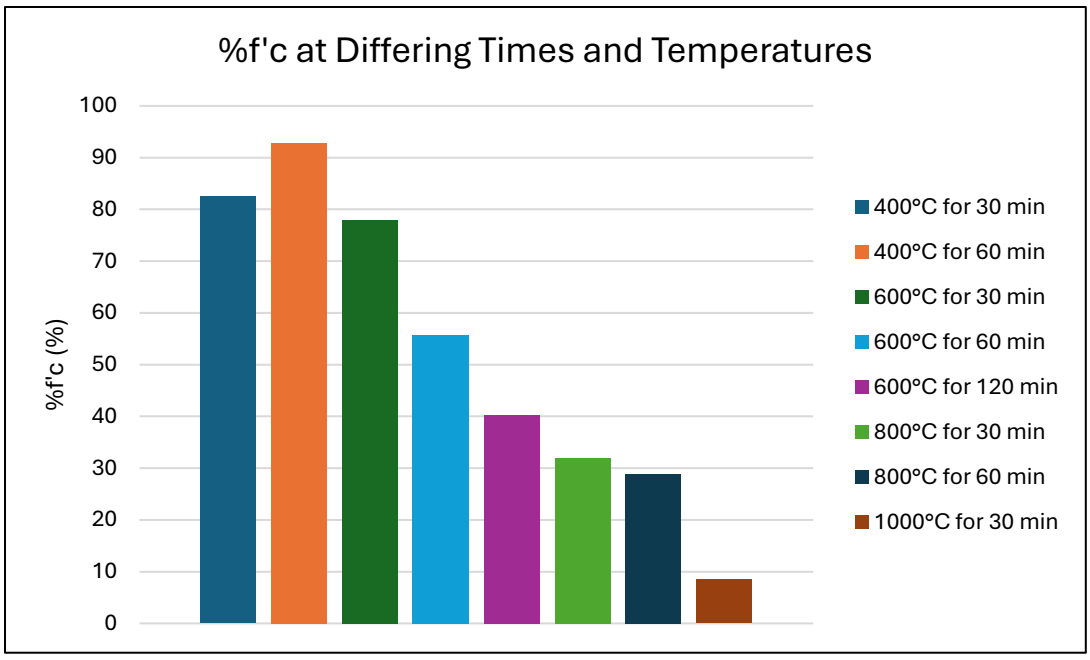

Figure 20. Chart. *%f'c* at differing temperatures and times.

There is an irregularity in the 400°C burns that lasted for 60 min, where the testing shows an increase in the residual capacity for the longer duration burn. This difference is viewed by the research team as variability within the experiment rather than an indication that increasing burn times at lower temperatures can improve the residual compressive strength. Rather, when viewing the overall picture, figure 20 indicates that temperature dominates over time in driving strength loss.

The measured residual strengths at the various temperatures fall outside of the ranges found in the literature (see table 9). This departure is not unexpected given differences in test configurations. The current work used 4 × 8-inch cylinders made from Quikrete 5000 and compression tested according to ASTM standards. Burns were conducted in an electric furnace to simulate damage caused to concrete bridge structures due to elevated temperatures. Further, the researchers limited their burn times to no more than 120 min, and all samples were allowed to cool to room temperature. Residual strength was normalized to batch-specific controls. Variations in concrete mix type, sample geometry, heating rates, peak-temperature uniformity, and post-burn handling can materially shift residual-strength outcomes [500], [501], [502], [503]. These facts can make cross-study comparisons challenging. Additionally, the explosive spalling observed in batch 3 demonstrates that nonuniform thermal damage may not be accounted for in the results reported by other researchers. Given these factors and the smaller sample size of this study, these results are generally consistent with what is reported in the literature. Further testing with different mixes would provide further validity.

Table 9. Experimental results versus literature.

Temperature (°C)	Results (%)	Literature (%)
400	87.7	50–80
600	62.9	30–50
800	30.4	10–30
1,000	10	<10

REBOUND HAMMER ONE-FACTOR REGRESSION

The first NDT method selected for this study was the RH. The RH provides a rapid and cost-effective means of assessing concrete surfaces. Because of its small size, the hammer is portable and can be carried into the field by bridge inspectors, maintenance personnel, or engineers. The device is easy to operate and enables large-scale screenings. These large screenings help to quickly identify areas of concrete that warrant closer evaluation. Although the RH has its limitations, the method offers a reliable, repeatable indicator that supports timely, defensible decision-making following a fire event.

Compressive Strength Calibration of Rebound Hammer

The first test analysis verified that the RH can reliably be used to estimate compressive strength. Figure 21 shows the relationship between *RH* and compressive strength for the test cylinders. Equation 9 is the numerical model that shows the relationship between the two variables. Both figure 21 and equation 9 show that each 1-unit increase in *RH* corresponds to roughly a 150-psi increase in compressive strength. The coefficient of determination suggests the model explains about 95 percent of the variance in strength. This would indicate a strong, approximately linear association between RH values and concrete compressive strength.

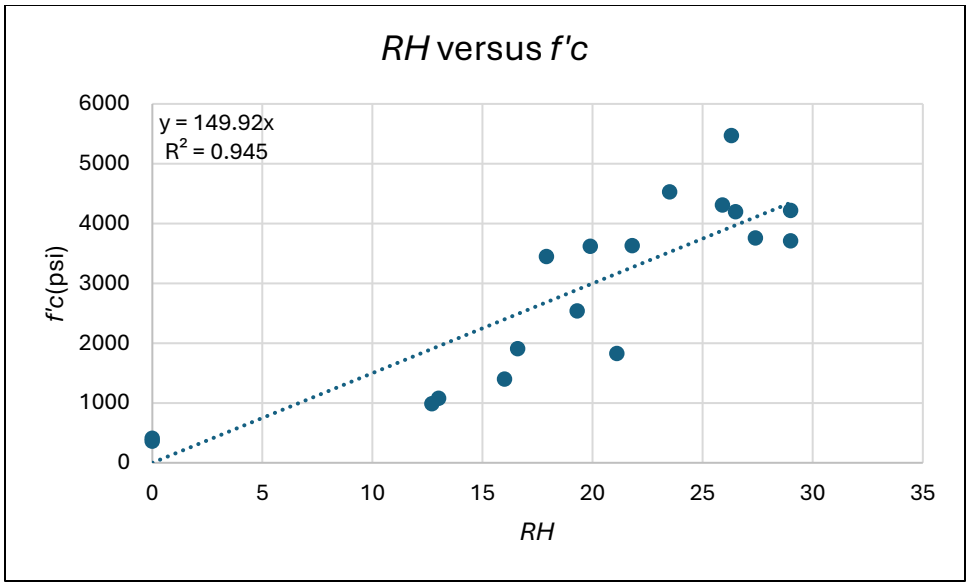

Figure 21. Graph. *RH* versus *f'c*.

$$f'c = 149.92RH \qquad \text{Equation 9}$$

This calibration provides a practical basis for estimating strength from *RH* during screening. However, there are some limitations. First, *RH* reflects the near-surface condition. Therefore, any estimates should be corroborated where interior damage may also be a possibility. Second, RH calibration curves are highly mix dependent. Water content, aggregate type, cement type, and admixtures can affect RH readings [504], [505], [506]. Finally, the RH can be influenced by the form and surface of the concrete being examined. Surface texture, shape, and size can all influence the results of the test [504], [507], [508].

Model to Estimate Residual Compressive Strength

Given the limitations noted above, this report adopts an alternative to predicting absolute compressive strength. Instead, this study hypothesizes that percent change in RH readings can serve as a practical indicator of the residual compressive capacity of concrete following a fire. In

laboratory settings for this study, RH measurements were obtained before and after thermal exposure to compute *%RH*. In field applications, this concept can be implemented by comparing RH values from fire-damaged concrete to adjacent or nearby, similar undamaged concrete to establish a local baseline. This approach prioritizes relative change over absolute strength, supporting timely screening and decision-making during post-fire assessments.

Figure 22 shows the relationship between *%RH* and *%f'c*, and it is expressed numerically in equation 10. This relationship shows a decreasing, nonlinear trend. Small changes in *RH* generally correspond to high remaining capacity. However, larger changes are associated with notable losses in concrete compressive strength. The curve flattens at high *%RH*, indicating extremely diminished residual capacity as the damage becomes severe.

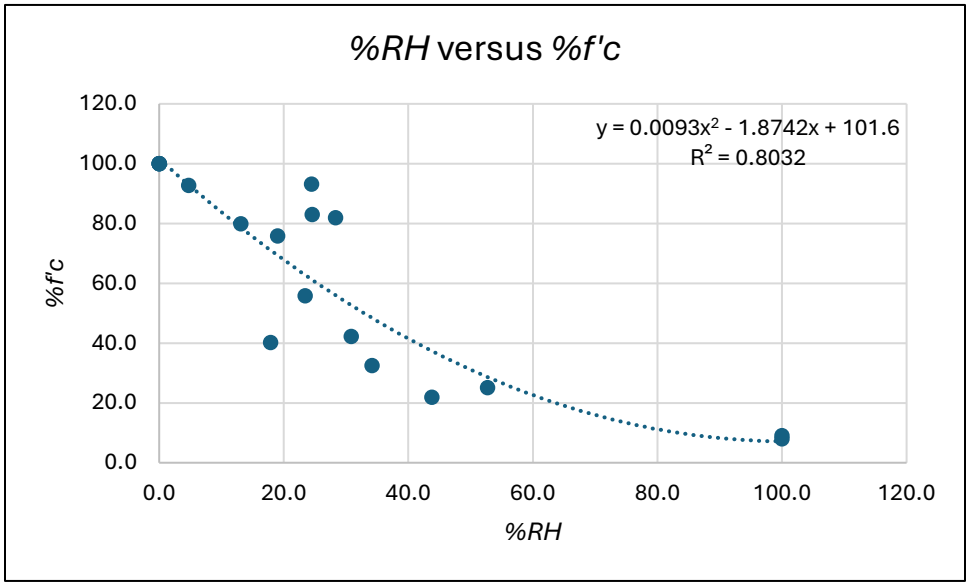

Figure 22. Graph. *%RH* versus *%f'c*.

$$\%f'c = 0.0093\%RH^2 - 1.87\%RH + 101.6 \qquad \text{Equation 10}$$

This model relating *%RH* and *%f'c* explains approximately 80 percent of the variance in residual strength for this dataset. This level of fit supports the model's use for screening, but it is not sufficient as a stand-alone basis for decision-making. Notably, the coefficient of determination increased as more samples were tested. Further testing may validate a stronger relationship between these variables.

Several factors likely contribute to the unexplained variability. First, the 400°C burns displayed atypical behavior, introducing nonuniform thermal-damage effects that the single variable model does not capture. Second, the RH exhibits a lower measurement bound, creating a floor effect. The smallest reliable reading was 10. For severely damaged concrete surfaces, the researchers could not obtain valid readings. In these cases, a reading of 0 was recorded. This floor effect reduces sensitivity at high damage levels and biases the fit. Given these limitations, RH readings should be corroborated with other NDT methods. These multivariate models, which incorporate differing NDTs into a single model, are presented in subsequent sections.

Estimating Surface Temperature Using Rebound Hammer Readings

Estimating concrete surface temperatures following thermal events is a frequent need in post-fire inspection and maintenance strategies. After cooling, the RH can provide an indirect indicator of surface temperature by measuring the surface hardness of the concrete [488]. This measurement is limited to the approximate upper 15 mm of concrete. Elevated temperatures reduce this hardness; therefore, lower rebound numbers after cooling generally correspond to higher surface temperatures during the thermal event [509], [510]. To use raw RH readings for temperature inference requires calibration to relate RH to known temperature histories for specific concrete mixes [509], [510].

Given variability in mix design, finish, absorbed water, carbonation, and fire exposure, a relative approach is more robust for field screening. Following the method described in Estimating Surface Temperature Using Rebound Hammer Readings to determine *%RH*, inspectors can begin to develop a curve to estimate the surface temperatures after cooling. This method can reduce mix design bias and offer a more universal indicator of surface temperatures.

Figure 23 shows the relationship between the percent change in RH readings compared to concrete surface temperatures when cooled to ambient temperature. The logarithmic model, shown in equation 11, shows a monotonic increase. Larger changes in RH are associated with higher estimated temperatures. The curve's shape indicates diminishing sensitivity at higher *%RH*. The R^2 value suggests that the relationship captures most variability in the dataset. This lends support to *%RH* as a screening proxy for temperature levels.

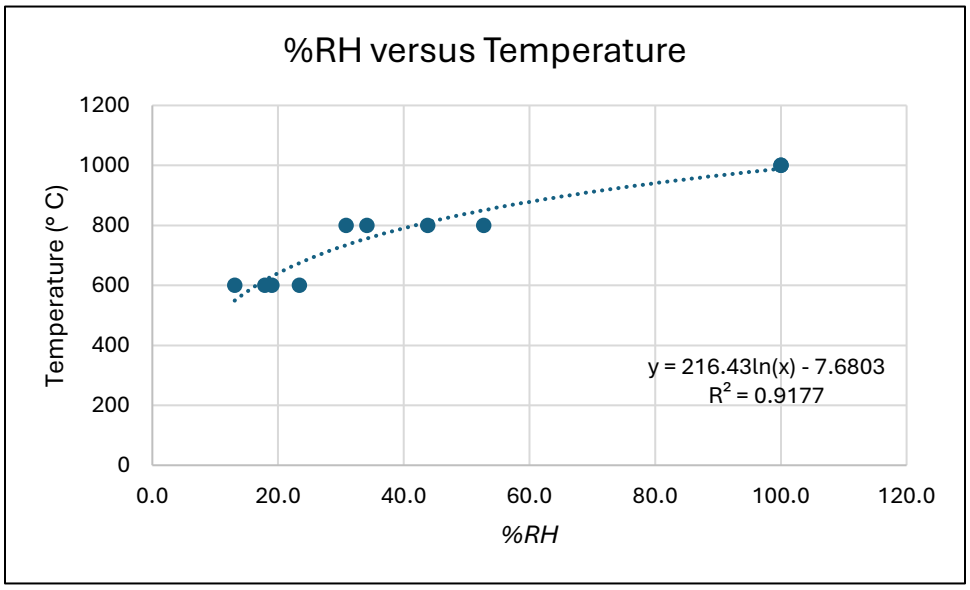

Figure 23. Graph. *%RH* versus temperature.

$$T_{surface} = 216.43 \ln(\%RH) - 7.68 \qquad \text{Equation 11}$$

The model present in equation 11 assumes a decrease in surface hardness with increasing temperatures. The 400°C burns exhibited the opposite trend. Because these tests violate the model's governing assumption and introduce bias into the relationship, the results from these tests are excluded from the calibration. Accordingly, the model is limited to estimating temperatures greater than 500°C or where *%RH* shows a decrease. Results should not be extrapolated to lower-temperature exposures. At these lower temperatures, different mechanisms dominate. Future research is required to further develop this model such that it will be able to incorporate lower temperatures.

ULTRASONIC PULSE VELOCITY ONE-FACTOR REGRESSION

UPV was selected as the other NDT method for this research. Like the RH, UPV provides a rapid and cost-effective means of assessing concrete condition in the field [511], [512], [513]. The equipment is portable and easy to use with straightforward instructions. Whereas the RH is only capable of testing the surface of concrete, UPV can probe deeper by examining internal inconsistencies [512], [513], [514]. It can detect cracking, delamination, and loss of concrete quality along the ultrasonic pulses [515]. When properly calibrated and applied systematically, UPV can estimate residual concrete strength [511], [514]. This allows inspectors and engineers to delineate zones of damage. These benefits provided by UPV support timely, defensible decisions after a thermal event [514].

Like the RH, the relationship between UPV and compressive strength is dependent upon mix design and condition. The velocity of the pulse traveling through the concrete is influenced by aggregate type, porosity, water content, and the presence of reinforcement [511], [513]. As a result, UPV alone cannot produce a universal strength estimate. UPV requires calibration specific to the mix design to develop the desired results.

Compressive Strength Calibration for Ultrasonic Pulse Velocity

Figure 24 plots the *UPV* against measured compressive strength for all cylinders. Equation 12 is the mathematical model of the polynomial trend line shown in figure 24. The curve shows a nonlinear, increasing relationship. As *UPV* increases, the estimated *f'c* also increases. The negative quadratic term produces a gentle plateau at higher velocities. This indicates that the model is most sensitive to low to mid-*UPV* range. This range is associated with deteriorated concrete.

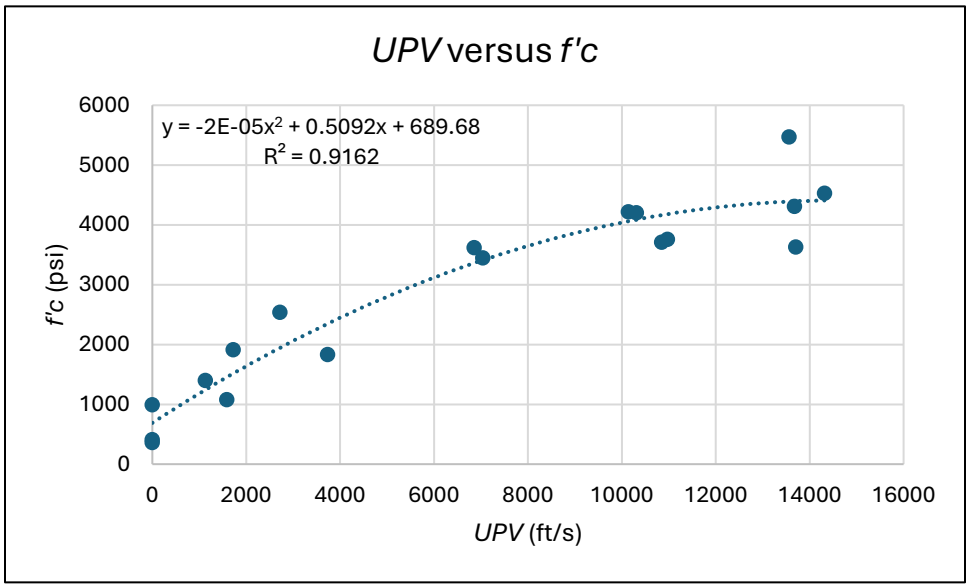

Figure 24. Graph. *UPV* versus *f'c*.

$$f'c = -2 \times 10^{-5}(UPV^2) + 0.51UPV + 689.68 \qquad \text{Equation 12}$$

The model has an R^2 value of approximately 0.92, meaning that the model explains most of the variance in the dataset. This high correlation indicates that the model is suitable for screening and preliminary strength estimations. This result has a known limitation in that the

relationship is only applicable to the test mix. This model should not be applied to other concrete mixes.

Model for Estimating Residual Compressive Strength

Given the limitations noted above, there is a need for a model that is less sensitive to mix-specific properties. This study hypothesizes that percent change in UPV readings can serve as a practical indicator of the residual capacity of fire-affected concrete. To evaluate this hypothesis, UPV measurements were taken pre- and post-burn. The change was computed per equation 6. For field application, this procedure can be implemented by comparing UPV values from fire-damaged concrete to nearby, similar undamaged concrete to establish a baseline. As with the RH approach, this method emphasizes relative changes over absolute strength. The purpose of this method is to improve robustness across varying concrete mix designs and site conditions. Furthermore, this method can support timely assessment and decision-making.

Figure 25 shows the relationship between *%UPV* and *%f'c*. This relationship is fitted with the quadratic model seen in equation 13. This model shows a strong, nonlinear decreasing trend. As *%UPV* increases, the remaining compressive strength decreases. Small UPV reading changes (0–20 percent) generally correspond to high residual compressive capacity (80–100 percent). On the opposite end of the model, large changes in *%UPV* (80–100 percent) align with a significantly reduced compressive strength (10–40 percent). The curve shows increasing sensitivity to higher *%UPV*, where strength declines quickly.

The coefficient of determination is shown to be approximately 0.96. This model explains most of the variability in the dataset, and the high correlation makes the model suitable for screening. Further testing is needed to determine whether this method can produce a universal model or it remains dependent on the mix design.

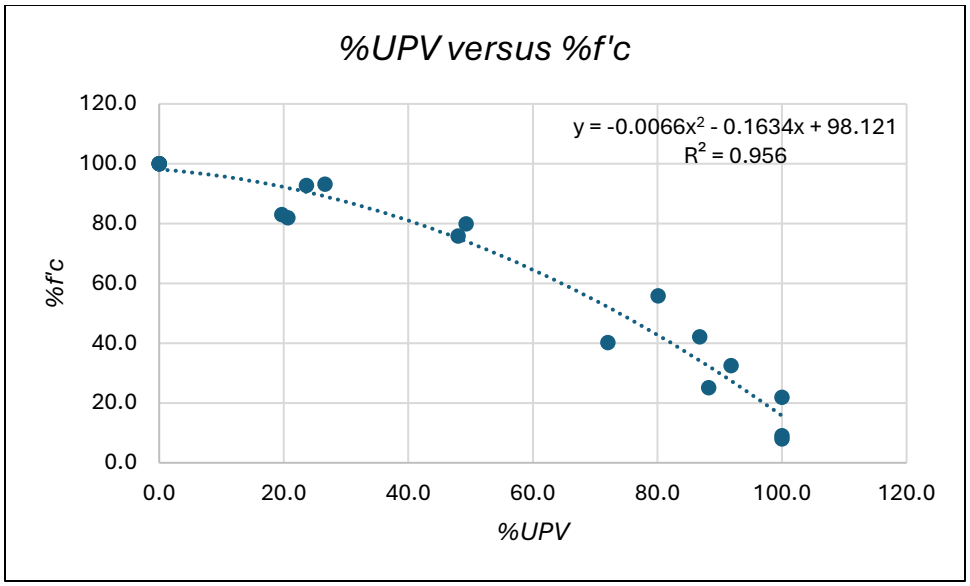

Figure 25. Graph. *%UPV* versus *%f'c*.

$$\%f'c = -0.0066(\%UPV^2) - 0.16\%UPV + 98.12 \qquad \text{Equation 13}$$

CRACK WIDTH ONE-FACTOR REGRESSION

During burn testing, the researchers documented fire-related distress for each heated specimen. Aside from the two explosive failures that fractured during ramp up, the predominant observations were cracking and minor discoloration. Notably, the maximum measured crack width showed an inverse relationship with residual compressive capacity. Wider cracks tended to coincide with lower remaining strength. This relationship (illustrated in figure 26) opens the possibility that crack width can be a practical screening indicator as engineers are making assessments of fire-damaged concrete.

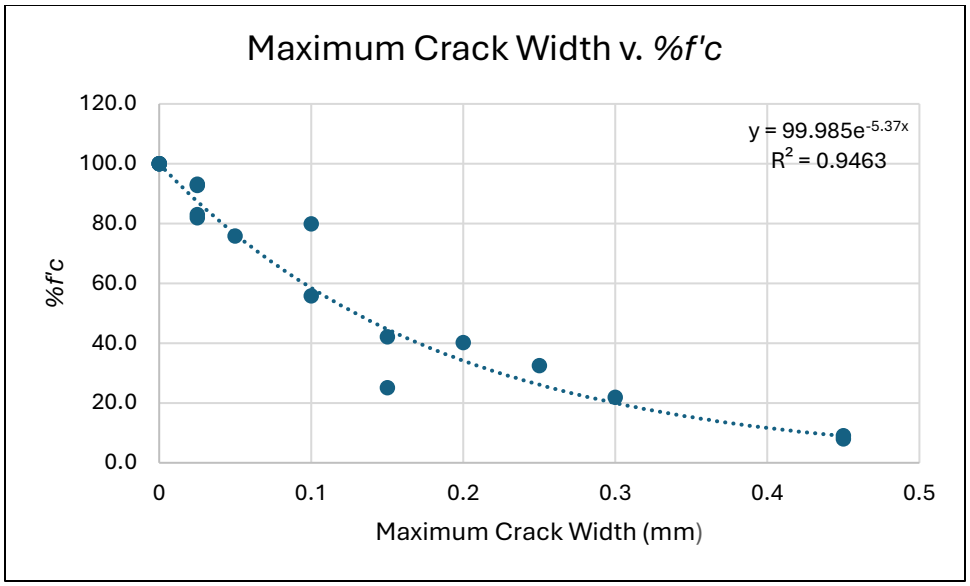

Figure 26. Graph. Maximum crack width versus *%f'c*.

$$\%f'c = 99.99e^{-5.37w_{c,max}}$$ Equation 14

Equation 14 is a fitted exponential decay model (see figure 26). This model shows a strong inverse relationship between the variables. As cracking width increases, the remaining compressive strength of the concrete decreases. Table 7 presents the observed crack width range (0–0.45 mm). Over this range, the compressive strength drops to approximately 10 percent for the widest cracks.

Despite the strong correlation observed in figure 26, the research team has reservations about using $w_{c,max}$ as a stand-alone predictor of residual compressive strength. The explosive failures of samples 3-1 and 3-5 would likely present as explosive spalling in the field. In small laboratory cylinders, visible surface cracking may dominate simply because it is one of the few damage modes available to scale. In full-scale members subjected to similar thermal demands, other defects, such as spalling, may present themselves. This change in defect presentation can

reduce the generality of a crack-width model. For these reasons, the crack-width model presented in equation 14 was not adopted as an independent assessment model.

Although maximum crack width alone may not reliably predict residual capacity, the observed relationship indicates that visible fire-related defects can carry diagnostic value. For this reason, maximum crack width will be retained as an explanatory variable within a multifactor regression analysis. Additional testing on larger samples, or full-scale representations of field components, could possibly be used to determine how visible defects relate to internal damage measures. This relationship could provide a robust model for estimating residual compressive strength.

MULTIFACTOR REGRESSION ANALYSES

This section presents the multifactor regression analyses performed on the given dataset. These regressions can be used to estimate the percentage of residual compressive strength for fire-damaged concrete using nondestructive indicators. Two OLS models were evaluated using specimens with complete datasets. The two-factor model treats the percent change in *RH* response and the percent change in *UPV* as independent variables. The three-factor model augments the two-factor model by including maximum crack width to incorporate visible damage. For both models, *%f'c* remains the dependent variable. These variables are defined in Multifactor Linear Regression Analysis.

Model development followed standard research practice. First, the coefficients were estimated by OLS. Then, the fit was summarized with the coefficient of determination, the adjusted coefficient of determination, and root mean square error. Basic diagnostics were performed to confirm model adequacy within the tested range. No interaction terms nor nonlinear transformations are included in the base specifications.

The linear specification was selected to maximize interpretability and auditability. Each coefficient represents a direct additive effect that can be readily traced and reviewed. Consistent with the field-oriented nature of the NDT methods, the models are portable and easy to implement. Inspectors with basic math skills can perform the calculations on a clipboard or Excel worksheet. This facilitates transparent application, rapid replication, and consistent documentation following fire events.

To use these models, *%f'c* should be adopted as a reduction factor for the design compressive strength of the concrete. For example, for load rating purposes, assume that the design compressive strength of the concrete member is 3,000 psi. If, following fire damage, *%f'c* is calculated at 80, the compressive strength of the concrete should be reduced to 2,400 psi, or 80 percent of the design compressive strength.

These models are not intended to be the sole criteria by which a bridge is assessed post-fire. They are intended to support screening and prioritization. Final determination regarding the health of a post-fire bridge structure will rely on engineering judgment informed by the whole body of evidence. Additional testing across varying concrete mix designs, geometries, and exposure conditions is required to confirm universality.

Two-Factor Linear Regression Analysis

As described previously, an OLS regression was used to estimate the percent residual compressive strength from the two NDT indicators (see Multifactor Linear Regression Analysis). Using the results from the 18 samples, a best fit model is presented in equation 15.

For field applications, the following information should be collected and calculated:

1. Obtain RH readings from similar, undamaged concrete and fire-damaged concrete and calculate *%RH* using equation 4.

2. Obtain UPV readings from similar, undamaged concrete and fire-damaged concrete and calculate *%UPV* using equation 6.
3. Using the information in steps 1 and 2, calculate the predicted *%f'c* using Equation 15.

$$\%f'c = 104.73 - 0.332\%RH - 0.631\%UPV \quad \text{Equation 15}$$

Uncertainty should be interpreted using the model's standard error as seen in table 10. As a practical rule, it can be interpreted that approximately 70 percent of comparable future observations can be expected to fall within ±8 percent of the calculated *%f'c*. For approximately 95 percent coverage, use a prediction interval of ±16 percent of the calculated value.

Table 10. Two-factor regression statistics.

Metric	Value
Multiple *R*	0.98
R^2	0.96
Adjusted R^2	0.95
Standard Error	7.33
Observations	18

Goodness of Fit

The two-factor OLS model provides a strong statistical fit for the data. As seen in table 10, both R^2 and adjusted R^2 are high. This indicates that roughly 96 percent of the variability in *%f'c* is explained by changes in *RH* response and *UPV*. The model's residual error represents the typical one-sigma (1σ) prediction uncertainty around the fitted values. Additionally, as seen in table 11, the F-test is highly significant, with a *p*-value of much less than

0.05. This demonstrates that the NDT predictors, taken together, explain a statistically meaningful share of the variation in *%f'c*. The two-factor coefficients are presented in table 12.

Residual plots for the NDT indicators show no domain outliers or discernible patterns (see figure 27 and figure 28). This indicates no strong evidence of nonlinearity or heteroscedasticity. The standardized residual plot (figure 29) and summary (table 13) further indicate that most observations fall within ±1.75,[5] the approximate reference band for 15 degrees of freedom (df). Samples 1-8 and 3-4 exhibit standard residuals of approximately 1.9 and −1.9, respectively, but are captured within ±2.1 of the 95 percent reference band. These samples merit attention as potential outliers.

These goodness of fit metrics only reflect in-sample performance. They do not guarantee accuracy under different circumstances. The results indicate that the proposed method shows promise as a screening approach for estimating residual compressive strength. Additional testing and external validation are required to confirm transferability. Further testing also provides the opportunity to refine the model.

Table 11. Two-factor analysis of variance (ANOVA).

	df	*SS*	*MS*	*F*	*Significance F*
Regression	2	18677	9338	173.7	1.23E−11
Residual	15	806	53.8		
Total	17	19483			

[5] This value was obtained from a t-distribution table due to the small sample size.

Table 12. Two-factor coefficients.

	Coefficients	Standard Error	t-Stat	*p*-Value	Lower 95%	Upper 95%
Intercept	104.73	2.85	36.71	4.19E−16	98.64	110.81
%RH	−0.332	0.091	−3.65	0.0024	−0.53	−0.14
%UPV	−0.631	0.069	−9.10	1.70E−07	−0.77	−0.48

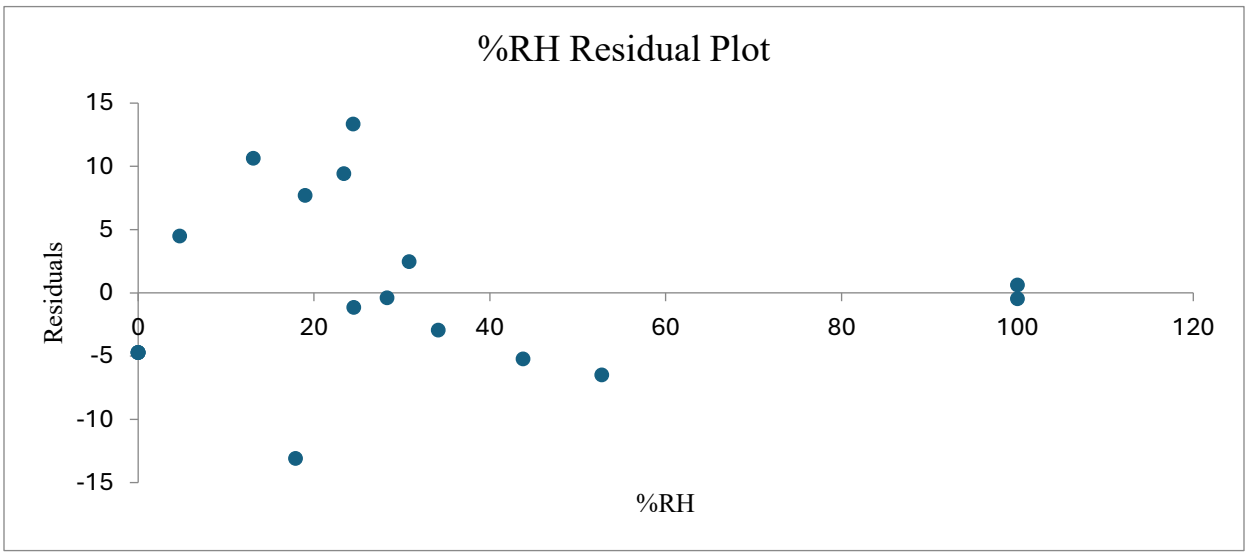

Figure 27. Plot. *%RH* residual plot for two-factor model.

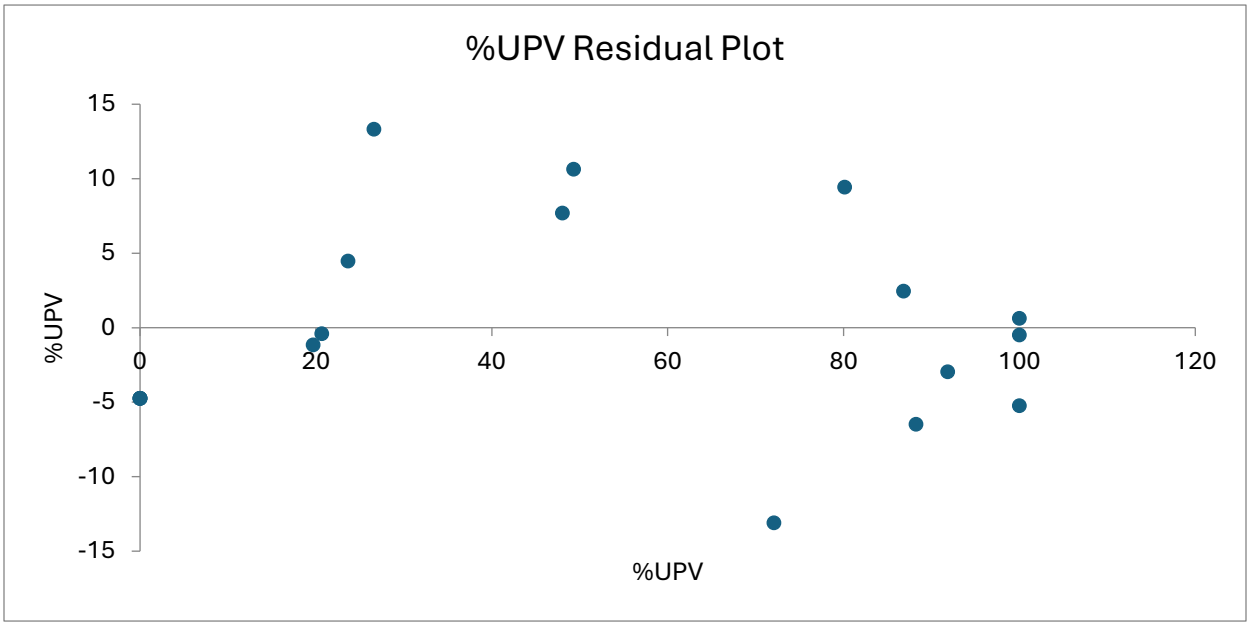

Figure 28. Plot. *%UPV* residual plot for two-factor model.

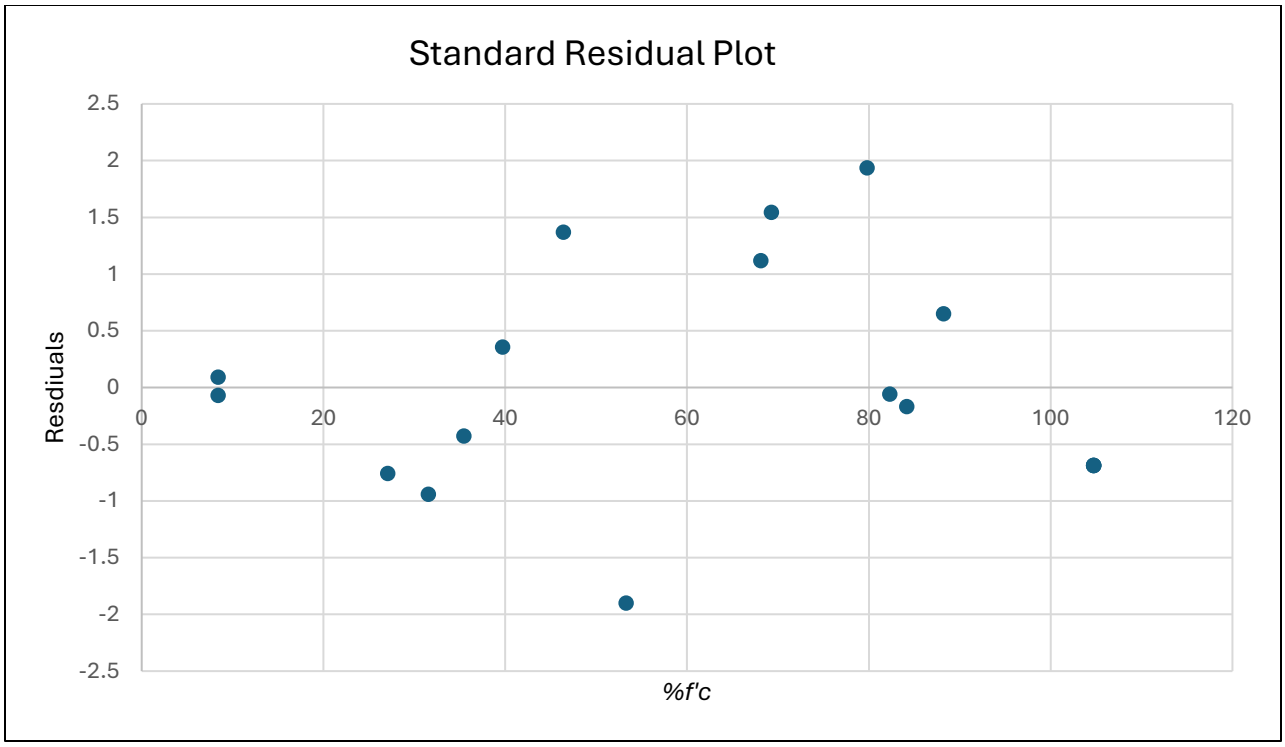

Figure 29. Plot. Standard residual plot for two-factor model.

Table 13. Residual output for two-factor model.

Batch Number	Sample Number	Predicted *%f'c*	Residuals	Standard Residuals
1	1	84.2	−1.2	−0.2
1	2	69.3	10.6	1.5
1	3	82.3	−0.4	−0.06
1	4	8.4	0.6	0.09
1	5	39.7	2.5	0.4
1	6	88.2	4.5	0.7
1	7	104.7	−4.7	−0.7
1	8	79.8	13.3	1.9
1	10	27.1	−5.2	−0.8
1	11	8.4	−0.5	−0.07
2	1	35.4	−2.9	−0.4
2	2	31.5	−6.4	−0.9
2	5	104.7	−4.7	−0.7
3	2	46.4	9.4	1.4
3	3	68.1	7.7	1.1
3	4	53.3	−13.1	−1.9
3	6	104.7	−4.7	−0.7
3	7	104.7	−4.7	−0.7

Two-Factor Model Coefficient Interpretation

The estimated slopes of both NDT indicators are negative and statistically significant. This indicates that larger *%RH* and *%UPV* values are associated with lower residual compressive strength after controlling the other indicator. For example, holding *%UPV* constant, a 1-point increase in *%RH* reduces *%f'c* by 0.332 point. The opposite is also true. Holding *%RH* constant, a 1-point increase in *%UPV* would decrease *%f'c* by 0.631 point.

Within the dataset, the UPV term carries roughly twice the weight of the RH term. This possibly reflects UPV's greater sensitivity to internal condition. The intercept is valued at

104.73. This exceeds the 100-point value for when *%RH* and *%UPV* values are 0. This is interpreted as a sampling variation and should not imply an increase in compressive strength.

Three-Factor Linear Regression Analysis

The second OLS model estimates the percent residual compressive strength from three indicators: *%RH*, *%UPV*, and $w_{c,max}$. The model was fit to the results from the 18 samples (see table 7 and table 8) and is presented in equation 16.

For field applications, the following information should be collected and calculated:

1. Obtain RH readings from similar, undamaged concrete and fire-damaged concrete and calculate *%RH* using equation 4.
2. Obtain UPV readings from similar, undamaged concrete and fire-damaged concrete and calculate *%UPV* using equation 6.
3. Obtain measurements of the maximum crack width that was a result of the fire damage using a standard bridge inspection crack gauge.
4. Using that information, calculate the predicted $\%f'c$ using equation 16:

$$\%f'c = 102.70 - 0.154\%RH - 0.537\%UPV - 61.1w_{c,mas} \quad \text{Equation 16}$$

Uncertainty is characterized by the model's standard error, as reported in table 14. As a practical rule, approximately 70 percent of comparable future observations can be expected to fall within ±7 percent of the calculated $\%f'c$. For approximately 95 percent coverage, use a prediction interval of ±16 percent of the calculated value.

Table 14. Three-factor regression statistics.

Metric	Value
Multiple R	0.98
R^2	0.97
Adjusted R^2	0.96
Standard Error	6.78
Observations	18

Table 15. Three-factor ANOVA.

	df	*SS*	*MS*	*F*	*Significance F*
Regression	3	18839	6280	136.5	1.33E−10
Residual	14	644	50.0		
Total	17	19483			

Goodness of Fit

The three-factor OLS model explains approximately 96 percent of the observed variation in percent residual strength, as shown in table 14. This indicates that changes in the independent variables account for nearly all the variability in *%f'c*. The standard error of 6.78 represents 1σ prediction uncertainty around the fitted values. Furthermore, as seen in table 15, the overall F-test is highly significant. This means that the indicators explain a statistically meaningful share of the variance relative to a null model with no predictors.

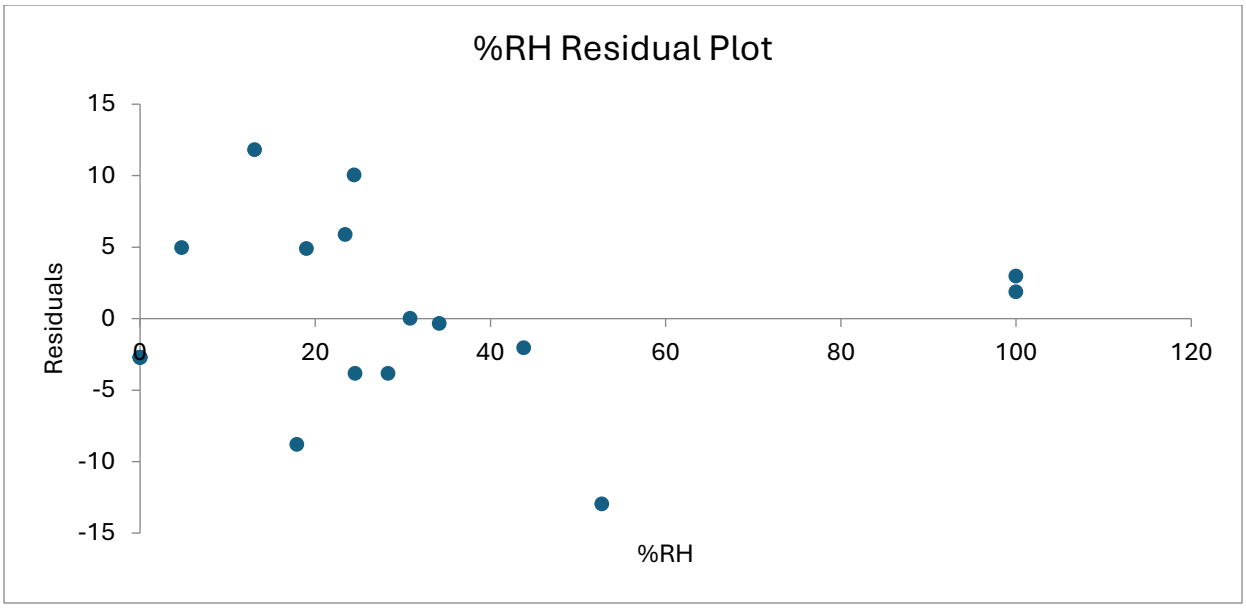

Figure 30. Plot. Three-factor *%RH* residual plot.

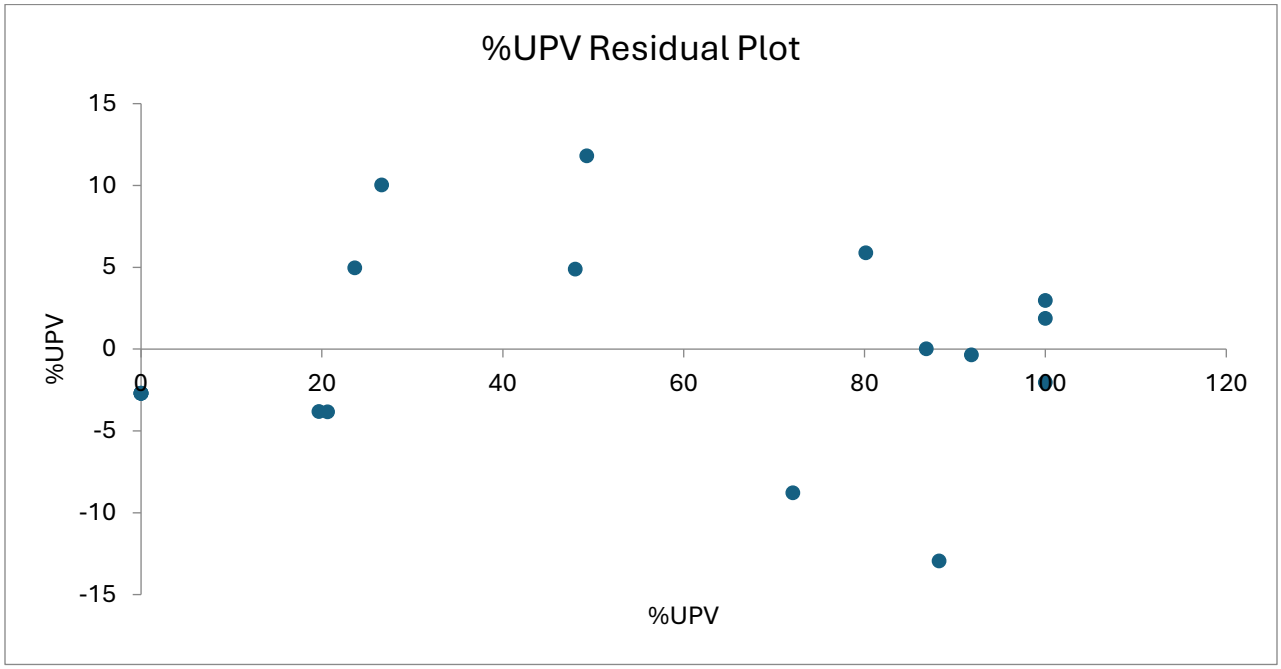

Figure 31. Plot. Three-factor *%UPV* residual plot.

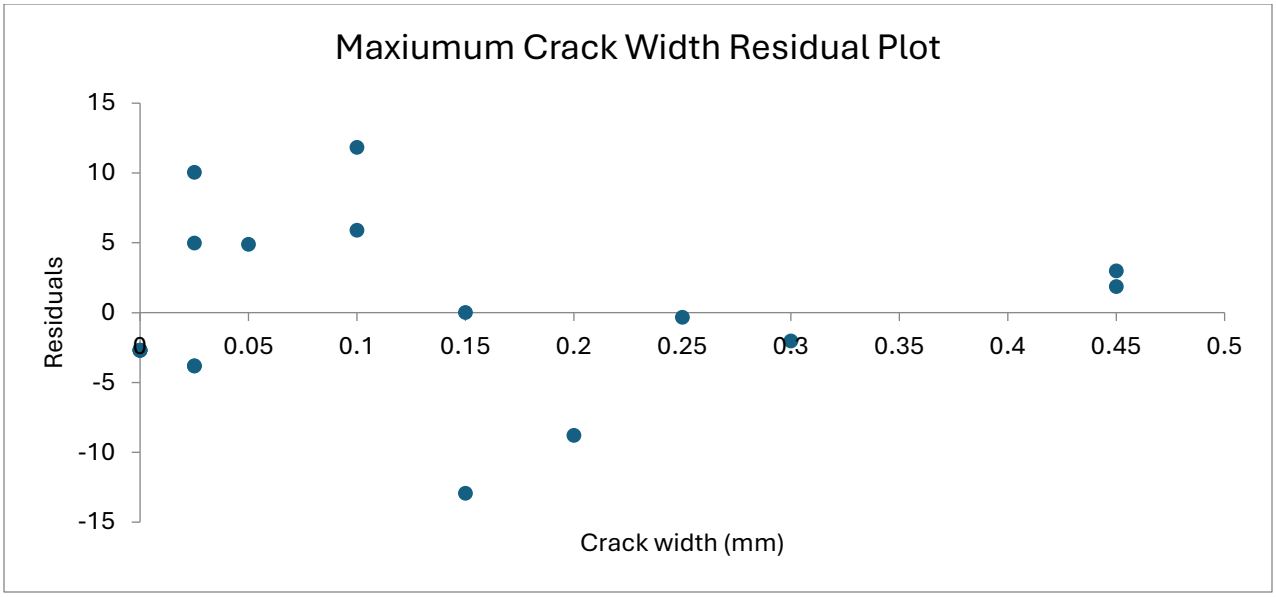

Figure 32. Plot. Three-factor maximum crack width residual plot.

Table 16. Three-factor residual output.

Batch Number	Sample Number	Predicted *%f'c*	Residuals	Standard Residuals
1	1	86.8	−3.8	−0.6
1	2	68.1	11.8	1.9
1	3	85.7	−3.8	−0.6
1	4	6.1	3.0	0.5
1	5	42.1	0.02	0.004
1	6	87.7	5.0	0.8
1	7	102.7	−2.7	−0.4
1	8	83.1	10.0	1.6
1	10	23.9	−2.0	−0.3
1	11	6.1	1.9	0.3
2	1	32.9	−0.3	−0.05
2	2	38.0	−12.9	−2.1
2	5	102.7	−2.7	−0.4
3	2	49.9	5.9	1.0
3	3	70.9	4.9	0.8
3	4	49.0	−8.8	−1.4
3	6	102.7	−2.7	−0.4
3	7	102.7	−2.7	−0.4

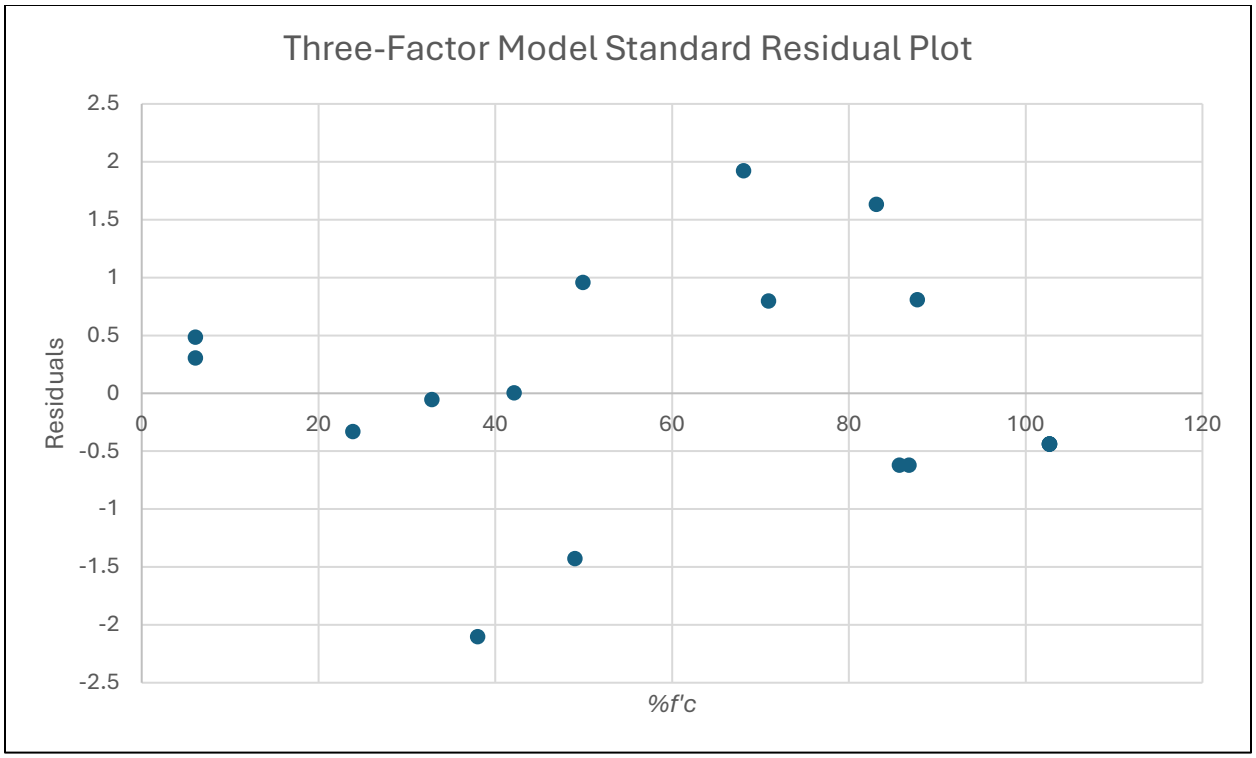

Figure 33. Plot. Three-factor standard residual plot.

Residual plots for the three independent variables (see figure 30–figure 32) show points scattered about zero, with no visible curvature. This indicates the absence of strong evidence of nonlinearity or heteroscedasticity over the dataset. Figure 33 presents the same conclusion for the standardized residual plot.

As summarized in table 16, 16 of the 18 observations fall within ±1.76, the approximate 90 percent reference band for 14 df. Samples 1-2 and 2-2 have standardized residuals of 1.9 and −2.1, respectively. Both numbers exceed the 90 percent band but remain within the 95 percent band. These samples should be treated as potential outliers and reviewed, but they do not invalidate the model. Taken together with the goodness of fit, the diagnostic supports adequacy of the model. As with the two-factor model, these findings are limited to the current dataset. Broader field application will require additional testing and validation to establish the universality of the model.

Three-Factor Model Coefficient Interpretation

Table 17 summarizes the coefficient results. For the three-factor model, the *%UPV* term remains the dominant predictor of residual compressive strength. The slope for *%UPV* is −0.537, meaning for each 1-point increase in *%UPV,* the predicted *%f'c* is reduced by about 0.54 point if other variables are held constant. For example, sample 2-1 saw a *%UPV* of 91.8. This result would reduce *%f'c* by approximately 49.3 points.

The crack-width slope was found to be −61.1 per millimeter of crack width. Every 0.10 mm of crack width corresponds to a reduction in *%f'c* of 6.1 points. Using sample 2-1 as an example, the recorded crack width is 0.25 mm. This corresponds to a decrease in *%f'c* of 15.3 points. This would indicate a meaningful effect; however, the 95 percent interval includes 0. This indicates that $w_{c,max}$ is suggestive but not conclusive.

Finally, the *%RH* slope is −0.154. This corresponds to an approximate 0.15-point drop in *%f'c* for every 1-point increase in *%RH*. Sample 2-1 shows a *%RH* of 34.5. This is reflected in a drop of 5.3 points in *%f'c*. Like $w_{c,max}$, the 95 percent interval for *%RH* also includes 0. Furthermore, this factor appears to have a smaller influence on the model compared to the other two variables. This leads to the possibility that *%RH* is not suggestive when *%UPV* and $w_{c,max}$ are included as independent variables.

Table 17. Three-factor coefficient data.

	Coefficients	Standard Error	t-Stat	*p*-Value	Lower 95%	Upper 95%
Intercept	102.70	2.85	36.02	3.33E-15	96.58	108.81
%RH	−0.154	0.13	−1.22	0.244	−0.426	0.118
%UPV	−0.537	0.08	−6.61	1.17E-5	−0.712	−0.363
$w_{c,max}$	−61.1	32.52	−1.88	0.0812	−130.86	8.64

Combining the effects for sample 2-1 yields a predicted residual strength of about 32.8 percent of $f'c$. Within the dataset, *%UPV* provides the clearest, most statistically robust signal. Crack width shows a plausible, but borderline influence on the model. *%RH* adds limited incremental information when *%UPV* and $w_{c,max}$ are included.

As detailed in Crack Width One-Factor Regression, there are known constraints on using crack width as a stand-alone factor. Incorporating it into a multifactor regression does not resolve those concerns. Although adding $w_{c,max}$ improves the overall fit, the improvement is not decisive. These findings support treating the three-factor model as requiring extensive further research into the nature of visual damage to concrete post-thermal event. The ability to quantify the fire-related defects is paramount in determining if this factor can generate a useful relationship with $\%f'c$.

CHAPTER 9. RECOMMENDATIONS

GDOT should **implement periodic training for bridge inspection and maintenance personnel,** focused on post-fire response. The curriculum should include: (1) a brief review of bridge-fire history and common trends; (2) common critical temperatures, damage mechanisms, and indicators; (3) inspection and NDT techniques; and (4) practical exercises that simulate initial post-fire assessment and decision-making.

GDOT should **procure common NDT tools,** including RHs and ultrasonic pulse devices to support rapid, portable, and cost-effective condition screening of fire-damaged concrete. Used together, these tools provide complementary information on near-surface hardness and internal condition. If budget constraints limit acquisition to a single device, UPV is recommended as a higher priority purchase due to its sensitivity to interior defects and stronger predictive value.

GDOT should **invest in further development and external validation of universal curves** for estimating residual concrete strength. The two-factor model, described in Two-Factor Linear Regression Analysis, presently shows the strongest performance. It should be prioritized for further testing and calibration. In parallel, the three-factor framework, presented in Three-Factor Linear Regression Analysis, warrants research to integrate visual metrics that are normalized on a 0–100 scale into the model. Drone imagery and artificial intelligence present a unique opportunity to aid in the development of this model. Both efforts should include larger sample sizes, varying sample shapes, varying concrete mix designs, and field trials to confirm transferability before operational adoption. This should include a pilot program involving GDOT and research teams to validate and refine the model.

GDOT should **develop and validate concrete criticality models based on the Quiel et al.** [58] **framework** that explicitly account for loss of concrete cover following a fire.

Incorporating as-found concrete cover will align screening outputs with observed field damage. This will provide more conservative and defensible classifications of damage criticality.

Alternatively, GDOT could **develop a calibration library using UPV and RH across common concrete mix designs and ages** across the state. These calibrations can be used to determine concrete compressive strength.

CHAPTER 10. CONCLUSIONS

Post-fire triage inspections of a bridge structure must be fast and repeatable. This report offers a workflow to accomplish this goal. First, inspectors should start with systematic visual documentation to localize distress. From this visual inspection, if conditions warrant, they can then apply rapid NDT methods to quantify the condition of the structural elements. With further development, these readings from concrete bridge elements can be converted into linear models to estimate the residual capacity of concrete following a fire. In the research team's dataset, the two-factor model was found to be the most reliable. The typical uncertainty of the model was found to be ±8 percent. If properly developed, this model shows promise in becoming a valuable tool in the assessment of bridge structures following thermal events.

This model is transparent and portable. It is easy to use and can be calculated by hand. It uses low-cost NDT methods that are accessible at various skill levels and can easily be deployed in the field. This model is a means of initial assessment. Final structural capacity determinations can only be made via engineering judgment and structural analysis.

Inspectors operate under time pressure and public scrutiny. Their first duty is to ensure the safety of the traveling public. The recommended investments in people, tools, and methods can help the Department accomplish this goal in the face of the challenges presented by bridge fires.

REFERENCES

1. Ibrahim, E.A.; Goff, D.; Keyvanfar, A.; Jonaidi, M., "Assessing Post-Fire Damage in Concrete Structures: A Comprehensive Review," *Buildings,* vol. 15, no. 3, 2025, https://doi.org/10.3390/buildings15030485.

2. Moradi, M.J.; Mehrpour, G.; Adelzadeh, M.; Hajiloo, H., "Structural damage levels of bridges in vehicular collision fires: Predictions using an artificial neural network (ANN) model," *Engineering Structures,* vol. 295, 2023, https://doi.org/10.1016/j.engstruct.2023.116840.

3. Gong, X.; Agrawal, A.K., "Numerical Simulation of Fire Damage to a Long-Span Truss Bridge," *Journal of Bridge Engineering,* vol. 20, no. 10, 2014, https://doi.org/10.1061/(ASCE)BE.1943-5592.0000707.

4. Hu, J.; Carvel, R.; Usamani, A., "Bridge fires in the 21st Century: A literature review," *Edinburgh Research Explorer,* 2021, https://doi.org/10.1016/j.firesaf.2021.103487.

5. Zheng, X.; Jian, J.; Liu, L.; Sun, B.; Zhang, K.; Gao, H., "Static and Dynamic Performance Analysis of Cable-Stayed Bridges with Cables Damaged Fire," *Buildings,* vol. 14, 2024, https://doi.org/10.3390/buildings14040884.

6. Zhang, G.; Zhao, X.; Lu, Z.; Song, C.; Li, X.; Tang, C., "Review and discussion on fire behavior of bridge girders," *Journal of Traffic and Transportaion Engineering,* vol. 9, no. 3, pp. 422-446, 2022, https://doi.org/10.1016/j.jtte.2022.05.002.

7. Lee, J.; Choi, K.; Yoon, J.; Chung, C.H., "Numerical analysis-based structural behavior assessment of a cable-stayed bridge under tanker fire," *Structure and Infrastructure Engineering,* vol. 19, no. 12, 2023, https://doi.org/10.1080/15732479.2022.2053553.

8. De Silva, D.; Miano, A.; De Rosa, G.; Di Meglio, F.; Prota, A.; Nigro, E., "Analitycal fire fragility assessment for bridges considering fire scenarios variability," *Engineering Structures,* vol. 325, 2025, https://doi.org/10.1016/j.engstruct.2024.119442.

9. Kodur, V.; Naser, M.Z., "Fire hazard in transportation infrastructure: Review, assessment, and mitigation strategies," *Frontiers of Structural and Civil Engineering,* vol. 15, pp. 46-60, 2021, https://doi.org/10.1007/s11709-020-0676-6.

10. Zhu, Z.; Quiel, S.E.; Khorasani, N.E., "Bivariate structural-fire fragility curves for simple-span overpass bridges with composite steel plate girders," *Structural Safety,* vol. 100, 2023, https://doi.org/10.1016/j.strusafe.2022.102294.

11. Pagan-Martinez, J.J.; Paya-Zaforteza, I.; Hospitaler-Perez, A., "Post-fire assessment of composite steel-concrete box-girder bridges: Lessons from a recent incident," *Journal of Construction Steel Research,* vol. 214, 2014, https://doi.org/10.1016/j.jcsr.2023.108425.

12. Senthilkumar, T.; Ajiboye, T.K., "Effect of Heat Treatment Processes on the Mechanical Properties of Medium Carbon Steel," *Journal of Minerals & Materials Characterization & Engineering,* vol. 11, no. 2, pp. 143-152, 2012.

13. Liu, Z.; Bai, S.L.; Yang, K.; Han, M., "Experimental studies on yield behavior of steel under rapid heating," *International Journal of Plasticity,* vol. 17, no. 5, pp. 691-701, 2001, https://doi.org/10.1016/S0749-6419(00)00022-X.

14. Gordon, J.A.; Bozeman, S.C.; Fisher, E.C.; Isgor, O.B.; Tucker, J.D., "Heating duration effects on post-fire structural steel mechanical properties," *Fire Safety Journal,* vol. 140, 2023, https://doi.org/10.1016/j.firesaf.2023.103848.

15. Shi, Y.; Luo, Z.; Zhou, X.; Xue, X.; Li, J., "Post-fire mechanical properties of titanium–clad bimetallic steel in different cooling approaches," *Journal of Construction Steel Research,* vol. 191, 2022, https://doi.org/10.1016/j.jcsr.2022.107169.

16. Kim, I.T.; Cha, K.H.; Jeong, Y.S.; Shin, A.S., "Visual Inspection of the Heavy-Duty Paint Systems Used in Steel Bridges for Assessing the Level of Fire Damage," *Coatings,* vol. 12, 2022, https://doi.org/10.3390/coatings12111697.

17. Dan, W.J.; Gou, R.B.; Yu, M.; Ge, Y.B.; Li, T.J., "Experimental study on the post-fire mechanical behaviours of structural steels," *Journal of Constructional Steel Research,* vol. 199, 2022, https://doi.org/10.1016/j.jcsr.2022.107629.

18. Georgali, B.; Tsakiridis, P.E., "Microstructure of fire-damaged concrete. A case study," *Cement and Concrete Composits,* vol. 27, no. 2, pp. 255-259, 2005, https://doi.org/10.1016/j.cemconcomp.2004.02.022.

19. Miao, K.; Pan, Z.; Fang, X.; Chen, A., "Fire-induced damage behaviour in corrosion-damaged concrete: Thermal-mechanical coupling phase field meso-scale modeling," *Journal of the Mechanics and Physics of Solids,* vol. 196, 2025, https://doi.org/10.1016/j.jmps.2025.106041.

20. Lottman, B.B.G.; Koenders, E.A.B.; Blom, C.B.M.; Walraven, "Spalling of fire exposed concrete," *Horon,* vol. 62, no. 3, pp. 129-166, 2017.

21. Kim, H.J.; Kim, H.Y.; Lee, J.S.; Kwan, K.H., "An Experimental Study on Thermal Damage and Spalling of Concrete Under Loading Conditions in a Tunnel Fire," *Journal of Asian Architecture and Building Engineering,* vol. 10, no. 11, pp. 375-382, 2011, https://doi.org/10.3130/jaabe.10.375.

22. Lubloy, E., "The relationship between conctere composition and structural stability in case of fire," *Construction and Building Materials,* vol. 431, 2024, https://doi.org/10.1016/j.conbuildmat.2024.136545.

23. Grace, N.F.; Mohamed, M.E.; Chynoweth, M.; Kose, N.; Bebawy, M, "Effect of Elevated Temperatures on the Mechanical Properties and Relaxation of CFRP Strands," *Journal of Composites for Construction,* vol. 25, no. 3, 2021, https://doi.org/10.1061/(ASCE)CC.1943-5614.0001127.

24. Lou, G.B.; Hou, J.; Qi, H.H.; Li, F.X.; Song, Z.H.; Li, G.Q., "Prestress loss of twisted wire strands and parallel wire strands at elevated temperatures," *Engineering Structures,* vol. 291, 2023, https://doi.org/10.1016/j.engstruct.2023.116483.

25. Banoth, I.; Agarwal, A., "Effect of Heating Rate on Bond Behavior Between Steel and Concrete at Elevated Temperatures," *Advances in Structural Engineering,* vol. 74, pp. 89-98, 2020, https://doi.org/10.1007/978-981-15-4079-0_8.

26. Bingol, A.F.; Gul, R., "Residual bond strength between steel bars and concrete after elevated temperatures," *Fire Safety Journal,* vol. 44, no. 6, pp. 854-859, 2009, https://doi.org/10.1016/j.firesaf.2009.04.001.

27. Wang, Y.; Zhang, B.; Liu, Z.; Gao, Y.; Fu, C., "Effect of temperature on the bond-slip between I-shaped steel and concrete," *Advances in Structural Engineering,* vol. 24, no. 10, 2021, https://doi.org/10.1177/1369433221993551.

28. Banoth, I.; Agarwal, A., "Bond between deformed steel rebars and concrete at elevated temperatures," *Fire Safety Journal,* vol. 145, 2024, https://doi.org/10.1016/j.firesaf.2024.104133.

29. Ibrahim, A.; Abdelkhalek, S.; Zayed, T.; Qureshi, A.H.; Abdelkader, E.M., "A Comprehensive Review of the Key Deterioration Factors of Concrete Bridge Decks," *Buildings,* vol. 14, no. 11, 2024, https://doi.org/10.3390/buildings14113425.

30. Faris, N.; Zayed, T.; Fares, A., "Review of Condition Rating and Deterioration Modeling Approaches for Concrete Bridges," *Buildings,* vol. 15, no. 2, 2025, https://doi.org/10.3390/buildings15020219.

31. Vishwanath, B.S.; Banerjee, S., "Considering uncertainty in corrosion process to estimate life-cycle seismic vulnerability and risk of aging bridge piers," *Reliability Engineering & System Safety,* vol. 232, 2023, https://doi.org/10.1016/j.ress.2022.109050.

32. Devendiran, D.K.; Banerjee, S., "Influence of Combined Corrosion–Fatigue Deterioration on Life-Cycle Resilience of RC Bridges," *Journal of Bridge Engineering,* vol. 28, no. 5, 2023, https://doi.org/10.1061/JBENF2.BEENG-5708.

33. Panchireddi, B.; Ghosh, J., "Cumulative vulnerability assessment of highway bridges considering corrosion deterioration and repeated earthquake events," *Bulletin of Earthquake Engineering,* vol. 17, pp. 1603-1638, 2018, https://doi.org/10.1007/s10518-018-0509-3.

34. Peris-Sayol, G.; Paya-Zaforteza, I.; Balasch-Parisi, S.; Alos-Moya, J., "Detailed analysis of the causes of bridge fires and their associated damage levels," *ASCE Journal of Performance and Constructed Facilities,* vol. 31, no. 3, 2017, DOI:10.1061/(ASCE)CF.1943-5509.0000977.

35. Kodur, V.; Gu, L.; Garlock, M.E.M., "Review and Assessment of Fire Hazard in Bridges," *Transporation Research Record: Journal of the Transportation Research Board,* vol. 2172, no. 1, 2010, https://doi.org/10.3141/2172-03.

36. Abedi, M.; Naser, M.Z., "RAI: Rapid, Autonomous and Intelligent machine learning approach to identify fire-vulnerable bridges," *Applied Soft Computing,* Vols. 113, Part A, 2021, https://doi.org/10.1016/j.asoc.2021.107896.

37. Hajiloo, H.; Green, M.F., "The thermal assessment of GFRP reinforced concrete bridge decks in fire scenarios," *Fire Safety Journal,* vol. 137, 2023, https://doi.org/10.1016/j.firesaf.2023.103777.

38. Eva, L.; Viktor, H.; Oliver, C.; Andras, B.; Zsolt, C., "Bridges after the fire – Experiences, tests and repair methods," *Ain Shams Engineering Journal,* vol. 14, no. 11, 2023, https://doi.org/10.1016/j.asej.2023.102519.

39. De Melo, M.; Wheatley, R.; Gibbin, N.; Gonzalez-Quesada, M.; Harwood, K., "Assessment and Repair of a Fire-Damaged Pre-stressed Concrete Bridge," *Structural Engineering International,* vol. 24, no. 3, pp. 408-413, 2014, https://doi.org/10.2749/101686614X13844300210272.

40. Godart, B.; Berthellemy, J.; Lucus, J.P., "Diagnosis, Assessmenet, and Repair of the Mathilde Bridge Close to Collapse during a Fire," *Hal Open Science,* vol. 25, no. 3, pp. 331-338, 2015, DOI: 10.2749/101686615X14210663188691.

41. Chen, Y.; Xu, Z.; Huang, Y.; Xu, Q.; Rao, R., "Damage analysis and assessment of concrete T-girder bridge based on fire scene numerical reconstruction," *Advances in Bridge Engineering,* vol. 5, 2024, https://doi.org/10.1186/s43251-024-00140-6.

42. Pant, U.; Shrestha, J.K., "Framework for assessing bridge quality index based on the correlation of non-destructive test results," *Heliyon,* vol. 10, no. 4, 2024, https://doi.org/10.1016/j.heliyon.2024.e26392.

43. Herki, B.A.; Khatib, J.; Ramadhan, Z.; Hamadameen, B., "Condition Assessment of Building Concrete Structures Using NDTs-Case Study," in *1st International Conference on Recent Academic Studies*, Konya, Turkiye, 2023.

44. Kilic, G., "Wavelet analysis and NDT for condition assessment of historic Masonry Bridge," *Structures,* vol. 45, pp. 275-283, 2022, https://doi.org/10.1016/j.istruc.2022.09.008.

45. Chi, J.H.; Peng, P.C., "Study of the structural safety assessment of steel bridge subjected in post-fire," *Construction and Building Materials,* vol. 247, 2020, https://doi.org/10.1016/j.conbuildmat.2020.118587.

46. Otsuki, Y.; Nguyen, S.T.; La, H.M.; Wang, Y., "Autonomous Ultrasonic Thickness Measurement of Steel Bridge Members Using a Climbing Bicycle Robot," *Journal of Engineering Mechanics,* vol. 149, no. 8, 2023, https://doi.org/10.1061/JENMDT.EMENG-7000.

47. Akgul, F., "Inspection and evaluation of a network of concrete bridges based on multiple NDT techniques," *Structure and Infrastructure Engineering,* vol. 17, no. 8, pp. 1076-1095, 2021, https://doi.org/10.1080/15732479.2020.1790016.

48. Alsharqawi, M.; Zayed, T.; Dabous, S.A., "Common practices in assessing conditions of concrete bridges," in *International Conference on Advances in Sustainable Construction Materials & Civil Engineering Systems*, [online], 2017, https://doi.org/10.1051/matecconf/201712002016.

49. Rapaport, G., "Applications of State of the Art NDT Techniques in Bridge Inspections," *CE Papers,* vol. 6, pp. 155-162, 2023, https://doi.org/10.1002/cepa.2083.

50. Johanis, M.B., "Study of Fire Damaged Concrete Structure," Universiti Malaysia Pahang, Pekan, Malaysia, 2012.

51. Gordon, J.A.; Bozeman, S.C.; Fisher, E.C.; Isgor, O.B.; Tucker, J.D., "Heating duration effects on post-fire structural steel mechanical properties," *Fire Safety Journal,* vol. 140, 2023, https://doi.org/10.1016/j.firesaf.2023.103848.

52. Liu, J.C.; Tan, K.H.; Yao, Y., "A new perspective on nature of fire-induced spalling in concrete," *Construction and Building Materials,* vol. 140, pp. 581-590, 2018, https://doi.org/10.1016/j.conbuildmat.2018.06.204.

53. Lee, D.; Liu, J.; Lim, R.; Chan, J.L.; Foong, S., "Geometrical-Based Displacement Measurement with Pseudostereo Monocular Camera on Bidirectional Cascaded Linear Actuator," *Transactions on Mechatronics,* vol. 26, no. 4, pp. 1923-1931, 2021, https://doi.org/10.1109/TMECH.2021.3079935.

54. Murcinkova, Z.; Baron, P.; Pollak, M., "Study of the Press Fit Bearing-Shaft Joint Dimensional Parameters by Analytical and Numerical Approach," *Advances in Materials Science and Engineering,* 2018, https://doi.org/10.1155/2018/2916068.

55. Yue, Q.; Li, L.; Zhang, X., "Failure mechanism and bearing capacity analysis of the underpinning structure with relative displacement," *Engineering Failure Analysis,* vol. 148, 2023, https://doi.org/10.1016/j.engfailanal.2023.107205.

56. Sun, Z.; Santos, J.; Caetano, E.; Oliveira, C., "Interpreting cumulative displacement in a suspension bridge with a physics-based characterisation of environment and roadway/railway loads," *Journal of Civil Structural Health Monitoring,* vol. 12, pp. 387-397, 2022, https://doi.org/10.1007/s13349-022-00647-4.

57. Park, J.S.; Ham, H.M.; Ahn, Y.H., "Expansion Joints Risk Prediction System Based on IoT Displacement Device," *Electronics,* vol. 12, 2023, https://doi.org/10.3390/electronics12122713.

58. Quiel, S.; Zhu, Z.; Murphy, T.; Lopez, M.; Artmont, F., "Characterizing Design-Basis Fire Exposure for Highway Bridges," Lehigh University - Adavanced Technology for Larger Structural Systems, Bethlehem, PA, 2024.

59. Gallo, M.; De Silva, D.; Nigro, E., "Fire vulnerability assessment of bridges: a performance-based approach procedure with unconventional fire scenarios," *Structures,* vol. 71, 2025, https://doi.org/10.1016/j.istruc.2024.108019.

60. Kodur, V.K.R.; Gil, A.M.; Naser, M.Z., "Fire-induced collapse of an I-95 overpass in Philadelphia: Causes, collapse mechanism, and mitigation strategies," *Engineering Structures,* vol. 303, 2024, https://doi.org/10.1016/j.engstruct.2024.117578.

61. Davidson, M.T.; Harik, I.E.; Davis, D.B., "Fire Impact and Passive Fire Protection of Infrastructure: State of the Art," *Journal of Performance of Constructed Facilities,* vol. 27, no. 2, 2011, https://doi.org/10.1061/(ASCE)CF.1943-5509.0000295.

62. Liu, Z.; Li, G.Q.; Paya-Zaforteza, I.; Cai, C.S.; Huang, Q., "Fire Hazards in Bridges: State of the Art, Recent Progress, and Current Research Gaps," *Journal of Bridge Engineering,* vol. 28, no. 7, 2021, https://doi.org/10.1061/JBENF2.BEENG-5790.

63. "DeKalb Street Bridge," Bridgeport Founders Day, [Online]. Available: https://bridgeportfoundersday.org/frosty-falls-the-dekalb-street-bridge/?utm_source=chatgpt.com. [Accessed 16 July 2025].

64. Sullivan, N., "The DeKalb Street Bridge Fire," The Historical Society of Montgomery County PA, [Online]. Available: https://hsmcpa.org/the-dekalb-street-bridge-fire/. [Accessed 16 July 2025].

65. "Newspapers.com," Ancestry.com, [Online]. Available: https://www.newspapers.com/article/the-evening-news-1924-reward-offered-for/135105588/. [Accessed 16 July 2025].

66. flickr, "DeKalb Street Bridge fire April 14, 1924, 12 of 15," 23 January 2015. [Online]. Available: https://www.flickr.com/photos/rich701/16163422800/in/photostream/. [Accessed 15 November 2025].

67. "Beyond 41," Safety, Agriculture, Villages and Environment, Inc., [Online]. Available: https://web.archive.org/web/20060827115502/https://www.save41.org/beyond.htm. [Accessed 16 July 2025].

68. Covered Spans of Yesteryear, "Bellbank, Chester County," Covered Spans of Yesteryear. [Online]. [Accessed 17 July 2025].

69. Kohut, S.B.A.R., Crossing Under Cover: Covered Bridges of Chester County Pennsylvania and Surrounding Regions, Atglen, PA: Schiffer Publishing, Ltd., 2023.

70. Robinson, R., "Rebirth of a Covered Bridge?," Lancaster Online, 11 September 2013. [Online]. Available: https://lancasteronline.com/news/rebirth-of-a-covered-bridge/article_1d8cb336-391d-5e40-a830-3f293f27f140.html. [Accessed 17 July 2025].

71. Caswell, "Documenting North America's past & present covered bridges," Covered Spans of Yesteryear, 2024. [Online]. Available: https://www.lostbridges.org/details.aspx?id=PA%2F38-15-21_2x&loc=n. [Accessed 11 November 2025].

72. Mann, D.A., "Big Four Bridge fire's cause, damage not yet determined," News and Tribute, 9 May 2008. [Online]. Available: https://archive.today/20130223061530/http://www.news-tribune.net/clarkcounty/local_story_129105311.html?keyword=secondarystory. [Accessed 17 July 2025].

73. Hill, B., "Footsteps on the Big Four," *Louisville Magazine,* pp. 40-43, 2010.

74. Garlock, M.; Paya-Zoforteza, I.; Kodur, V., "Fire Hazard in Bridges: Review, Assessment, and Repair Strategies," *Engineering Structures,* vol. 35, pp. 89-98, 2012, https://doi.org/10.1016/J.ENGSTRUCT.2011.11.002.

75. "Kentucky Crews Battle Big Four Bridge Fire," Firehouse, 16 May 2008. [Online]. Available: https://www.firehouse.com/photo-story/article/10566872/kentucky-crews-battle-big-four-bridge-fire. [Accessed 17 July 2025].

76. "Big Four Bridge," Wikipedia, 10 October 2025. [Online]. Available: https://en.wikipedia.org/wiki/Big_Four_Bridge. [Accessed 15 November 2025].

77. Lehman, E.D., "The Legend of Pleasure Beach," Bridgeport Library: Bridgeport History Center, [Online]. Available: https://bportlibrary.org/hc/entertainment/the-legend-of-pleasure-beach/. [Accessed 17 July 2025].

78. Sattanni, R., "Remembering the Pleasure Beach Bridge: Bridge Fire Closed the Beach," Patch.com, 11 August 2019. [Online]. Available: https://patch.com/connecticut/bridgeport/remembering-pleasure-beach-bridge. [Accessed 17 July 2025].

79. Motavalli, J., "Pleasure Beach: A Place for Birds and People," Audubon, March-April 2012. [Online]. Available: https://www.audubon.org/magazine/pleasure-beach-place-birds-and-people#:~:text=The%20wooden%20swing%20bridge%20that,well%20be%20on%20the%20moon. [Accessed 17 July 2025].

80. Christopher, M., "Pleasure Beach and Long Beach," Abandoned America, 3 April 2022. [Online]. Available: https://www.abandonedamerica.us/pleasure-and-long-beach#:~:text=Jeanette%20Scinto%20remembers%20that%20day%3A,time%20was%20the%20end%20of. [Accessed 17 July 2025].

81. Burgeson, J., "Humans are gone from Pleasure Beach, and so have the shore birds," CTPost, 1 August 2010. [Online]. Available: https://www.ctpost.com/news/article/humans-are-gone-from-pleasure-beach-and-so-have-598691.php#:~:text=The%20cranky%20swing%20bridge%2C%20which,much%20beyond%20the%20talking%20stage. [Accessed 17 July 2025].

82. Calusen, C.A.; White, R.H.; Wacker, J.P.; Lebow, S.T.; Dietenberger, M.A.; Zelinka, S.L.; Stark, N.M., "Laboratory investigation of fire protected coatings for creosote-treated timber railroad bridges," U.S. Forest Service, Madison, Wisconsin, 2014.

83. Leff, D.K., "Loneliest Beach in the Megalopolis," Wayfarer Magazine, 5 August 2024. [Online]. Available: https://www.wayfarermagazine.com/p/loneliest-beach-in-the-megalopolis-9a3. [Accessed 17 July 2025].

84. Font, A., "The Night the Dumbarton Rail Bridge Went Up in Flames," KQED, 8 January 2018. [Online]. Available: https://www.kqed.org/news/11639835/the-night-the-dumbarton-rail-bridge-went-up-in-flames#:~:text=New%20details%20were%20released%20last,the%20Dumbarton%20Rail%20Bridge. [Accessed 20 July 2025].

85. Kazak, D., "FIREFIGHTERS: Dumbarton rail bridge destroyed," Palo Alto Weekly, 7 January 1998. [Online]. Available: https://web.archive.org/web/20040814110454/https://www.paloaltoonline.com/weekly/morgue/news/1998_Jan_7.FIRE.html. [Accessed 20 July 2025].

86. Schneider, E.J.;, "Construction Problems, Dumbarton Bridge, Central California Railway," in *American Society of Civil Engineers*, New York, NY, 1913.

87. Doyle, J., "Mysterious Fire On Trestle Probed / Rail bridge near Dumbarton collapsed into S.F. Bay," SFGate, 5 January 1998. [Online]. Available: https://www.sfgate.com/news/article/mysterious-fire-on-trestle-probed-rail-bridge-3016220.php. [Accessed 20 July 2025].

88. Budzynski, B.W., "The I-59/I-20 Corridor, the largest project in the history of Birmingham, Ala., looks to reinvent the city's business district," Roads & Bridges, 7 June 2019. [Online]. Available: https://www.roadsbridges.com/asphalt/highway-construction/article/10651859/the-i-59-i-20-corridor-the-largest-project-in-the-history-of-birmingham-ala-looks-to-reinvent-the-citys-business-district. [Accessed 20 July 2025].

89. Wright, W.; Lattimer, B.; Woodworth, M.; Nahid, M.; Sotelino, E., "Highway Bridge Fire Hazard Assessment Draft Guide Specification for Fire Damage Evaluation in Steel Bridges," Virginia Polytechnic Institute and State University, Blacksburg, VA, 2013.

90. Deseret News, "Fatal crash, blast rock Birmingham," Deseret News, 6 January 2002. [Online]. Available: https://www.deseret.com/2002/1/6/19630041/fatal-crash-blast-rock-birmingham/#:~:text=interstate%20Saturday%2C%20killing%20one%20person,of%20the%20state%27s%20busiest%20interchanges. [Accessed 20 July 2025].

91. Riley, C., "Alabama Interstate Bridge Collapse Snarls Traffic, Forces Rapid Repair," Construction Equipment Guide, 19 February 2002. [Online]. Available: https://www.constructionequipmentguide.com/alabama-interstate-bridge-collapse-snarls-traffic-forces-rapid-repair/1919#:~:text=Best%20known%20as%20%E2%80%9CMalfunction%20Junction%2C%E2%80%9D,flames%20and%20cause%20massive%20damage. [Accessed 20 July 2025].

92. Byington, P., "Atlanta I-85 fire and bridge collapse reminds Birmingham of "Malfunction Junction" interstate closures in the early 2000s," Bham Now, 19 December 2020. [Online]. Available: https://bhamnow.com/2017/03/31/atlanta-i-85-fire-and-bridge-collapse-reminds-birmingham-of-malfunction-junction-interstate-closures-in-the-early-2000s/#:~:text=death%20of%20trucker%20Tim%20Dyson,Gorrie%20in%20just%2038. [Accessed 20 July 2025].

93. Walsh, L., "What ALDOT learned from 2002, 2004 malfunction junction bridge collapses," ABC 33/40 News, 31 March 2017. [Online]. Available: https://abc3340.com/news/local/what-aldot-learned-from-2002-2004-malfunction-junction-bridge-collapses. [Accessed 20 July 2025].

94. Brasfield & Gorrie, "I-65 Emergency Bridge Replacement," Brasfield & Gorrie, 2025. [Online]. Available: https://www.brasfieldgorrie.com/projects/i-65-emergency-bridge-replacement/. [Accessed 15 November 2025].

95. Firehouse, "Fuel Tanker Flips, burns At Busy Alabama Interstate Interchange," Firehouse, 21 October 2004. [Online]. Available: https://www.firehouse.com/home/news/10516690/fuel-tanker-flips-burns-at-busy-alabama-interstate-interchange. [Accessed 20 July 2025].

96. The Portal Bridge Link, "A New and Improved Northeast Corridor Link," Portal Bridge Capacity Enhancement, 1 January 2007. [Online]. Available: https://web.archive.org/web/20110715104707/http://www.portalbridgenec.com/pdfs/PortalBridgeLink-Issue1.pdf. [Accessed 21 July 2025].

97. Leir, R., "Fire boat in town's future," The Observer, 1 February 2012. [Online]. Available: https://www.theobserver.com/2012/02/01/fire-boat-in-town%E2%80%99s-future/#:~:text=Back%20on%20May%2012%2C%202005%2C,River%20between%20Kearny%20and%20Secaucus. [Accessed 21 July 2025].

98. McGeehan, P., "Trains Crawl Back Into Service After Kearny Bridge Fire," The New York Times, 14 May 2005. [Online]. Available: https://www.nytimes.com/2005/05/14/nyregion/trains-crawl-back-into-service-after-kearny-bridge-fire.html. [Accessed 21 July 2025].

99. Associated Press, "Electrical work was faulty before bridge fire, Amtrak says," Brotherhood of Locomotive Engineers and Trainmen, 6 June 2005. [Online]. Available: https://ble-t.org/news/electrical-work-was-faulty-before-bridge-fire-amtrak-says/#:~:text=KEARNY%2C%20N,improperly%20installed%2C%20Amtrak%20officials%20said. [Accessed 21 July 2025].

100. McGeehan, P., "Repairing New Jersey bridge may take a year, Amtrak says," Brotherhood of Locomotive Engineers and Trainmen, 19 May 2005. [Online]. Available: https://ble-t.org/news/repairing-new-jersey-bridge-may-take-a-year-amtrak-says/#:~:text=Fire%20broke%20out%20at%20the,Newark%20until%20the%20next%20morning. [Accessed 21 July 2025].

101. Belsen, K., "Approval Given for Jersey Rail Bridges," The New York Times, 31 December 2008. [Online]. Available: https://www.nytimes.com/2009/01/01/nyregion/01bridge.html. [Accessed 21 July 2025].

102. Bajwa, C.S.; Easton, E.P.; Adkins, H.; Cuta, J.; Klynyshyn, N.; Suffield, S., "The MacArthur Maze Fire and Roadway Collapse: A “Worst Case Scenario” for Spent Nuclear Fuel Transportation?," in *ASME 2012 Pressure Vessels and Piping Conference*, Toronto, Ontario, Canada, 2012, https://doi.org/10.1115/PVP2012-78637.

103. CalTrans, "Emergency Ramp Replacement Project: MacArthur Maze/580 Deck Collapse," CalTrans, 30 April 2007. [Online]. Available: https://web.archive.org/web/20080706183313/https://dot.ca.gov/dist4/newsreleases/mazeupdate43007.pdf. [Accessed 21 July 2025].

104. WJE, "MacArthur Maze Fire and Collapse," WJE, [Online]. Available: chrome-extension://efaidnbmnnnibpcajpcglclefindmkaj/https://www.wje.com/assets/pdfs/projects/MacArthur_Maze_Fire_and_Collapse.pdf#:~:text=as%20the%20MacArthur%20Maze,880. [Accessed 21 July 2025].

105. Astaneh-Asi, A.; Noble, C.R.; Son, J.; Wemhoff, A.P.; Thomas, M.P.; McMichael, L.D., "Fire Protection of Steel Bridges and the Case of the MacArthur Maze Fire Collapse," in *TCLEE 2009*, Oakland, California, 2009, https://doi.org/10.1061/41050(357)69.

106. Cabanataun, M., "A-MAZE-ING / His reputation on the line, contractor finishes repair early, and I-580 opens," SFGate, 25 Man 2007. [Online]. Available: https://www.sfgate.com/bayarea/article/a-maze-ing-his-reputation-on-the-line-2592154.php. [Accessed 21 July 2025].

107. Franchini, A.; Barake, B.; Galasso, C.; Garlock, M.E.M.; Mulligan, J.; Quiel, S.; Torero, J.L., "Integrating fire safety into bridge design is essential for resilient infrastructure," *National Library of Medicine,* vol. 15, no. 1, 2024, https://doi.org/10.1038/s41467-024-49593-3.

108. Matier, P.; Ross, A., "CHP recommends no charges for Maze trucker," SFGate, 17 March 2008. [Online]. Available: https://www.sfgate.com/crime/article/CHP-recommends-no-charges-for-Maze-trucker-3224012.php. [Accessed 15 November 2025].

109. "Paramount Boulevard Bridge Reopens 115 Days After Fire Destroyed Predecessor," KCAL News, 19 May 2012. [Online]. Available: https://www.cbsnews.com/losangeles/news/paramount-boulevard-bridge-reopens-115-days-after-fire-destroyed-predecessor/. [Accessed 31 July 2025].

110. Giulani, L; Crosti, C.; Gentili, F., "Vulnerability of Bridges to Fire," *Bridge Maintenance, Safety, Management, Resilience, and Sustainability,* pp. 1565-1572, 2012.

111. Zawadowska, A.; Giuliani, L.; Hertz, K.D., "Experimental study on the mechanical properties of fire exposed concrete," *Safety Science,* vol. 142, 2021, https://doi.org/10.1016/j.ssci.2021.105357.

112. "Pomona Freeway Open," Channel 4 Los Angeles, 18 December 2011. [Online]. Available: https://www.nbclosangeles.com/news/local/pomona-freeway-open/1914616/#:~:text=The%20driver%20of%20a%20double,long%20stretch%20of%20freeway. [Accessed 31 July 2025].

113. Associated Press, "So. Cal tanker fire will force freeway demolition," Deseret, 15 December 2011. [Online]. Available: https://www.deseret.com/2011/12/15/20238476/so-cal-tanker-fire-will-force-freeway-demolition/#:~:text=The%20cause%20of%20the%20crash%2C,brakes%20overheated%2C%20remained%20under%20investigation. [Accessed 31 July 2025].

114. Sumwalk, R.L.; Weener, E.F.; Dinh-Zarr, T.B., "Fire Damage to Bridge and Subsequent Collapse," National Transportation Safety Board, Washington, D.C., 2018.

115. Zhu, Z.; Quiel, S.E.; Naito, C.J., "Resiliency of Prestressed Concrete Beams Exposed to Fire," The Pennsylvania Department of Transportation, Harrisburg, PA, 2023.

116. NOCoE, "I-85 Bridge Collapse and Rebuild," National Operations Center of Excellence, 27 August 2018. [Online]. Available: https://transportationops.org/case-studies/i-85-bridge-collapse-and-rebuild#:~:text=On%20March%2030%2C%202017%2C%20a,carries%20243%2C000%20vehicles%20per%20day. [Accessed 21 July 2025].

117. CNN Wire, "After I-85 fire, states are taking a closer look under their bridges," New Richmond, 20 May 2017. [Online]. Available: https://www.wtvr.com/2017/05/20/after-i-85-fire-states-are-taking-a-closer-look-under-their-bridges#:~:text=These%20tubes%20were%20meant%20for,GDOT%20Commissioner%20Russell%20McMurry%20said. [Accessed 21 July 2025].

118. Biondi, E., "ACTION: Documentation and Treatment of Materials Stored Under a Highway Bridge," Federal Highway Administration, 11 November 2023. [Online]. Available: https://www.fhwa.dot.gov/bridge/inspection/documentation_and_treatment_of_materials_stored_under_highway_bridge.cfm#:~:text=remind%20the%20State%20Departments%20of,Way. [Accessed 23 July 2025].

119. C.W. Matthews Contracting Company, "I-85 Bridge Collapse/Repair," C.W. Matthews Contracting Company, 2017. [Online]. Available: https://cwmatthews.com/projects/i-85-bridge-collapse-repair/. [Accessed 15 November 2025].

120. Honey Run Coverd Bridge Association, "ABOUT HONEY RUN COVERED BRIDGE ASSOCIATION," Honey Run Coverd Bridge Association, [Online]. Available: https://www.hrcoveredbridge.org/abouthrcba?utm_source=chatgpt.com. [Accessed 25 July 2025].

121. Witcher, T.R., "Fifty Years of Preservation: Historic American Engineering Record," *Civil Engineering,* vol. 89, no. 1, pp. 40-43, 2019.

122. Robertson, M., "132-year-old Honey Run Covered Bridge, the last of its kind, destroyed by wildfire," SFGate, 9 November 2018. [Online]. Available: https://www.sfgate.com/california-wildfires/article/honey-run-covered-bridge-destroyed-chico-fire-13379409.php?utm_source=chatgpt.com. [Accessed 25 July 2025].

123. Matt, J., "Paradise Redux," Places, March 2024. [Online]. Available: https://www.sfgate.com/california-wildfires/article/honey-run-covered-bridge-destroyed-chico-fire-13379409.php?utm_source=chatgpt.com. [Accessed 25 July 2025].

124. Derbeken, J.V., "No Audit of PG&E High-Voltage Power Line Linked to Camp Fire: Investigation," NBC Bay Area, 21 November 2018. [Online]. Available: https://www.nbcbayarea.com/news/local/no-audit-of-pge-high-voltage-power-line-linked-to-camp-fire-investigation/202581/. [Accessed 25 July 2025].

125. Zimmermann, J., "November 2018 Camp Fire," National Oceanic and Atmospheric Association, Salt Lake City, Utah, 2020.

126. Brown, T.; Leach, S.; Wachter, B.; Garunio, B, "The Extereme 2018 Northern California Fire Season," *American Meterological Society,* pp. S1-S4, 2020, https://doi.org/10.1175/BAMS-D-19-0275.1.

127. Maranghides, A.; Link, E.D.; Mell, W.; Hawks, S.; Brown, C.; Walkton, W.D., "A Case Study of Camp Fire," U.S. Department of Commerce, Washington, D.C., 2023, https://doi.org/10.6028/NIST.TN.2252.

128. Vermont Covered Bridge Society, "Honey Run Covered Bridge Lost to Fire," Vermont Covered Bridge Society, [Online]. Available: https://www.vermontbridges.org/california-honey_run_bridge_lost.shtml?utm_source=chatgpt.com. [Accessed 25 July 2025].

129. White, R., "One of just two historic covered bridges in Washington burns in Whitman County fire," The Spokesman-Review, 14 September 2020. [Online]. Available: https://www.spokesman.com/stories/2020/sep/14/one-of-just-two-historic-covered-bridges-in-washin/#:~:text=A%20landmark%20102,still%20burning%20in%20Whitman%20County. [Accessed 25 July 2025].

130. The Bridge Hunter's Chronicles, "Great Western Fires Destroy Iconic Historic Bridges," The Bridge Hunter's Chronicles, 12 September 2020. [Online]. Available: https://bridgehunterschronicles.wordpress.com/2020/09/12/great-western-fires-destroy-iconic-historic-bridges/#:~:text=One%20of%20the%20most%20heart,the%20last%20encased%20truss%20span. [Accessed 25 July 2025].

131. Pine Creek Community Restoration, "History in flames as fires decimate a railroad town and its iconic bridge," Pine Creek Community Restoration, 10 September 2020. [Online]. Available: https://www.pinecreekcommunityrestoration.org/history-in-flames-as-fires-decimate-a-railroad-town-and-its-iconic-bridge/#:~:text=,%E2%80%9D. [Accessed 25 July 2025].

132. Reilly, M.J.; et al., "Cascadia Burning: The historic, but not historically unprecedented, 2020 wildfires in the Pacific Northwest, USA," *Ecosphere,* vol. 13, no. 6, 2022, https://doi.org/10.1002/ecs2.4070.

133. Higuera, P.E.; Abatzoglou, J.T., "Record-setting climate enabled the extraordinary 2020 fire season in the western United States," *Global Change Biology,* 2020, https://doi.org/10.1111/gcb.15388.

134. Giardinelli, C.; et al, "2020 Labor Day fires increase public awareness, money to wildfire fight," KATU 2 ABC, 10 September 2022. [Online]. Available: https://katu.com/news/wildfire-season/2020-labor-day-fires-increase-public-awareness-money-to-wildfire-fight?utm_source=chatgpt.com. [Accessed 25 July 2025].

135. O'Sullivan, J., "Washington state's wildfires have now destroyed more than 626,000 acres, 181 homes," The Seattle Times, 11 September 2020. [Online]. Available: https://www.seattletimes.com/seattle-news/environment/washington-states-wildfires-have-now-destroyed-more-than-626000-acres181-homes/. [Accessed 25 July 2025].

136. Cronwell, P., "1-year-old from Renton killed, parents burned while fleeing Cold Springs fire in Washington state," The Seattle Times, 9 September 2020. [Online]. Available: https://www.seattletimes.com/seattle-news/1-year-old-killed-parents-burned-while-fleeing-cold-springs-fire/. [Accessed 25 July 2025].

137. "Demolition begins on CT overpass damaged in I-95 tanker fire; part of highway to remain closed," 6 ABC Action News, 3 May 2024. [Online]. Available: https://6abc.com/post/where-is-i-95-closed-fiery-crash-norwalk-connecticut-tanker-fire/14760581/#:~:text=For%20three%20hours%2C%20flames%20raged,gallons%20of%20fuel%2C%20caught%20fire. [Accessed 31 July 2025].

138. Cobin, H.F., "Norwalk's Fairfield Ave bridge to be demolished following gasoline tanker fire on I-95," Nancy on Norwalk, 2 May 2024. [Online]. Available: https://www.nancyonnorwalk.com/gasoline-tanker-crash-ignites-i-95-blaze-in-norwalk/#:~:text=tanker%20truck%20carrying%208%2C500%20gallons,hot%20enough%20to%20melt%20steel. [Accessed 31 July 2025].

139. "The Norwalk Fire Department responded to a multi vehicle accident on I-95 near exit 14," City of Norwalk, 3 May 2024. [Online]. Available: https://www.norwalkct.gov/CivicAlerts.aspx?AID=2464. [Accessed 31 July 2025].

140. "DANIEL CARTER BEARD BRIDGE INSPECTION," Facility Inspection & Transportation, [Online]. Available: https://fitengineering.us/portfolio/daniel-carter-beard/#:~:text=The%20Daniel%20Carter%20Beard%20,and%20nearly%20160%20feet%20tall. [Accessed 31 July 2025].

141. "I-471 Daniel Carter Beard Bridge," Cincinnati Transit, [Online]. Available: https://cincinnati-transit.net/bigmac.html#:~:text=Construction%20of%20the%20I,71. [Accessed 31 July 2025].

142. "Daniel Carter Beard Bridge," Structurae, [Online]. Available: https://structurae.net/en/structures/daniel-carter-beard-bridge#:~:text=bridge%20has%20a%20main%20span,the%20Boy%20Scouts%20of%20America. [Accessed 31 July 2025].

143. Swartsell, N., "'One man who likes to start fires': Prosecutor says Big Mac Bridge blaze a random act of arson," NPR, 27 June 2025. [Online]. Available: https://www.wvxu.org/local-news/2025-06-27/prosecutor-big-mac-bridge-fire-arson. [Accessed 31 July 2025].

144. Sanderson, E., "Prosecutor: Man set Big Mac Bridge fire 'because he likes to set fires'," WLWT 5, 27 June 2025. [Online]. Available: https://www.wlwt.com/article/prosecutor-big-mac-bridge-fire-investigation-suspects-sentenced/65219697. [Accessed 31 July 2025].

145. "I-471 Fire Media Center," Ohio Department of Transportation, 1 November 2024. [Online]. Available: https://www.transportation.ohio.gov/about-us/news/district-8/i-471-remains-closed-after-bridge-fire#:~:text=continue%20through%20December. [Accessed 31 July 2025].

146. "I-471 Bridge [12/10 Update]," City of Cincinnati, 11 December 2024. [Online]. Available: https://www.cincinnati-oh.gov/cityofcincinnati/traffic-alerts/i-471-bridge-1210-update/#:~:text=Components%20Starting%20to%20Arrive%20Bronze,January. [Accessed 31 July 2025].

147. Zhang, F.; Shi, L.; Liu, S.; Shi, J.; Shi, C.; Xiang, T., "CFD-Based Fire Risk Assessment and Control at the Historic Dong Wind and Rain Bridges in the Western Hunan Region: The Case of Huilong Bridge," *Sustainability,* vol. 14, no. 19, 2022, https://doi.org/10.3390/su141912271.

148. Cui, Z.; Chun, Q., "Experimental and numerical study on fire development process and fire risk assessment of historic timber lounge bridges," *Heritage Science,* vol. 12, 2024, https://doi.org/10.1186/s40494-024-01525-6.

149. Mostofi, S.; Altunisik, A.C.; Akbulut, Y.E.; Okur, F.Y., "A Simulation-Based Investigation on Thermal Responses of Suspension Bridge Tower Under Different Fire Scenarios," *Arabian Journal for Science and Engineering,* vol. 50, pp. 1945-1967, 2024, https://doi.org/10.1007/s13369-024-09063-w.

150. Zhao, X.; Zhang, G.; Tang, C.; Wang, S.; Lu, Z., "Evaluating fire performance of through continuous composite steel Warren-truss bridge girders: Experimental and numerical investigation," *Engineering Structures,* vol. 326, 2025, https://doi.org/10.1016/j.engstruct.2024.119591.

151. Song, C.; Zhang, G.; Li, X.; Kodur, V., "Experimental and numerical study on failure mechanism of steel-concrete composite bridge girders under fuel fire exposure," *Engineering Structures,* vol. 247, 2021, https://doi.org/10.1016/j.engstruct.2021.113230.

152. Gong, X.; Agrawal, A.K., "Safety of Cable-Supported Bridges during Fire Hazards," *Journal of Bridge Engineering,* vol. 21, no. 4, 2016, https://doi.org/10.1061/(ASCE)BE.1943-5592.0000870.

153. Chen, W.; Chen, X.; Shen, R.; Qi, D.; Li, Z., "Fire resistance analysis and protection measures for cable components of suspension bridges," *Journal of Constructional Steel Research,* vol. 220, 2024, https://doi.org/10.1016/j.jcsr.2024.108852.

154. Song, X.; Wang, Z.; Ge, S.; Li, W.; Lu, J.; An, W., "Study on flame height and temperature distribution of double-deck bridge fire based on large-scale fire experiments," *Thermal Science and Engineering Progress,* vol. 47, 2024, https://doi.org/10.1016/j.tsep.2023.102319.

155. Zhang, G.; Yuan, Z.; Ding, Y.; Xu, F.; Tang, C.; Wang, S., "Fire behavior of composite steel truss bridge girders: numerical investigation and design strategies," *Advances in Bridge Engineering,* vol. 5, no. 36, 2024, https://doi.org/10.1186/s43251-024-00150-4.

156. Li, Y.; Wang, Z.; Wang, C.; Zhang, Y., "Fire effect of steel bridge structure with consideration of leaked combustion fuel on asphalt bridge deck," *Case Studies in Thermal Engineering,* vol. 59, 2024, https://doi.org/10.1016/j.csite.2024.104594.

157. Zhang, Y.K.; Yuan, P.; Geng, B.; Shang, J.N.; Long, B., "A Study on the Thermodynamic Response of Double-Armed Thin-Walled Piers under an FRP Anti-Collision Floating Pontoon Fire," *Buildings,* vol. 14, no. 7, 2024, https://doi.org/10.3390/buildings14071969.

158. Ciftcioglu, A.O.; Naser, M.Z., "Identifying and estimating causal effects of bridge failures from observational data," *Journal of Infrastructure Intelligence and Reslience,* vol. 3, no. 1, 2024, https://doi.org/10.1016/j.iintel.2023.100068.

159. Lee, G.C.; Mohan, S.B.; Huang, C.; Fard, B.N., "A Study of U.S. Bridge Failures 1980-2012," MCEER, Buffalo, NY, 2013.

160. Quiel, S.E.; Pessiki, S.P., "Bridges, Fire, and the Structural Engineer," *Structure,* vol. 25, no. 6, pp. 12-13, 2018.

161. Choi, J.; Haj-Ali, R.; Kim, H.S., "Integrated fire dynamic and thermomechanical modeling of a bridge under fire," *Structural Engineering and Mechanics,* vol. 42, no. 5, 2012, https://doi.org/10.12989/sem.2012.42.6.815.

162. Hedden, J.; Quagliata, M.; Wandzilak, T., "Emergency Renovation," *Steel Bridge News,* pp. 36-39, 2010.

163. Kodur, V.; Aziz, E.; Dwaikat, M., "Evaluating Fire Resistance of Steel Girders in Bridges," *Journal of Bridge Engineering,* vol. 18, no. 7, 2012, https://doi.org/10.1061/(ASCE)BE.1943-5592.0000412.

164. Dowling, V.P., "Ignition of timber bridges in bushfires," *Fire Safety Journal,* vol. 22, no. 2, pp. 145-168, 1994, https://doi.org/10.1016/0379-7112(94)90070-1.

165. De Silva, D.; Gallo, M.; De Falco, L.; Nigro, E., "Fire risk assessment of bridges: from state of the art to structural vulnerability mitigation," *Journal of Civil Structural Health Monitoring,* vol. 13, pp. 1613-1632, 2023, https://doi.org/10.1007/s13349-023-00670-z.

166. NFPA, "Standard for Road Tunnels, Bridges, and Other Limited Access Highways," National Fire Protection Association, Quincy, MA, 2017.

167. Regan, J.W., "Heat Release Rate Characterization of NFPA 1403 Compliant Training Fuels," *Fire Technology,* vol. 57, pp. 1847-1867, 2021, https://doi.org/10.1007/s10694-021-01092-3.

168. Babrauskas, V.; Peacock, R.D., "Heat release rate: The single most important variable in fire hazard," *Fire Safety Journal,* vol. 18, no. 3, pp. 255-272, 1992, https://doi.org/10.1016/0379-7112(92)90019-9.

169. Lattimer, B.Y.; Beitel, J.J., "Evaluation of heat release rate equations used in standard test methods," *Fire and Materials,* vol. 22, no. 7, pp. 167-173, 1999, https://doi.org/10.1002/(SICI)1099-1018(1998070)22:4%3C167::AID-FAM649%3E3.0.CO;2-M.

170. Baheti, A.; Lange, D.; Matsagar, V., "Appropriate Fire Intensity Measures for Reinforced Concrete Beam and Column Elements," *Engineering Structures,* Vols. 323, Volume A, 2025, https://doi.org/10.1016/j.engstruct.2024.119223.

171. Hasemi, Y., "Surface Flame Spread," in *SFPE Handbook of Fire Protection Engineering*, New York, NY, Springer, 2016, https://doi.org/10.1007/978-1-4939-2565-0_23, pp. 705-723.

172. Fernandez-Pello, A.C., "Flame Spread Modeling," *Combustion Science and Technology,* vol. 39, no. 1-6, pp. 119-134, 1984, https://doi.org/10.1080/00102208408923786.

173. Fernandez-Pello, A.C.; Hirano, T., "Controlling Mechanisms of Flame Spread," *Combustion Science and Technology,* vol. 32, no. 1-4, pp. 1-31, 1983, https://doi.org/10.1080/00102208308923650.

174. Gollner, M.J.; Miller, C.H.; Tang, W.; Signh, A.V., "The effect of flow and geometry on concurrent flame spread," *Fire Safety Journal,* vol. 91, pp. 68-78, 2017, https://doi.org/10.1016/j.firesaf.2017.05.007.

175. Fernandez-Pello, A.C., "Flame spread in a forward forced flow," *Combustion and Flame,* vol. 36, pp. 63-78, 1979, https://doi.org/10.1016/0010-2180(79)90046-4.

176. Bu, R.; Zhou, Y.; Huang, X.; Fan, C., "Flame spread over convex and inclined flat surfaces," *Fire Safety Journal,* vol. 141, 2023, https://doi.org/10.1016/j.firesaf.2023.103955.

177. Wichman, I.S., "Theory of opposed-flow flame spread," *Progress in Engergy and Combustion Science,* vol. 18, no. 6, pp. 553-593, 1992, https://doi.org/10.1016/0360-1285(92)90039-4.

178. Zhang, Y.; Fang, J.; Tian, F.; Song, L.; Singh, A.V., "Upward flame spread over discrete thick fuels under mixed convection flow," *Fire Safety Journal,* vol. 135, 2023, https://doi.org/10.1016/j.firesaf.2022.103723.

179. Chen, A.; Yang, S.; Dong, X., "Studies of the combined effects of some important factors on the likelihood of flashover.," *Fire and Materials,* 2011, https://doi.org/10.1002/fam.1045.

180. Ruan, H.; Xia, T.; Wang, Y., "Investigation of flashover occurrence criterion based on thermal equilibrium theory," *Journal of Building Engineering,* vol. 92, 2024, https://doi.org/10.1016/j.jobe.2024.109658.

181. Kim, H.J.; Lilley, D.G., "Flashover: A Study of Parameter Effects on Time to Reach Flashover Conditions," *Journal of Propulsion and Power,* vol. 18, no. 3, 2002, https://doi.org/10.2514/2.5982.

182. Fujiwara, K.; Shibahara, M., "Thermal transport mechanism at a solid-liquid interface based on the heat flux detected at a subatomic spatial resolution," *Physical Review E,* vol. 105, 2022, https://doi.org/10.1103/PhysRevE.105.034803.

183. Yi, W.T.; Cui, X.C.; Du, Z.; Liu, W., "Remove measurment of transient heat flux based on the thermomagnetic effect," *Measurement Science and Technology,* vol. 35, 2024, DOI: 10.1088/1361-6501/ad3e20.

184. Childs, P.R.N.; Greenwood, J.R.; Long, C.A., "Heat flux measurement techniques," *Journal of Mechanical Engineering Science,* vol. 213, no. 7, 1999, https://doi.org/10.1177/095440629921300702.

185. Lloyd, J.; Guinyard, T.; Murphy, S., "Bridge to Be Demolished After Tanker Fire," NBC 7 San Diego, 15 December 2011. [Online]. Available: https://www.nbcsandiego.com/news/local/tanker-fire-60-freeway-bridge-demolition/1913777/. [Accessed 25 July 2025].

186. Leite, R.M.; Centeno, F.R., "Effect of tank diameter on thermal behavior of gasoline and diesel storage tanks fires," *Journal of Hazardous Materials,* vol. 342, pp. 544-552, 2018, https://doi.org/10.1016/j.jhazmat.2017.08.052.

187. Okamoto, K.; Yamasaki, H.; Matsouka, I.; Ichikawa, T.; Matsouka, H.; Saeki, Y.; Honma, M., "Burning behavior and fire hazards of petroleum liquid combustible spills," *Journal of Loss Prevention in the Process Industires,* vol. 90, 2024, https://doi.org/10.1016/j.jlp.2024.105346.

188. Zhao, J.; Song, G.; Zhang, X.; Li, Y.; Zhang, J.; Yang, R., "Experimental investigation and modeling of the spread and burning behaviors of continuous spill fires on a water surface," *Process Safety and Environmental Protection,* vol. 168, pp. 88-95, 2022, https://doi.org/10.1016/j.psep.2022.09.071.

189. Hu, X.J.; Ye, C.H.; Xia, M.Q.; Li, J.X.; Zhang, P.H., "Experimental study of the effect of delayed ignition on the ethanol spill fire behaviour with different channel width in tunnel environment," *International Communiations in Heat and Mass Transfer,* vol. 160, 2025, https://doi.org/10.1016/j.icheatmasstransfer.2024.108335.

190. Ooi, J.B.; Rajanren, J.R.; Ismail, H.M.; Swamy, V.; Wang, X, "Improving combustion characteristics of diesel and biodiesel droplets by graphite oxide addition for diesel engine applications," *International Journal of Energy Research,* 2017, https://doi.org/10.1002/er.3787.

191. Zhang, Z.; Lv, J.; Li, W.; Long, J.; Wang, S.; Tan, D.; Yin, Z., "Performance and emission evaluation of a marine diesel engine fueled with natural gas ignited by biodiesel-diesel blended fuel," *Energy,* vol. 256, 2022, https://doi.org/10.1016/j.energy.2022.124662.

192. He, Z.; Man, J.; Li, G.; Li, H.; Song, Y.; Liu, T. Song, C., "Study on Fire Plume and Surface Temperature Field of Components in Mid Through Steel Box Ribbed Arch Bridge Under Tanker Fire," *Fire Technology,* vol. 61, pp. 2327-2359, 2024, https://doi.org/10.1007/s10694-024-01684-9.

193. Cui, C.; Chen, A.; Ma, R., "Stability assessment of a suspension bridge considering the tanker fire nearby steel-pylon," *Journal of Constructional Steel Research,* vol. 172, 2020, https://doi.org/10.1016/j.jcsr.2020.106186.

194. Quiel, S.; Yokayama, T.; Mueller, K.; Bregman, L.; Marjanishvili, S., "Mitigating the effects of a tanker truck fire on a cable-stayed bridge," in *International Conference on Performance-based and Life-cycle Structural Engineering*, Brisbane, Queensland, Australia, 2015, https://doi.org/10.14264/uql.2016.539.

195. Yu, M.; Chen, Q.; Yao, X; Guo, X.; Hao, T.; Wang, H., "High-Temperature Properties of Long-Span Double-Deck Suspension Bridge under a Tanker Fire," *Advances in Civil Engineering,* 2021, https://doi.org/10.1155/2021/2631346.

196. Wu, X.; Huang, T.; Au, F.T.K.; Li, J., "A Localized Fire Model for Prediction the Surface Temperature of Box Girder Bridges Subjected to Tanker Truck Fire," *Fire Technology,* vol. 56, pp. 2059-2087, 2020, https://doi.org/10.1007/s10694-020-00966-2.

197. Lee, J.Y.;Kim, H., "Fire Characteristics for Spill Rate of Light Oil and Methanol," *Journal of the Korean Society of Safety,* vol. 31, no. 5, pp. 54-60, 2016, https://doi.org/10.14346/JKOSOS.2016.31.5.54.

198. Date, A.W., "Combustion of Particles and Droplets," in *Analytic Combustion*, Singapore, Springer, 2020, https://doi.org/10.1007/978-981-15-1853-9_10, pp. 263-306.

199. Chang, L.; Rangwala, A., "Hydrocarbon Fuel Burning Analysis Using a Variable B-Number on Turbulent Water Surface with Immersed Thermal Conductors," *Combustion Science and Technology,* 2025, https://doi.org/10.1080/00102202.2025.2453035.

200. Lei, J.; Deng, W.; Liu, Z.; Mao, S.; Saito, K.; Tao, Y.; Wu, H.; Xie, C., "Experimental study on burning rates of large-scale hydrocarbon pool fires under controlled wind conditions," *Fire Safety Journal,* vol. 127, 2022, https://doi.org/10.1016/j.firesaf.2021.103517.

201. Mao, S.; Liu, S.; Yu, S.; Li, B.; Hao, W.; Chen, H., "Experimental investigation of the burning characteristics of aviation fuel under atmospheric crosswind conditions," *Fuel,* Vols. 332, Part 1, 2023, https://doi.org/10.1016/j.fuel.2022.125981.

202. Hong, M.C.; Merci, B.; Beji, T., "On the use of natural and forced convection correlations in predictive CFD simulations of liquid pool fires," *Fire Safety Journal,* vol. 137, 2023, https://doi.org/10.1016/j.firesaf.2023.103765.

203. Sung, K.; Chen, J.; Brundy, M.; Hamins, A., "The characteristics of a 1 m methanol pool fire," *Fire Safety Journal,* vol. 120, 2021, https://doi.org/10.1016/j.firesaf.2020.103121.

204. Wang, Z.; Hou, S.; Muchen, Z.; Xu, J.; Gao, Z.; Cozzani, V.; Zhang, B., "Assessment of the mass burning rate of LNG pool fires by a validated CFD model," *Process Safety and Environmental Protection,* vol. 168, pp. 642-653, 2022, https://doi.org/10.1016/j.psep.2022.10.019.

205. Zhang, B.; Laboureur, D.M.; Gopalaswami, N.; Mannan, M.S., "Experimental Study of a Liquefied Natural Gas Pool Fire on Land in the Field," *Industrial & Engineering Chemistry Research,* vol. 57, no. 42, pp. 14297-14306, 2018, https://doi.org/10.1021/acs.iecr.8b02087.

206. Zhai, X.; Chen, P.; Sun, S.; Liu, Y.; Li, L., "Experimental study on heat transfer and propagation speed of spill fire on porous media substrate with micro-inclination," *International Communications in Heat and Mass Transfer,* Vols. 145, Part B, 2023, https://doi.org/10.1016/j.icheatmasstransfer.2023.106860.

207. Hu, X.J.; Ye, C.H.; Li, J.X.; Shang, R.X.; Zhang, P.H., "Experimental study of the effect of delayed ignition on ethanol spill fire behavior on inclined surfaces," *International Journal of Thermal Sciences,* vol. 203, 2024, https://doi.org/10.1016/j.ijthermalsci.2024.109136.

208. Kong, D.; Yang, H.; He, Y., "Impact of wind on in-situ burning behavior of spilled oil on open water," *Journal of Loss Prevention in the Process Industries,* vol. 60, 2020, https://doi.org/10.1016/j.jlp.2020.104147.

209. Li, H.; Li, Z.; Wang, Q.; Huang, Y.; Tang, F., "Heat transfer and spread characteristics of continuous ethanol spill fires on sand substrates," *Process Safety and Environmental Protection,* vol. 176, pp. 528-536, 2023, https://doi.org/10.1016/j.psep.2023.06.032.

210. Ye, C.; Hu, X.; Xia, M.; Li, J.; Zhang, P., "Experimental investigation on the combustion phenomena and heat transfer mechanism of ethanol spill fire with different initial fuel temperatures," *Journal of Thermal Analysis and Calorimetry,* vol. 149, pp. 2351-2363, 2024, https://doi.org/10.1007/s10973-023-12796-9.

211. Zhao, J.; Song, G.; Zhang, X.; Li, Y.; Zhang, J.; Yang, R., "Experimental investigation and modeling of the spread and burning behaviors of continuous spill fires on a water surface," *Process Safety and Environmental Protection,* pp. 88-95168, 2022, https://doi.org/10.1016/j.psep.2022.09.071.

212. Li, Y.; Meng, D.; Yang, L.; Shuai, J., "Experimental study on the burning rate of continuously released spill fire on open surface with measurement of burning fuel thickness," *Case Studies in Thermal Engineering,* vol. 36, 2022, https://doi.org/10.1016/j.csite.2022.102217.

213. Hynynen, J.; Quant, M.; Pramanik, R.; Olofosson, A.; Li, Y.Z.; Arvidson, M.; Andersson, P., "Electric vehicle fire safety in enclosed spaces," *RISE,* 2023.

214. Li, D.; Zhu, G.; Zhu, H.; Yu, Z.; Gao, Y.; Jiang, X., "Flame spread and smoke temperature of full-scale fire test of car fire," *Case Studies in Thermal Engineering,* Vols. 10, No. C, pp. 315-324, 2017, https://doi.org/10.1016/j.csite.2017.08.001.

215. Zhu, H.; Gao, Y.; Guo, H., "Experimental investigation of burning behavior of a running vehicle," *Case Studies in Thermal Engineering,* vol. 22, 2020, https://doi.org/10.1016/j.csite.2020.100795.

216. Shintani, Y.; Kakae, N.; Harada, K., "Experimental Investigation of Burning Behavior of Automobiles," in *6th Asian-Oceania Symposium on Fire Science and Technology*, Daegu, Korea, 2004.

217. Kang, S.; Kwon, M.; Choi, J.Y.; Choi, S., "Full-scale fire testing of battery electric vehicles," *Applied Energy,* vol. 332, 2023, https://doi.org/10.1016/j.apenergy.2022.120497.

218. Tewarson, A., "Fire Environment In Partially Vented Automobile Crash Fires," *Fire Safety Science,* vol. 8, pp. 1205-1216, 2005, http://dx.doi.org/10.3801/IAFSS.FSS.8-1205.

219. Xu, P.; Zhu, D.; Li, L; Chen, K.; Lin, B.; Li, L., "Study on the key parameters of vehicle fires for the growth stage in tunnels," *Fire and Materials,* vol. 48, no. 1, pp. 128-137, 2023, https://doi.org/10.1002/fam.3172.

220. Bai, L; Cheng, F.; Dong, Y., "Ignition Characteristics and Flame Behavior of Automotive Lubricating Oil on Hot Surfaces," *Processes,* vol. 12, no. 11, 2024, https://doi.org/10.3390/pr12112522.

221. Park, Y.; Ryu, J.; Ryou, H.S., "Experimental Study on the Fire-Spreading Characteristics and Heat Release Rates of Burning Vehicles Using a Large Scale Calorimeter," *Energies,* vol. 12, 2019, http://dx.doi.org/10.3390/en12081465.

222. Koromila, I.A.; Spyrou, K.J., "Design Fire Methodology for Vehicle Spaces Onboard Ships," *Fire Technology,* vol. 59, pp. 1725-1759, 2023, https://doi.org/10.1007/s10694-023-01403-w.

223. Shi, B.; Jia, K.; Ge, S.; He, C.; Zhao, J., "Numerical simulation study on temperature characteristics of double-deck suspension bridge in vehicle fires," *Case Studies in Thermal Engineering,* vol. 65, 2025, https://doi.org/10.1016/j.csite.2024.105626.

224. Timilsina, S.; Yazdani, N.; Beneberu, E., "Post-fire analysis and numerical modeling of a fire-damaged concrete bridge," *Engineering Structures,* vol. 244, 2021, https://doi.org/10.1016/j.engstruct.2021.112764.

225. Woodworth, M.A., "Fire Hazard Assessment for Highway Bridges with Thermal Mechanical Modeling," 27 June 2013. [Online]. Available: https://vtechworks.lib.vt.edu/bitstream/handle/10919/23683/Woodworth_MA_D_2013.pdf#:~:text=Year. [Accessed 28 July 2025].

226. Phares, B.; Wipf, T.; Sievers, R.; Hosteng, T., "Covered Bridge Security Manual," May 2013. [Online]. Available: https://www.fpl.fs.usda.gov/documnts/fplgtr/fpl_gtr223.pdf#:~:text=ing%20neglect%2C%20arson%2C%20vandalism%2C%20and,of%20complexity%20to%20the%20situation. [Accessed 28 July 2025].

227. National Society for the Preservation of Covered Bridges, "Arson Reduction Incentive," National Society for the Preservation of Covered Bridges, 25 July 2025. [Online]. Available: https://www.coveredbridgesociety.org/arson.htm#:~:text=Over%20the%20past%20five%20decades%2C,to%20their%20historic%20covered%20bridges. [Accessed 28 July 2025].

228. The Columbus Dispatch, "Ohio's Historic Bridges Falling Prey to Arsonists," Firehouse, 4 September 2013. [Online]. Available: https://www.firehouse.com/home/news/11141007/ohio-historic-bridges-falling-prey-to-arsonists. [Accessed 28 July 2025].

229. Jordan, F., "Prosecutor: Big Mac Bridge fire caused by 'one man who set the fire because he likes to set fires'," WCPO Cinicinnati, 27 June 2025. [Online]. Available: https://www.wcpo.com/news/local-news/following-sentencing-of-all-4-suspects-prosecutor-to-discuss-conclusion-of-big-mac-bridge-fire-case#:~:text=and%20last%20updated%206%3A32%20PM%2C,Jun%2027%2C%202025. [Accessed 28 July 2025].

230. Solis, N.; Vives, R.; Winton, R.; Dixson, B.; Ahn, A., "Arson is behind the massive fire that shut down the 10 Freeway, officials say," Los Angeles Times, 13 November 2023. [Online]. Available: https://www.latimes.com/california/story/2023-11-13/10-freeway-closure-snarls-commute-after-huge-downtown-los-angeles-fire. [Accessed 28 July 2025].

231. Deliso, M., "I-10 freeway in Los Angeles reopens; search for person of interest in fire continues," ABC News, 19 November 2023. [Online]. Available: https://abcnews.go.com/US/person-interest-sought-connection-10-freeway-fire-los/story?id=105006373. [Accessed 28 July 2025].

232. OSHA, "Fire Watch Duties during Hot Work," [Online]. Available: https://www.osha.gov/sites/default/files/publications/OSHA4188.pdf?utm_source=chatgpt.com. [Accessed 28 July 2025].

233. Li, Y.; Wang, Z.; Wang, C.; Zhang, Y.; Ma, H.; Liu, L., "Fire Effect and Performance of Bridge Pylon Columns under Construction," *Fire,* vol. 6, no. 10, 2023, https://doi.org/10.3390/fire6100387.

234. Duchon, Vives, R., "All lanes of Interstate 15 reopen after massive bridge fire," 7 May 2014. [Online]. Available: https://www.latimes.com/local/lanow/la-me-ln-interstate-15-in-hesperia-reopens-both-directions-20140507-story.html. [Accessed 28 July 2025].

235. El-Ghobashy, T., "Metro-North Service Resumes After Bridge Fire," The Wall Street Journal, 20 September 2010. [Online]. Available: https://www.wsj.com/articles/SB10001424052748703989304575503881216032288?gaa_at=eafs&gaa_n=ASWzDAjFZmjtzo_WpxVzsK7Nt3lm1P9tzlpI32-YX6hiYDorE-EDrmkWkOJO&gaa_ts=688a7a61&gaa_sig=xQDUkeQrOWOCNZb7RL-9wNy0dXd1I-nJnJAwb-7GV6gY4u4lOaH5CY7bUvDyAWmZ_Rm_CqbzrUT_lJf. [Accessed 30 July 2025].

236. Zhou, H.; Leng, J.; Zhou, M.; Chun, Q., "China's unique woven timber arch bridges," *ICE Proceedings Civil Engineering,* vol. 171, no. 3, 2018, http://dx.doi.org/10.1680/jcien.17.00046.

237. Di Virgillo, G.; Evans, J.P.; Blake, S. A.P.; Armstrong, M.; Dowdy, A.J.; Sharples, J.; McRae, R., "Climate Change Increases the Potential for Extreme Wildfires," *Geophysical Research Letters,* vol. 46, no. 14, pp. 8517-8526, 2019, https://doi.org/10.1029/2019GL083699.

238. Refai, R., "Bridges and Wildfire Events: Identifying Information Gaps in Bridge Protecton in the Context of Resistance to Wildland Fire Events," FPInnovations, Vancourver, British Columbia, Canada, 2020.

239. Cunningham, C.X.; Williamson, G.J.; Bowman, D.M.J.S., "Increasing frequency and intensity of the most extreme wildfires on Earth," *Nature, Ecology, & Evolution,* vol. 8, pp. 1420-1425, 2024, https://doi.org/10.1038/s41559-024-02452-2.

240. Hansen, T.G., "Wildfire Damage of Geotechnical Assets," in *Rocky Mountain Geo-Conference*, Westminster, Colorado, 2022, https://doi.org/10.1061/9780784484517.008.

241. Dissanayake, A.P.; Setunge, S.; Venkatesan, S.; Moinuddin, K.A.M.; Sutherland, D., "Numerical assessment of composite bridges subjected to Wildland Urban Interface (WUI) fires," in *Maintenance, Safety, Risk, Management, and Live-Cycle Performance of Bridges*, 2018, Numerical assessment of composite bridges subjected to Wildland Urban Interface (WUI) fires.

242. Kganyago, M.; Shikwambana, L., "Assessment of the Characteristics of Recent Major Wildfires in the USA, Australia, and Brazil in 2018-2019 Using Multi-Source Satellite Products," *Remote Sensing,* vol. 12, 2020, http://dx.doi.org/10.3390/rs12111803.

243. Varga, K.; Jones, C.; Trugman, A.; Carvalho, L.M.V.; McLoughlin, N.; Seto, D.; Thompson, C.; Daum, K., "Megafires in a Warming World: What Wildfire Risk Factors Lead to California's Largest Recorded Wildfire," *Fire,* vol. 5, 2022, https://doi.org/10.3390/fire5010016.

244. Cruz, M.G.; Hoffman, C.M.; Fernandes, P.M., "Global Synthesis of Quantification of Fire Behavior Characteristics in Forests and Shrublands: Recent Progress," *Fire Science and Management,* vol. 11, no. 8, 2025, https://doi.org/10.1007/s40725-024-00241-5.

245. Sullivan, A.L., "Inside the Inferno: Fundamental Processes of Wildland Fire Behaviour - Part 1: Combustion Chemistry and Heat Release," *Fire Science and Management,* vol. 3, pp. 132-149, 2017, https://doi.org/10.1007/s40725-017-0057-0.

246. Balik, J.A.; Coop, J.D.; Krawchuk, M.A.; Naficy, C.E.; Parisien, M.A.; Parks, S.A.; Stevens-Rumann, C.S.; Whitman, E., "Biogeographic patterns of daily wildfire spread and extremes across North America," *Frontiers,* 2024, https://doi.org/10.3389/ffgc.2024.1355361.

247. Duwane, A.; Castellnou, M.; Brotons, L, "Towards a comprehensive look at global drivers of novel extreme wildfire events," *Climatic change,* vol. 162, 2021, https://doi.org/10.1007/s10584-021-03066-4.

248. Nauslar, N.J.; Abatzoglou, J.T.; Marsh, P.T., "The 2017 North Bay and Southern California Fires: A Case Study," *Fire,* vol. 1, no. 18, 2018, http://dx.doi.org/10.3390/fire1010018.

249. Dunbar, U.; Selamet, S., "Fire load and fire growth characteristics in modern high-rise buildings," *Fire Safety Journal,* vol. 135, 2023, https://doi.org/10.1016/j.firesaf.2022.103710.

250. Fontana, M.; Kohler, J.; Fischer, K.; De Sanctis, G., "Fire Load Density," in *SFPE Handbook of Fire Protection Engineering*, New York, NY, Springer, 2016, https://doi.org/10.1007/978-1-4939-2565-0_35.

251. Nayak, N.; Subramanian, L.P., "Fuel loads and their composition, and compartment characteristics in educational, office, and library buildings," *Fire and Materials,* vol. 48, no. 2, pp. 208-221, 2023, https://doi.org/10.1002/fam.3178.

252. Ding, Y.; Cheung, W.K.; Zhang, Y.; Huang, X., "Digitized fuel load survey in commercial and university office buildings for fire safety assessment," *Fire Safety Journal,* Vols. 150, Part B, 2024, https://doi.org/10.1016/j.firesaf.2024.104287.

253. Price, O.F.; Gordon, C.E., "The potential for LiDAR technology to map fire fuel hazard over large areas of Australian forest," *Journal of Environmental Management,* vol. 181, pp. 663-673, 2016, https://doi.org/10.1016/j.jenvman.2016.08.042.

254. Dzolev, I.; Laban, M.; Draganic, S., "Survey based fire load assessment and impact analysis of fire load increment on fire development in contemporary dwellings," *Safety Science,* vol. 135, 2021, https://doi.org/10.1016/j.ssci.2020.105094.

255. Chow, W.K., "Fuel Load and Peak Heat Release Rate Correlations in Post-Flashover Room Fires," *Heat Transfer Engineering,* vol. 31, no. 3, pp. 250-254, 2010, https://doi.org/10.1080/01457630903304681.

256. Gazi, M.E.; Sonnier, R.; Giraud, S.; Batistella, M.; Basak, S.; Dumazert, L.; Hajj, R.; Hage, R.E., "Fire Behavior of Thermally Thin Materials in Cone Calorimeter," *Polymers,* vol. 13, 2021, https://doi.org/10.3390/polym13081297.

257. Zhu, W.; Xu, N.; Hower, J.C., "Unveiling the predictive power of machine learning in coal gross calorific value estimation: An interpretability perspective," *Energy,* vol. 318, 2025, https://doi.org/10.1016/j.energy.2025.134781.

258. De Paulo, E.H.; Dos Santos, F.D.; Folli, G.S.; Santos, L.P.; Nascimento, M.H.C.; Moro, M.K.; Da Cunha, P.H.P.; Castro, E.V.R.; Neto, A.C.; Filgueiras, P.R., "Determination of gross calorific value in crude oil by variable selection methods applied to 13C NMR spectroscopy," *Fuel,* vol. 311, 2022, https://doi.org/10.1016/j.fuel.2021.122527.

259. Dhamodaran, G.; Esakkimuthu, G.S.; Palani, T., "Feasibility of adding N-Butanol and di isopropyl ether with gasoline on its physico-chemical properties," *Petroleum Science and Technology,* vol. 40, no. 4, 2022, https://doi.org/10.1080/10916466.2021.2003383.

260. Patel, N.; Shadangi, K.P.; Kar, P.K., "Pyrolytic oil blended gasoline as future fuel: pyrolysis mechanism, fuel properties, and composition analysis," *Advances in Chemical and Environmental Engineering,* vol. 29, pp. 86400-86417, 2022, https://doi.org/10.1007/s11356-022-19776-w.

261. Ismaila, A.; Nasiru, R.; Kaisan, M.U.; Garba, N.N., "Determination of Energy of Plant Biomass for Domestic and Small-Scale Industrial Heating Applications," *FUDMA Journal of Sciences,* vol. 8, no. 1, pp. 362-368, 2024, https://doi.org/10.33003/fjs-2024-0801-.

262. Ozyuguran, A.; Yaman, S., "Prediction of Calorific Value of Biomass from Proximate Analysis," *Energy Procedia,* vol. 107, pp. 130-136, 2017, https://doi.org/10.1016/j.egypro.2016.12.149.

263. Finney, M.A.; Cohen, J.D.; Forthofer, J.M; McAllister, S.S.; Gollner, M.J.; Gorham, D.J.; Saito, K.; Akafuah, N.K.; Adam, B.A.; English, J.D., "Role of buoyant flame dynamics in wildfire spread," *Environmental Sciences,* vol. 112, no. 32, 2015, https://doi.org/10.1073/pnas.1504498112.

264. Battaglia, F.; Mcgrattan, K.; Rehm, R.; Baum, H., "Simulating fire whirls," *Combustion Theory and Modelling,* vol. 4, no. 2, pp. 123-138, 2000, https://doi.org/10.1088/1364-7830/4/2/303.

265. Xiao, T.; Gupta, V.; MacFarlane, A.R.W.; Kennedy, C.; Dunn, M.J.; Kourmatzis, A.; Torero, J.L.; Masri, A.R., "On the structure of buoyant fires with varying levels of fuel-turbulence," *Combustion and Flame,* vol. 257, 2023, https://doi.org/10.1016/j.combustflame.2023.112993.

266. Tokami, T.; Hachijo, T.; Miyano, T.; Gotoda, H., "Spatiotemporal dynamics of a buoyancy-driven turbulent fire," *Physical Review E,* vol. 101, 2020, https://doi.org/10.1103/PhysRevE.101.042214.

267. Khan, N.; Suterland, D.; Wadhwani, R.; Moinuddin, K., "Physics-Based Simulation of Heat Load on Structures for Improving Construction Standards for Bushfire Prone Areas," *Frontiers in Mechanical Engineering,* vol. 5, 2019, https://doi.org/10.3389/fmech.2019.00035.

268. Wei, J.; Zhang, C., "A refined cylinder fire model for thermal radiation calculation from localized fire to exposed horizontal surface," *International Journal of Heat and Mass Transfer,* vol. 227, 2024, https://doi.org/10.1016/j.ijheatmasstransfer.2024.125539.

269. Lattimer, B.Y.; Mealy, C.; Beitel, J., "Heat Fluxes and Flame Lengths from Fires Under Ceilings," *Fire Technology,* vol. 49, pp. 269-291, 2012, https://doi.org/10.1007/s10694-012-0261-1.

270. Huang, X.; Wang, Y.; Zhu, H.; He, L.; Tang, F.; Wen, J., "Experimental study on the radiant heat flux of wall-attached fire plume generated by rectangular sources," *International Journal of Thermal Sciences,* vol. 159, 2020, https://doi.org/10.1016/j.ijthermalsci.2020.106605.

271. Fan, X.; Tang, F.; Zhu, N.; Hu, L., "Study on the flame radiative heat transfer and near-field radiation heat flux predictive model of vehicle fires in a tunnel," *International Journal of Heat and Mass Transfer,* vol. 228, 2024, https://doi.org/10.1016/j.ijheatmasstransfer.2024.125666.

272. Michaletz, S.; Johnson, E.A., "How forest fires kill trees: A review of the fundamental biophysical processes," *Scandinavian Journal of Forest Research,* vol. 22, no. 6, 2007, http://dx.doi.org/10.1080/02827580701803544.

273. Heskestad, G., "Fire Plumes, Flame Height, and Air Entrainment," in *SFPE Handbook of Fire Protection Engineering*, New York, NY, Springer, 2016, https://doi.org/10.1007/978-1-4939-2565-0_13, pp. 396-428.

274. Drysdale, D., "Diffusion Flames and Fire Plumes," in *An Introduction to Fire Dynamics*, 2011, https://doi.org/10.1002/9781119975465.ch4.

275. Sun, X.; Zhang, X.; Tang, F.; Ren, F.; Lv, J.; Chen, X.; Hu, L., "Experimental study of ejected fire plume from an opening under facing wind passing through the roof," *Fire Safety Journal,* vol. 141, 2023, https://doi.org/10.1016/j.firesaf.2023.103973.

276. Heskestad, G., "Engineering relations for fire plumes," *Fire Safety Journal,* vol. 7, no. 1, pp. 25-32, 1984, https://doi.org/10.1016/0379-7112(84)90005-5.

277. Kaczorek-Chrobak, K.; Fangrat, J., "Combustible Material Content vs. Fire Properties of Electric Cables," *Energies,* vol. 13, 2020, http://dx.doi.org/10.3390/en13236172.

278. Chen, C.; Chen, J.; Zhao, X.; Shi, C., "Experimental investigation on combustion characteristics of steel cable for cable-stayed bridge," *Journal of Thermal Analysis and Caloimetry,* vol. 134, pp. 2317-2327, 2018, https://doi.org/10.1007/s10973-018-7689-6.

279. Guo, Q.; Root, K.J.; Carlton, A.; Quiel, S.E.; Naito, C.J., "Framework for rapid prediction of fire-induced heat flux on concrete tunnel liners with curved ceilings," *Fire Safety Journal,* vol. 109, 2019, https://doi.org/10.1016/j.firesaf.2019.102866.

280. Kodur, V.; Gil, A., "Fire hazard in concrete bridges: review, assessment and mitigation strategies," *Structure and Infrastructure Engineering,* 2022, https://doi.org/10.1080/15732479.2022.2152465.

281. Jiang, H.; Teng, J.; Wang, D.; Zhou, L.; Chen, Y., "Numerical Investigation of the Wan'an Bridge Fire and the Protection Effect of Intumescent Flame-Retardant Coatings," *Fire,* vol. 8, no. 5, 2025, https://doi.org/10.3390/fire8050184.

282. Li, H.T.; Young, B., "Material properties of cold-formed high strength steel at elevated temperatures," *Thin-Walled Structures,* vol. 115, pp. 289-299, 2017, https://doi.org/10.1016/j.tws.2017.02.019.

283. Chen, J.; Young, B.; Uy, B., "Behavior of High Strength Structural Steel at Elevated Temperatures," *Jounral of Structural Engineering,* vol. 132, no. 12, 2006, https://doi.org/10.1061/(ASCE)0733-9445(2006)132:12(1948).

284. Li, G.Q.; Song, L.X., "Mechanical properties of TMCP Q690 high strength structural steel at elevated temperatures," *Fire Safety Journal,* vol. 116, 2020, https://doi.org/10.1016/j.firesaf.2020.103190.

285. Wang, W.; Zhang, Y.; Xu, L.; Li., X., "Mechanical properties of high-strength Q960 steel at elevated temperature," *Fire Safety Journal,* vol. 114, 2020, https://doi.org/10.1016/j.firesaf.2020.103010.

286. Rezaeian, A.; Keshavarz, M.; Hajjari, E., "Mechanical properties of steel welds at elevated temperatures," *Journal of Construction Steel Reserch,* vol. 167, 2020, https://doi.org/10.1016/j.jcsr.2019.105853.

287. Senin, S.F.; Talaha, N.A.A.; Hamid, R., "Condition Assessment of Fire-Affected RC Slab Via GPR Signal Reflections Analysis and Visual Inspection Method," *International Journal of Engineering and Technology,* vol. 8, no. 12, 2018, https://doi.org/10.14419/ijet.v8i1.2.24874.

288. Stefan, R.; Foglar, M., "Visualization and analysis of concrete specimens damage after fire and blast experiments," *Materials Science and Engineering,* vol. 596, 2019, DOI:10.1088/1757-899X/596/1/012040.

289. Mukupa, W.; Hancock, C.; Roberts, G.; Al-Manasir, K.; De Ligt, H.; Chen, Z., "Visual inspection of fire-damaged concrete based on terrestrial laser scanner data," *Applied Geomatics,* vol. 9, pp. 143-158, 2017, https://doi.org/10.1007/s12518-017-0188-9.

290. Short, N.R.; Purkiss, J.A.; Guise, S.E., "Assessment of fire damaged concrete using colour image analysis," *Construction and Building Materials,* vol. 15, no. 1, pp. 9-15, 2001, https://doi.org/10.1016/S0950-0618(00)00065-9.

291. Zhang, G.; Song, C.; Li. X.; He, S.; Huang, Q., "Fire Performance of Continuous Steel-Concrete Composite Bridge Girders," *KSCE Journal of Civil Engineering,* vol. 28, no. 3, pp. 973-984, 2021, https://doi.org/10.1007/s12205-021-0985-x.

292. Nahid, M.N.H.; Sotelino, E.D.; Lattimer, B.Y., "Thermo-Structural Response of Highway Bridge Structures with Tub Girders and Plate Girders," *Journal of Bridge Engineering,* vol. 22, no. 10, 2017, https://doi.org/10.1061/(ASCE)BE.1943-5592.0001029.

293. Shen, K.; Jiang, Z.; Zhao, J.; Ahou, Z.; Wu, Q.; Qiang, Q.; Wang, H., "Fire-resistance design and experimental research for the stay cables of super-long span cable-stayed bridge," *Advances in Bridge Engineering,* vol. 6, 2025, https://doi.org/10.1186/s43251-024-00153-1.

294. Liu, Z.; Lou, G.; Hou, J.; Li, G., "Designing a Two-Level Steel Cable-stayed Bridge against Fires," *Structural Engineering International,* vol. 33, no. 4, pp. 569-575, 2023, https://doi.org/10.1080/10168664.2023.2171331.

295. Li, Q.; Guo, H.; Zhou, J.; Wang, M., "Fridge Fire Vulnerability Hierarchy Assessment Based on Weighted Topsis Method," *Sustainability,* vol. 14, 2022, https://doi.org/10.3390/su142114174.

296. Pizarro, A.; Manfreda, S.; Tubaldi, E., "The Science behind Scour at Bridge Foundations: A Review," *Water,* vol. 12, 2020, http://dx.doi.org/10.3390/w12020374.

297. Wang, C.; Yu, X.; Liang, F., "A review of bridge scour: mechanism, estimation, monitoring and countermeasures," *Natural Hazards,* vol. 87, pp. 1881-1906, 2017, https://doi.org/10.1007/s11069-017-2842-2.

298. Deng, L.; Cai, C.S., "Bridge Scour: Prediction, Modeling, Monitoring, and Countermeasures—Review," *Practice Periodical on Structural Design and Construction,* vol. 15, no. 2, 2009, https://doi.org/10.1061/(ASCE)SC.1943-5576.0000041.

299. Kazemain, A.; Yee, T.; Oguzmert, M.; Amirgholy, M.; Yang, J.; Goff, D., "A review of bridge scour monitoring techniques and developments in vibration based scour monitoring for bridge foundations," *Advances in Bridge Engineering,* vol. 4, 2023, https://doi.org/10.1186/s43251-023-00081-6.

300. Wardhana, K.; Hadipriono, F.C., "Analysis of Recent Bridge Failures in the United States," *Journal of Performance of Constructed Facilities,* vol. 17, no. 3, 2003, https://doi.org/10.1061/(ASCE)0887-3828(2003)17:3(144).

301. DeMello, N.; Bridge, J.A., "A generalized, model-free framework for assessing scour-induced bridge pier instability," *Engineering Structures,* vol. 309, 2024, https://doi.org/10.1016/j.engstruct.2024.118086.

302. Irhayyim, A.; Gunaratne, M.; Fioklou, A., "Assessment of scoured bridges subjected to ship impact," *Structures,* vol. 36, pp. 635-649, 2022, https://doi.org/10.1016/j.istruc.2021.12.023.

303. Shi, X.; Zhou, Z.; Ruan, X., "Forensic Diagnosis on the Overall Collapse of a Composite Box-Girder Bridge," *Structural Engineering International,* vol. 28, no. 1, pp. 51-59, 2018, https://doi.org/10.1080/10168664.2018.1431424.

304. Fiorillo, G.; Ghosn, M., "Fragility analysis of bridges due to overweight traffic load," *Structure and Infrastructure Engineering,* vol. 14, no. 5, pp. 619-633, 2018, https://doi.org/10.1080/15732479.2017.1380675.

305. Biezma, M.V.; Schanack, F., "Collapse of Steel Bridges," *Journal of Performance of Constructed Facilities,* vol. 21, no. 5, 2007, https://doi.org/10.1061/(ASCE)0887-3828(2007)21:5(398).

306. Al-Rashed, R.; Abdelfatah, A.; Yehia, S., "Identifying the Factors Impacting Bridge Deterioration in the Gulf Cooperation Council," *Designs,* vol. 7, 2023, https://doi.org/10.3390/designs7060126.

307. Rao, A.S.; Lepech, M.D.; Kiremidjian, A.S.; Sun, X.Y., "Simplified structural deterioration model for reinforced concrete bridge piers under cyclic loading, " *Structure and Infrastructure Engineering,* vol. 13, no. 1, 2017, https://doi.org/10.1080/15732479.2016.1198402.

308. Milic, I.; Ivankovic, A.M.; Syrkov, A.; Skokandic, D., "Bridge failures, forensic structural engineering and recommendations for design of robust structures," *Gradeviner,* vol. 73, 2021, https://doi.org/10.14256/JCE.3234.2021.

309. Adhikari, R.; Bhatt, L.; Baruwal, R.; Gautam, D.; Rupakhety, R., "Failure investigation of a propped cantilever truss bridge," *Advances in Bridge Engineering,* vol. 5, 2024, https://doi.org/10.1186/s43251-024-00115-7.

310. Malerba, P.G., "Bridge vulnerabilities and collapses: the Italian experience," *Structures and Infrastructure Engineering,* vol. 20, no. 7-8, pp. 976-1001, 2024, https://doi.org/10.1080/15732479.2023.2277362.

311. Zucca, M.; Tattoni, S.; Di Castri, M.; Simoncelli, M., "On the collapse of a post-tensioned reinforced concrete truss bridge during the construction phases," *Engineering Failure Analysis,* vol. 158, 2024, https://doi.org/10.1016/j.engfailanal.2024.107999.

312. Xu, F.Y.; Zhang, M.J.; Wang, L.; Zhang, J.R., "Recent Highway Bridge Collapses in China: Review and Discussion," *Journal of Performance of Constructed Facilities,* vol. 30, no. 5, 2016, https://doi.org/10.1061/(ASCE)CF.1943-5509.0000884.

313. AASHTO LRFD Bridge Design Specifications, Washington, DC: American Association of State Highway and Transportation Officials, 2024.

314. Huang, C.; Chen, L.; He, L.; Zhuo, W., "Comparative assessment of seismic collapse risk for non-ductile and ductile bridges: a case study in China," *Bulletin of Earthquake Engineering,* vol. 19, 2021, https://doi.org/10.1007/s10518-020-00946-5.

315. Abuassi, M.; Bisharah, M., "Machine learning-based assessment of seismic performance in fiber-reinforced polymer (FRP) retrofitted bridges," *Asian Journal of Civil Engineering,* vol. 26, pp. 975-987, 2025, https://doi.org/10.1007/s42107-024-01217-3.

316. Pei, L., "Exploring the Impact of Dynamic Winds on Bridge Safety," *Highlights in Science, Engineering, and Technology,* vol. 137, 2025, https://doi.org/10.54097/sxyffv14.

317. Larsen, A.; Larose, G.L., "Dynamic wind effects on suspension and cable-stayed bridges," *Journal of Sound and Vibration,* vol. 334, pp. 2-28, 2015, https://doi.org/10.1016/j.jsv.2014.06.009.

318. Fang, G.; Pang, W.; Zhao, L.; Xu, K.; Cao, S.; Ge, Y., "Tropical-cyclone-wind-induced flutter failure analysis of long-span bridges," *Engineering Failure Analysis,* vol. 132, 2022, https://doi.org/10.1016/j.engfailanal.2021.105933.

319. Martinelli, L.; Domaneschi, M., "Effect of structural control on wind fatigue mitigation in suspension bridges," *International Journal of Structural Engineering,* vol. 8, no. 4, 2018, https://dx.doi.org/10.1504/IJSTRUCTE.2017.089386.

320. Rackauskaite, E.; Kotsovinos, P.; Jeffers, A.; Rein, G., "Computational analysis of thermal and structural failure criteria of a multi-storey steel frame exposed to fire," *Engineering Structures,* vol. 180, pp. 524-543, 2019, https://doi.org/10.1016/j.engstruct.2018.11.026.

321. Yazici, C., "Mechanical Properties of S235 Steel Protected with Intumescent Coatings Under High Temperatures: An Experimental Study," *Buildings,* vol. 14, no. 6, 2024, https://doi.org/10.3390/buildings14061597.

322. Chen, W.; Qin, Q.; Wang, X.; Li, J.; Liang, M.; Chen, Z.; Yang, T., "Study on the Fire Resistance of Axially Restrained H-Shaped Steel Beams Under Real Fire," *Applied Sciences,* vol. 15, no. 13, 2025, https://doi.org/10.3390/app15137424.

323. AISC, Specifications for Structural Steel Buildings, Chicago, IL: American Insittute of Steel Construction, 2022.

324. Li, Y.; Wang, M.; Li, G.; Jiang, B., "Mechanical properties of hot-rolled structural steels at elevated Temperatures：A review," *Fire Safety Journal,* vol. 119, 2021, https://doi.org/10.1016/j.firesaf.2020.103237.

325. Yan, X.; Xia, Y.; Blum, H.B.; Gernay, T., "Elevated temperature material properties of advanced high strength steel alloys," *Journal of Construction Steel Research,* vol. 174, 2020, https://doi.org/10.1016/j.jcsr.2020.106299.

326. ASTM, Test Methods for Fire Tests of Building Construction and Materials, West Conshohocken, PA: ASTM International, 2024, https://doi.org/10.1520/E0119-24..

327. Wang, X.; Chen, W.; Li, J.; Yang, T., "Fire Resistance Performance of Constrained H-Shaped Steel Columns with Uneven Vertical Temperature Distributions," *Buildings,* vol. 14, no. 19, 2024, https://doi.org/10.3390/buildings14092826.

328. Jiang, B.; Yin, Z.; Zhang, J.; Fan, C.; Li, Y., "Effect of rotational restraint conditions on performance of steel columns in fire," *Engineering Structures,* vol. 238, 2021, https://doi.org/10.1016/j.engstruct.2021.112237.

329. Liu, G.; Meng, H.; Qu, G.; Wang, L.; Ren, L.; Lu, H., "Real-time monitoring and prediction method of commercial building fire temperature field based on distributed optical fiber sensor temperature measurement system," *Journal of Building Engineering,* vol. 70, 2023, https://doi.org/10.1016/j.jobe.2023.106403.

330. Rodrigues, J.P.C.; Neves, I.C.; Valente, J.C., "Experimental research on the critical temperature of compressed steel elements with restrained thermal elongation," *Fire Safety Journal,* vol. 35, no. 2, pp. 77-98, 2000, https://doi.org/10.1016/S0379-7112(00)00018-7.

331. Jiang, B.; Chen, Z.; Yin, Z.; Xiao, L., "Buckling and critical temperatures of restrained H-section steel columns in fire considering dynamic effect," *Fire Safety Journal,* vol. 141, 2023, https://doi.org/10.1016/j.firesaf.2023.104006.

332. Pournaghshband, A.; Afshan, S.; Foster, A.S.J., "Structural fire performance of axially and rotationally restrained stainless steel columns," *Thin-Walled Structures,* vol. 137, pp. 561-572, 2019, https://doi.org/10.1016/j.tws.2019.01.010.

333. Huang, Z.F.; Tan, K.H.; Ting, S.K., "Heating rate and boundary restraint effects on fire resistance of steel columns with creep," *Engineering Structures,* vol. 28, no. 6, pp. 805-817, 2006, https://doi.org/10.1016/j.engstruct.2005.10.009.

334. Valente, J.C.; Neves, I.C., "Fire resistance of steel columns with elastically restrained axial elongation and bending," *Journal of Constructional Steel Research,* vol. 52, no. 3, pp. 319-331, 1999, https://doi.org/10.1016/S0143-974X(99)00033-4.

335. Yang, J.; Shi, Y.; Wang, W.; Xu, L.; Al-azzani, H., "Experimental and numerical studies on axially restrained cold-formed steel built-up box columns at elevated temperatures," *Journal of Constructional Steel Research,* vol. 171, 2020, https://doi.org/10.1016/j.jcsr.2020.106143.

336. Bailey, C.G., "The influence of the thermal expansion of beams on the structural behaviour of columns in steel-framed structures during a fire," *Enineering Structures,* vol. 22, no. 7, pp. 755-768, 2000, https://doi.org/10.1016/S0141-0296(99)00028-0.

337. Huang, D.; Kodur, V.; Wang, W., "Temperature-dependent properties of high-strength steel for evaluating the fire resistance of structures," *Advances in Structural Engineering,* vol. 26, no. 12, 2023, https://doi.org/10.1177/13694332231175232.

338. Azhari, F.; Apon, A.A.H.; Heidarpour, A.; Zhao, X.L.; Hutchenson, C.R., "Mechanical response of ultra-high strength (Grade 1200) steel under extreme cooling conditions," *Construction and Building Materials,* vol. 175, pp. 790-803, 2018, https://doi.org/10.1016/j.conbuildmat.2018.04.191.

339. Keranen, L.; Kangaspouskari, M.; Niskanen, J., "Ultrahigh-strength steels at elevated temperatures," *Journal of Constructional Steel Research,* vol. 183, 2021, https://doi.org/10.1016/j.jcsr.2021.106739.

340. Shi, Y.; Tu, C.; Wu, Y.; Liu, D.; Meng, L.; Ban, H., "Numerical investigations of fire-resistant steel welded I-section columns under elevated temperatures," *Journal of Construction Steel Research,* vol. 177, 2021, https://doi.org/10.1016/j.jcsr.2020.106464.

341. Sauca, A.; Chichi, R.; Zhang, C.; Choe, L., "Critical Temperature of Axially Loaded Steel Members with Wide-Flange Shapes Exposed to Fire," *Engineering Journal,* vol. 58, no. 1, 2021, https://doi.org/10.62913/engj.v58i1.1219.

342. Zhong, Y.; Su, A.; Zhao, O., "Post-fire local buckling behaviour of cold-formed S700 high strength steel circular hollow sections under axial compression: Experiments, modelling and design," *Thin-Walled Structures,* vol. 184, 2023, https://doi.org/10.1016/j.tws.2022.110511.

343. Maia, E.; Couto, C.; Real, P.V.; Lopes, N., "Critical temperatures of class 4 cross-sections," *Journal of Construction Steel Research,* vol. 121, pp. 370-382, 2016, https://doi.org/10.1016/j.jcsr.2016.02.017.

344. Wozniczka, P., "Critical temperature of laterally unrestrained steel plate girders with slender section," *Engineering Structures,* vol. 291, 2023, https://doi.org/10.1016/j.engstruct.2023.116242.

345. Liu, X.; Kuang, S.; Luo, W.; Xie, Z., "Examination of the Behavior of Double Cold-Formed Steel Columns with Σ-Shaped Sections Subjected to Non-Uniform Temperature Conditions," *Fire Technology,* vol. 61, pp. 1491-1533, 2021, https://doi.org/10.1007/s10694-024-01651-4.

346. Roszkowski, P.; Fangrat, J., "Critical temperature of roof trapezoidal steel sheets based on fire resistance tests," *Fire Safety Journal,* vol. 141, 2023, https://doi.org/10.1016/j.firesaf.2023.103855.

347. Laim, L.; Craveiro, H.D.; Simoes, R.; Escudiro, A.; Mota, A., "Experimental analysis of cold-formed steel columns with intermediate and edge stiffeners in fire," *Thin-Walled Structures,* vol. 146, 2020, https://doi.org/10.1016/j.tws.2019.106481.

348. Quan, C.; Kuckler, M., "Cross-section resistance and design of stainless steel CHS and EHS at elevated temperatures," *Engineering Structures,* vol. 285, 2023, https://doi.org/10.1016/j.engstruct.2023.115996.

349. Quan, C.; Kucukler, M., "Stability and design of stainless steel hollow section columns at elevated temperatures," *Engineering Structures,* vol. 297, 2023, https://doi.org/10.1016/j.engstruct.2023.116935.

350. Zhang, C.; Jia, B.; Wang, J., "Influence of artificial cooling methods on post-fire mechanical properties of Q355 structural steel," *Construction and Building Materials,* vol. 252, 2020, https://doi.org/10.1016/j.conbuildmat.2020.119092.

351. Jeanneret, C.; Nicoletta, B.; Robertson, L.; Gales, J.; Kostovinos, P., "Guidance for the post-fire structural assessment of prestressing steel," *Engineering Structures,* vol. 235, 2021, https://doi.org/10.1016/j.engstruct.2021.112023.

352. Ren, S.; Li, G.; Gu, S.; Kong, C.; Han, F.; Li, X.; Gu, Y., "Effect of fire high temperature on mechanical degradation and fracture behavior of steel," *KSCE Journal of Civil Engineering,* vol. 29, no. 1, 2025, https://doi.org/10.1016/j.kscej.2024.100007.

353. Qi, H.H.; Hou, J.; Lou, G.B.; Jiang, Y.; Zhong, B.; Li, G.Q., "Experimental and numerical study on fire-induced collapse of unprotected steel framed structures," *Journal of Constructional Steel Research,* vol. 218, 2024, https://doi.org/10.1016/j.jcsr.2024.108730.

354. Mackiewicz, M.; Krentowski, J.R.; Knyziak, P.; Kowalski, R., "The influence of the fire temperature on the condition of steel roof structure," *Engineering Failure Analysis,* vol. 146, 2023, https://doi.org/10.1016/j.engfailanal.2023.107080.

355. Zheng, Y.H.; Zhong, W.H.; Zhang, Y.; Tan, Z.; Duan, S.C.;Meng, B.; Gao, Y.; Wang, H.C., "Failure mechanism of steel frames with angle steel-bolted connections exposed to fire under progressive collapse condition," *Engineering Failure Analysis,* vol. 155, 2024, https://doi.org/10.1016/j.engfailanal.2023.107744.

356. Jiang, H.; Jin, C.; Yan, L.; Li, Q, Lu, W., "Design method for the relocation of plastic hinges in prefabricated steel beams with corrugated webs," *Plos One,* vol. 16, no. 2, 2021, https://doi.org/10.1371/journal.pone.0246439.

357. Song, X.; Li, H.; Zhang, J., "Experimental investigation into ultra-low cycle fatigue behavior of composite members in spatial grid structures," *Advances in Structural Engineering,* vol. 23, no. 12, 2020, https://doi.org/10.1177/1369433220916941.

358. Cao, Y.; Jiang, J.; Lu, Y.; Chen, W.; Ye, J., "Progressive collapse of steel structures exposed to fire: A critical review," *Journal of Construction Steel Research,* vol. 207, 2023, https://doi.org/10.1016/j.jcsr.2023.107985.

359. Tide, H.R., "Integrity of Structural Steel After Exposure to Fire," *Engineering Journal,* vol. 35, no. 1, 1998, https://doi.org/10.62913/engj.v35i1.691.

360. Guo, Z. Xing, Z.; Xhang, H.; Zhang, H.; Chen, L.; Chen, Y., "Anti-collapse performance assessment of steel beam-column substructures with all-welded connections after exposure to fire," *Journal of Construction Steel Research,* vol. 197, 2022, https://doi.org/10.1016/j.jcsr.2022.107465.

361. Sun, R.; Burgess, I.W.; Huang, Z.; Dong, G., "Progressive failure modelling and ductility demand of steel beam-to-column connections in fire," *Engineering Structures,* vol. 89, pp. 66-78, 2015, https://doi.org/10.1016/j.engstruct.2015.01.053.

362. Fan, S.; Duan, S.; Zeng, S.; Wu, Y.; Ding, R., "Experimental study and numerical simulation analysis of the Bolted-Welded hybrid connection joint of steel frame under fire," *Structures,* vol. 41, pp. 77-78, 2022, https://doi.org/10.1016/j.istruc.2022.04.100.

363. Pancikiewicz,K.; Maslak, M.; Pazdanowski, M.; Stankiewicz, M.; Zajdel, P., "Changes in the microstructure of selected structural alloy steel grades identified after their simulated exposure to fire temperature," *Case Studies in Construction Materials,* vol. 18, 2023, https://doi.org/10.1016/j.cscm.2023.e01923.

364. Zhang, Y.; Cheng, L.; Pan, A.; Hu, C.; Wu, K., "Phase Transformation Temperature Prediction in Steels via Machine Learning," *Materials,* vol. 17, no. 5, 2024, https://doi.org/10.3390/ma17051117.

365. Li, Z.; Yuan, Q.; Xu, S.; Zhou, Y.; Liu, S.; Xu, G., "In Situ Observation of the Grain Growth Behavior and Martensitic Transformation of Supercooled Austenite in NM500 Wear-Resistant Steel at Different Quenching Temperatures," *Materials,* vol. 16, no. 10, 2023, https://doi.org/10.3390/ma16103840.

366. Shin, J.H.; Song, J.Y.; Ma, Y.W., "Effects of Annealing Temperature on Microstructural Evolution and Mechanical Properties in Cold-Rolled High-Nitrogen Austenitic Steel," *Metals,* vol. 14, no. 4, 2024, https://doi.org/10.3390/met14040389.

367. Yeli, G.; Auger, M.A.; Wilford, K.; Smith, G.D.W.; Bagot, P.A.J.; Moody, M.P., "Sequential nucleation of phases in a 17-4PH steel: Microstructural characterisation and mechanical properties," *Acta Materialia,* vol. 125, pp. 38-49, 2017, https://doi.org/10.1016/j.actamat.2016.11.052.

368. Liu, Y.; Han, S.; Yang, C.; Geng, R.; Yuan, X.; Li, Y.; Wang, C., "Evolution of Microstructures and Mechanical Properties with Tempering Temperature in a Novel Synergistic Precipitation Strengthening Ultra-High Strength Steel," *Materials,* vol. 17, no. 21, 2024, https://doi.org/10.3390/ma17215314.

369. Maslak, M.; Pazdanowski, M.; Stankiewicz, M.; Wassilkowska, A.; Zajdel, P.; Sielina, M., "Impact Fracture Surfaces as the Indicators of Structural Steel Post-Fire Susceptibility to Brittle Cracking," *Materials,* vol. 16, no. 8, 2023, https://doi.org/10.3390/ma16083281.

370. Maslak, M.; Pazdanowski, M.; Stankiewicz, M.; Zajdel, P., "Post-Fire Susceptibility to Brittle Fracture of Selected Steel Grades Used in Construction Industry—Assessment Based on the Instrumented Impact Test," *Materials,* vol. 14, no. 14, 2021, https://doi.org/10.3390/ma14143922.

371. Simoncelli, M.; Aloisio, A.; Zucca, M.; Venturi, G.; Alaggio, R., "Intensity and location of corrosion on the reliability of a steel bridge," *Journal of Construction Steel Research,* vol. 206, 2023, https://doi.org/10.1016/j.jcsr.2023.107937.

372. Li, W.; Ge. B.; Li, Z.; Xing, G.; Jing, Y., "Post-fire mechanical properties and constitutive model of Q690 high-strength structural steel," *Engineering Failure Analysis,* vol. 160, 2024, https://doi.org/10.1016/j.engfailanal.2024.108232.

373. Jiang, S.; Zhu, S.; Guo, X.; Li, Z., "Full-scale fire tests on steel roof truss structures," *Journal of Construction Steel Research,* vol. 169, 2020, https://doi.org/10.1016/j.jcsr.2020.106025.

374. Shin, A.; Bhang, S.; Kim, H.; Han, T.; Lee, H.; Jeong, G.; Park, J., "Behavior of fluorine coatings on steel bridges at different temperatures upon exposure to a direct heat source," *Journal of Industrail and Engineering Chemistry,* vol. 97, pp. 402-410, 2021, https://doi.org/10.1016/j.jiec.2021.02.026.

375. Casaoli, A.; Boniardi, M.; Gerosa, R.; Rivolta, B., "Metallurgical Analysis as a Useful Method for Fire Investigation: the Case of Galvanized Steel Sheets," *Fire Technology,* vol. 58, pp. 553-570, 2021, https://doi.org/10.1007/s10694-021-01158-2.

376. Wang, Z.; Zhou, H.; Ma, S., "Effects of corrosion on post-fire mechanical properties of Q690 high-strength steel," *Journal of Construction Steel Research,* vol. 226, 2025, https://doi.org/10.1016/j.jcsr.2024.109255.

377. Chauhan, S.; Muthulingam, S., "Surface roughness characteristics of high–ductile thermo–mechanically treated steel rebar exposed to pitting corrosion and elevated temperature," *Construction and Building Materials,* vol. 404, 2023, https://doi.org/10.1016/j.conbuildmat.2023.133210.

378. Liu, D.; Liu, X; Fu, F.; Wang, W., "Nondestructive Post-fire Damage Assessment of Structural Steel Members Using Leeb Harness Method," *Fire Technology,* vol. 56, pp. 1777-1799, 2020, https://doi.org/10.1007/s10694-020-00954-6.

379. Ji, S.H.; Wang, W.D.; Chen, W.; Shi, Y.L.; Xian, W., "Lateral impact behaviour of post-fire steel-reinforced concrete-filled steel tubular members: Experiment and evaluation method," *Engineering Structures,* vol. 293, 2023, https://doi.org/10.1016/j.engstruct.2023.116612.

380. Meglio, E.; Davino, A.; Formisano, A., "Hardness Tests on New and Existing Steel Structures," *IEEE Xplore,* 2024, https://doi.org/10.1109/MetroLivEnv60384.2024.10615797.

381. Li, D.; Hu, S.; Liu, X.; Xie, Y. Feng, C., "Safety Performance Assessment Strategies of P91 Steel Based on Leeb Hardness," *Earth and Environmental Science,* vol. 295, no. 3, 2019, https://doi.org/10.1088/1755-1315/295/3/032096?urlappend=%3Futm_source%3Dresearchgate.net%26medium%3Darticle.

382. Felicetti, R.; Gambarova, P.G., "Assessment of the Residual Strength of Fire-Damaged Steel-Rebars," *Nondestructive Testing of Materials and Structures,* vol. 6, pp. 213-218, 2013, https://doi.org/10.1007/978-94-007-0723-8_31.

383. Citra, Z.; Antonius, A.; Biantoro, A., "Application of Ultrasonic and Coating Material Thickness Testing on Post-Fire Steel Construction," *Rekayasa Sipil,* vol. 19, pp. 234-240, 2025, https://doi.org/10.21776/ub.rekayasasipil.2025.019.02.12.

384. Chi, D.; Xu, Z.; Liu, H., "Detection and Imaging of Corrosion Defects in Steel Structures Based on Ultrasonic Digital Image Processing," *Metals,* vol. 14, no. 4, 2024, https://doi.org/10.3390/met14040390.

385. Peng, P.C.; Chi, J.H.; Cheng, J.W., "A study on behavior of steel structures subjected to fire using non-destructive testing," *Construction and Building Materials,* vol. 128, pp. 170-175, 2016, https://doi.org/10.1016/j.conbuildmat.2016.07.056.

386. Park, S.; Bokhari, I.; Alnuaimi, H.; Amjad, U.; Fleischman, R.; Kundu, T., "Early detection of steel tube welded joint failure using SPC-I nonlinear ultrasonic technique," *Structural Health Monitoring,* vol. 24, no. 1, 2024, https://doi.org/10.1177/14759217241235057.

387. Vera, J.; Neira, M.T.; Garcia, L.F.C., "Capability of the Liquid Penetrant Method to Detect Defects in Welds," in *LACCEI 2023*, Buenos Aires, Argentina, 2023, https://doi.org/10.18687/LACCEI2023.1.1.416.

388. Sumardani, N.I.; Setlawan, N.I.; Nuryandin, B.W.; Sumardani, D., "The Defect Analysis of Carbon Steel Pipe Welding Connections Using Non-Destructive Testing with the Penetrant Test Method," *Risenologi Jurnal,* vol. 5, no. 1, 2020, https://doi.org/10.47028/j.risenologi.2020.51.72.

389. Kumar, N.; Mallik, B.; Kilkarni, R.R., "Modification of dye/fluorescent penetrant testing in accordance with Industry 4.0," *Materials Joining and Manufacturing Processes,* vol. 55, pp. 40-44, 2025, https://doi.org/10.21741/9781644903612-7.

390. Xin, M.L.; Chen, Y.; Li, M.D.; Wang, Z.G., Gu, G.H., "The research of penetration testing in the FRP pipe applications," *Materials Science and Engineering,* vol. 292, 2018, https://doi.org/10.1088/1757-899X/292/1/012080.

391. Irek, P.; Rawicki, L.; Kaczmarek, K., "Dye Penetrant Testing of Welded Joints Made of Aluminium and its Alloys," *Biuletyn Instytutu Spawalnictwa,* pp. 14-22, 2016, http://dx.doi.org/10.17729/ebis.2016.3/2.

392. Cicic, D.T.; Amza, C.G.; Popescu, D.; Anania, F.D., "Automated Stand for Non-Destructive Testing Evaluation of Metal Products," *Applied Mechanics and Materials,* vol. 371, pp. 401-405, 2013, https://doi.org/10.4028/www.scientific.net/AMM.371.401.

393. Lu, Q.Y.; Wong, C.H., "Applications of non-destructive testing techniques for post-process control of additively manufactured parts," *Virtual and Physical Prototyping,* pp. 301-321, 2017, https://doi.org/10.1080/17452759.2017.1357319.

394. Sacarea, A.I.; Oancea, G.; Parv, L., "Magnetic Particle Inspection Optimization Solution within the Frame of NDT 4.0," *Processes,* vol. 9, no. 6, 2021, https://doi.org/10.3390/pr9061067.

395. Li, Y.; Kang, Y.; Chen, Y.; Guo, Y.; Duan, Z.; Feng, B., "Feature Enhancement Method for Magnetic Particle Testing Based on Isolation Strip," *IEEE Xplore,* vol. 73, 2024, https://doi.org/10.1109/TIM.2024.3373080.

396. Wu, Q.; Dong, K.; Qin, X.; Hu, Z.; Xiong, X., "Magnetic particle inspection: Status, advances, and challenges — Demands for automatic non-destructive testing," *NDT & E International,* vol. 143, 2024, https://doi.org/10.1016/j.ndteint.2023.103030.

397. Kumar, V.; Kumar, N., "Performance Characteristics of Weld Defect Inspection by Magnetic Particle Testing," *International Journal of Innovative Technology and Exploring Engineering,* vol. 9, no. 3, 2020, http://doi.org/10.35940/ijitee.C8856.019320.

398. Savranguler, E.N., "Analysis of Leakage Magnetic Field of Rectangular Shaped Defects in Magnetic Materials and Investigation of Magnetic Fluids in the Field," in *IEEE 14th International Conference Nanomaterials: Applications & Properties*, Riga, Latvia, 2024, https://doi.org/10.1109/NAP62956.2024.10739772.

399. Baumeyer, J.; Chatoux, H.; Pelletier, A. Marquie, P., "Industrial Application of AI-Based Assistive Magnetic Particle Inspection," *Applied Sciences,* vol. 14, no. 4, 2024, https://doi.org/10.3390/app14041499.

400. Alvarado, J.W.; Garcia, L.F.C.; Neir, M.T.; Flores, J.W.V., "Probability of Defects Detection in Welded joints Using the Magnetic Particle Method," *Archives of Metallurgy and Materials,* vol. 69, pp. 607-612, 2024, https://doi.org/10.24425/amm.2024.149789.

401. Pachideh, G.; Gholhaki, M.; Aljenabi, A.; Rezaifar, "Compressive strength ratios of concretes containing pozzolans under elevated temperatures," *Heliyon,* vol. 10, no. 5, 2024, https://doi.org/10.1016/j.heliyon.2024.e26932.

402. Li, P.; Liu, J.; Duan, S.; Huang, R., "Variation Pattern of the Compressive Strength of Concrete under Combined Heat and Moisture Conditions," *Materials,* vol. 16, no. 4, 2023, https://doi.org/10.3390/ma16041548.

403. Elsanadedy, H.M., "Residual Compressive Strength of High-Strength Concrete Exposed to Elevated Temperatures," *Advances in Materials Science and Engineering,* 2019, https://doi.org/10.1155/2019/6039571.

404. Cheng, F.P. Kodur, V.K.; Wang, T.C., "Stress-Strain Curves for High Strength Concrete at Elevated Temperatures," *Journal of Materials in Civil Engineering,* vol. 16, no. 1, 2004, https://doi.org/10.1061/(ASCE)0899-1561(2004)16:1(84).

405. Rukavina, M.J.; Gabrijel, I.; Grubesa, I.N.; Mladenovic, A., "Residual Compressive Behavior of Self-Compacting Concrete after High Temperature Exposure—Influence of Binder Materials," *Materials,* vol. 15, no. 6, 2022, https://doi.org/10.3390/ma15062222.

406. Abid, S.R.; Abbass, A.A.; Murali, G.; Al-Sarray, M.L.J.; Nader, I.A.; Ali, S.H., "Repeated Impact Response of Normal- and High-Strength Concrete Subjected to Temperatures up to 600 °C," *Materials,* vol. 15, no. 15, 2022, https://doi.org/10.3390/ma15155283.

407. Colakoglu, H.E.; Husem, M., "Investigation of the Change in Mechanical Properties of Concrete Subjected After High-Temperature Effect to Cyclic Lateral Load," *Arabian Journal for Science and Engineering,* vol. 50, 2025, https://doi.org/10.1007/s13369-024-09889-4.

408. Tantawy, M.A., "Effect of High Temperatures on the Microstructure of Cement Paste," *Journal of Materials Science and Chemistry Engineering,* vol. 5, no. 11, 2017, https://doi.org/10.4236/msce.2017.511004.

409. Yao, W.; Pang, J.; Liu, Y., "Performance Degradation and Microscopic Analysis of Lightweight Aggregate Concrete after Exposure to High Temperature," *Materials,* vol. 13, no. 7, 2020, https://doi.org/10.3390/ma13071566.

410. Li, L.; Zhang, Y.; Shi, Y.; Xue, Y.; Cao, M., "Surface Cracking and Fractal Characteristics of Cement Paste after Exposure to High Temperatures," *Fractal and Fractional,* vol. 6, no. 9, 2022, https://doi.org/10.3390/fractalfract6090465.

411. Anunai, R.; Siempu, R., "Behavior of High Strength Concrete Subjected to Elevated Temperature," *International Journal of Innovative Technology,* vol. 9, no. 2, 2019, http://doi.org/10.35940/ijitee.B8028.129219.

412. Fernandes, B.; Gil, A.M.; Bolina, F.L.; Tutikian, B.F., "Thermal damage evaluation of full scale concrete columns exposed to high temperatures using scanning electron microsopy and X-ray diffraction," *DYNA,* vol. 85, no. 207, pp. 123-128, 2018, http://doi.org/10.15446/dyna.v85n207.70593.

413. Jansson, R., "Fire spalling of concrete - A historical overview," *MATEC Web of Conferences,* vol. 6, 2013, https://doi.org/10.1051/matecconf/20130601001.

414. Khalaf, J.; Huang, Z., "The bond behaviour of reinforced concrete members at elevated temperatures," *Fire Safety Journal,* vol. 103, pp. 19-33, 2019, https://doi.org/10.1016/j.firesaf.2018.12.002.

415. Pena, D.L.; Albero, V.; Hospitaler, A., "Additional Fire Exposure Time for the Effect of Spalling in Reinforced Concrete Columns," *Fire Technology,* vol. 60, pp. 3147-3174, 2023, https://doi.org/10.1007/s10694-023-01401-y.

416. Monte, F.L.; Felicetti, R.; Rossino, C., "Fire spalling sensitivity of high-performance concrete in heated slabs under biaxial compressive loading," *Materials and Structures,* Vols. 52, number 14, 2019, https://doi.org/10.1617/s11527-019-1318-0.

417. Goswami, N.; Barma, B.; Faruque, H.; Nag, S. Alom, S., "Comparative Study on the Effect of Different Admixtures in Concrete," *International Journal for Research,* vol. 11, no. 8, 2023, https://doi.org/10.22214/ijraset.2023.55501.

418. Sam, V.S.; Anand, N.; Lubloy, E.; Andrushia, D., "Investigation on Key Influencing Factors Affecting Temperature Distribution in Concrete," *Periodica Polytechnica Civil Engineering,* Vols. 69, No. 1, 2025, https://doi.org/10.3311/PPci.37355.

419. Ma, Q.; Guo, R.; Zhao, Z.; Lin, Z.; He, K., "Mechanical properties of concrete at high temperature—A review," *Construction and Building Materials,* vol. 93, pp. 371-383, 2015, https://doi.org/10.1016/j.conbuildmat.2015.05.131.

420. Ferdiansyah, T.; Ismy, R.; Shahzad, S.; Rafiq, W.; Nadeen, K., "The Influence of the Water–Cement Ratio on Concrete Resistivity: A Temperature and Saturation Dependent Analysis Using an Experimental and Predictive Approach," *CivlEng,* vol. 6, no. 3, 2025, https://doi.org/10.3390/civileng6030038.

421. Wang, Y.; Cui, J.; Deng, J.; Zhou, H., "Experimental Study of Thermally Damaged Concrete under a Hygrothermal Environment by Using a Combined Infrared Thermal Imaging and Ultrasonic Pulse Velocity Method," *Materials,* vol. 16, no. 3, 2023, https://doi.org/10.3390/ma16031040.

422. Hager, I.; Mroz, K., "Role of Polypropylene Fibres in Concrete Spalling Risk Mitigation in Fire and Test Methods of Fibres Effectiveness Evaluation," *Materials,* vol. 12, no. 13, 2019, https://doi.org/10.3390/ma12233869.

423. Phan, L.T., "Pore pressure and explosive spalling in concrete," *Materials and Structures,* vol. 41, pp. 1623-1632, 2007, https://doi.org/10.1617/s11527-008-9353-2.

424. Khaliq, W.; Khan, H.A., "High temperature material properties of calcium aluminate cement concrete," *Construction and Building Materials,* vol. 94, pp. 475-487, 2015, https://doi.org/10.1016/j.conbuildmat.2015.07.023.

425. Pulkit, U.; Adhikary, S.D., "ffect of micro-structural changes on concrete properties at elevated temperature: Current knowledge and outlook," *Structural Concrete,* vol. 23, no. 4, pp. 1995-2014, 2021, https://doi.org/10.1002/suco.202000365.

426. Boudlebnane, M.A.; Belkadi, A.A.; Chiker, T., "Impact of Aggregate Properties on the Microstructural Performance of Concrete Exposed to High Temperatures: An Analytical Review," *International Journal of Advanced Natural Sciences and Engineering Researches,* Vols. 7, No. 7, 2023, https://doi.org/10.59287/ijanser.1421.

427. Hachemi, S.; Rahmouni, Z.E., "A Review on the Effect of Varied Sand Types in Concrete at High Temperature," *Journal of Engineering Research and Sciences,* vol. 1, no. 4, pp. 38-47, 2022, http://dx.doi.org/10.55708/js0104005.

428. Niry R., R.; Beaucour, A.L.; Herbert, R.; Noumowe, A.; Ledesert, B.; Bodet, R., "Thermal stability of differnet siliceous and calcareous aggregates subjected to high temperatures," *MATEC Web of Conferences,* vol. 6, 2013, http://dx.doi.org/10.1051/matecconf/20130607001.

429. Alhamad, A.; Yehia, S.; Lubloy, E.; Elchalakani, M., "Performance of Different Concrete Types Exposed to Elevated Temperatures: A Review," *Materials,* vol. 15, no. 14, 2022, https://doi.org/10.3390/ma15145032.

430. Kodur, V.K.R.; Sultan, M.A., "Effect of Temperature on Thermal Properties of High-Strength Concrete," *Journal of Materials in Civil Engineering,* vol. 15, no. 2, 2003, https://doi.org/10.1061/(ASCE)0899-1561(2003)15:2(101).

431. Belkadi, A.A.; Kessal, O.; Bensalem, S.; Aggoun, S.; Amouri, C.; Khouadjia, M.L.K., "Aggregate Type Influence on Microstructural Behavior of Concrete Exposed to Elevated Temperature," *Civil and Environmental Engineering Reports,* vol. 32, no. 1, pp. 19-42, 2022, https://doi.org/10.2478/ceer-2022-0002.

432. Teixeira, G.P.; Ribeiro, J.C.L.; Pedroti, L.G.; Nalon, G.H., "Effects of Post-Fire Rehydration on the Mechanical Properties of Slag-Modified Concrete," *Buildints,* vol. 15, no. 1, 2025, https://doi.org/10.3390/buildings15010136.

433. Aydin, F.; Akyurek, M.; Arslan, S.; Yilmaz, K., "Effects of concrete cover thickness and concrete strength on temperature transfer in high temperature exposed FRP reinforced concrete," *Revista de la Construccion,* vol. 22, no. 1, pp. 242-258, 2023, Thicker cover delays heat penetration and protects reinforcement, effectively raising the critical temperature for structural failure.

434. Bengar, H.A.; Zarrinkolaei, F.A., "Effect of steel fibers and concrete cover on bond behavior between steel deformed bar and concrete under high temperature," *Structures,* vol. 32, pp. 1507-1521, 2021, https://doi.org/10.1016/j.istruc.2021.03.062.

435. Ba, G.; Wu, W.; Dai, H.; Jiao, Y.; Zhang, J., "Numerical Modeling of Uniaxial Corroded Reinforced Concrete Columns Exposed to Fire," *Buildings,* vol. 14, no. 9, 2024, https://doi.org/10.3390/buildings14092737.

436. Ba, G.; Weng, X.; Liu, C.; Wiao, J., "Bond strength of corroded reinforcements in concrete after high-temperature exposure," *Construction and Building Mateials,* vol. 270, 2021, https://doi.org/10.1016/j.conbuildmat.2020.121400.

437. Liu, C.; Yan, L.; Ba, G.; Miao, J.; Liu, Y., "Experimental Evaluation of Bond Behavior between Corroded Reinforcing Bars and Concrete under Elevated Temperatures," *Journal of Materials in Civil Engineering,* Vols. 35, No. 8, 2023, https://doi.org/10.1061/JMCEE7.MTENG-15206.

438. Mydin, M.A.O.; Sor, N.H.; Bahrami, A.; Dulaimi, A.; Ozkilic, Y.O.; Althoey, F.; Jagadesh, P.; Isleem, H.F.; Tawfik, T.A., "Residual durability, mechanical, and microstructural properties of foamed concrete subjected to various elevated temperatures," *Engineering Science and Technology,* vol. 55, 2024, https://doi.org/10.1016/j.jestch.2024.101725.

439. "Andrushia A.D.; Anand, N.; Lubloy, E.; Prince, A.G.," *Advances in Structural Engineering,* vol. 24, no. 9, 2021, https://doi.org/10.1177/1369433220986637.

440. Mathews, M.E.; Anand, N.; Anrushia, A.D.; Kiran, T., "Investigation on Crack Control and Crack Pattern Analysis of Self-compacting Concrete Exposed to Standard Fire Exposure," *International RILEM Conference on Early-Age and Long-Term Cracking in RC Structures,* vol. 31, pp. 127-139, 2021, https://doi.org/10.1007/978-3-030-72921-9_11.

441. Moradi, M.S.; Tavana, M.H.; Habibi, M.R.; Amiri, M., "Effect of water to cement ratio on mechanical properties of FRC subjected to elevated temperatures: Experimental and soft computing approaches," *Heliyon,* 2024, https://doi.org/10.1016/j.heliyon.2024.e39513.

442. Golewski, G.L., "The Phenomenon of Cracking in Cement Concretes and Reinforced Concrete Structures: The Mechanism of Cracks Formation, Causes of Their Initiation, Types and Places of Occurrence, and Methods of Detection—A Review," *Buildings,* vol. 13, no. 3, 2023, https://doi.org/10.3390/buildings13030765.

443. Abyaneh, S.D.; Wong, H.S.; Buenfeld, N.R., "Simulating the effect of microcracks on the diffusivity and permeability of concrete using a three-dimensional model," *Computational Materials Science,* vol. 119, pp. 130-143, 2016, https://doi.org/10.1016/j.commatsci.2016.03.047.

444. Wu, Z.; Wong, H.S.; Buenfield, N.R., "Influence of drying-induced microcracking and related size effects on mass transport properties of concrete," *Cement and Concrete Research,* vol. 68, pp. 35-48, 2015, https://doi.org/10.1016/j.cemconres.2014.10.018.

445. Mac, M.J.; Yio, M.H.N.; Desbois, G.; Casanova, I.; Wong, H.S.; Buenfeld, N.R., "3D imaging techniques for characterising microcracks in cement-based materials," *Cement and Concrete Research,* vol. 140, 2021, https://doi.org/10.1016/j.cemconres.2020.106309.

446. Yuan, M.; Quiang, S.; Xu, Y.; Li, Y.; Xu, W., "Research on Cracking Mechanism of Early-Age Restrained Concrete under High-Temperature and Low-Humidity Environment," *Materials,* vol. 14, no. 15, 2021, https://doi.org/10.3390/ma14154084.

447. Smarzewski, P., "Study of Toughness and Macro/Micro-Crack Development of Fibre-Reinforced Ultra-High Performance Concrete After Exposure to Elevated Temperature," *Materials,* vol. 12, no. 8, 2019, https://doi.org/10.3390/ma12081210.

448. Wroblewska, J.; Kowalski, R., "Assessing concrete strength in fire-damaged structures," *Construction and Building Materials,* vol. 254, 2020, https://doi.org/10.1016/j.conbuildmat.2020.119122.

449. Wu, Z.; Wong, H.S.; Chen, C.; Buenfeld, N.R., "Anomalous water absorption in cement-based materials caused by drying shrinkage induced microcracks," *Cement and Concrete Research,* vol. 115, pp. 90-104, 2019, https://doi.org/10.1016/j.cemconres.2018.10.006.

450. Winnefeld, F.; Leemann, A.; German, A.; Lothenbach, B., "CO2 storage in cement and concrete by mineral carbonation," *Current Opinion in Green and Sustainable Chemistry,* vol. 38, 2022, https://doi.org/10.1016/j.cogsc.2022.100672.

451. Liu, Z.; Sun, C.; Qu, J., "Coupling Effects of Stress and Carbonation on Concrete Durability: A Review," *Materials,* vol. 17, no. 22, 2024, https://doi.org/10.3390/ma17225438.

452. Hager, I., "Behaviour of cement concrete at high temperature," *Bulletin of the Polish Academy of Sciences,* vol. 6, no. 1, pp. 145-154, 2013, https://doi.org/10.2478/bpasts-2013-0013.

453. Colombo, M.; Felicetti, R., "New NDT techniques for the assessment of fire-damaged concrete structures," *Fire Safety Journal,* vol. 42, no. 6-7, pp. 461-472, 2007, https://doi.org/10.1016/j.firesaf.2006.09.002.

454. Hager, I., "Colour Change in Heated Concrete," *Fire Technology,* vol. 50, pp. 945-958, 2014, https://doi.org/10.1007/s10694-012-0320-7.

455. Lee, J.; Choi, K.; Hong, K, "Color and Material Property Changes in Concrete Exposed to High Temperatures," *Journal of Asian Architecture and Building Engineering,* vol. 8, no. 1, 2008, https://doi.org/10.3130/jaabe.8.175.

456. Annerel, E.; Taerwe, L., "Revealing the temperature history in concrete after fire exposure by microscopic analysis," *Cement and Concrete Research Branch,* vol. 39, no. 12, pp. 1239-1249, 2009, https://doi.org/10.1016/j.cemconres.2009.08.017.

457. Annerel, E.; Taerwe, L., "Methods to quantify the colour development of concrete exposed to fire," *Construction and Building Materials,* vol. 25, no. 10, pp. 3989-3997, 2011, https://doi.org/10.1016/j.conbuildmat.2011.04.033.

458. Mohammed, H.; Ahmed, H.; Kurda,R.; Alyousef, R.; Deifalla, A.F., "Heat-Induced Spalling of Concrete: A Review of the Influencing Factors and Their Importance to the Phenomenon," *Materials,* vol. 15, no. 5, 2022, https://doi.org/10.3390/ma15051693.

459. Moccia, F.; Ruiz, M.F.; Muttoi, A., "Spalling of concrete cover induced by reinforcement," *Engineering Structures,* vol. 237, 2021, https://doi.org/10.1016/j.engstruct.2021.112188.

460. Mohammed, H.; Sultangaliyeve, F.; Wrzykowski, M.; terrasi, G.P.; Bisby, L., "Heat-induced explosive spalling of self-prestressing, self-compacting concrete slabs," *Construction and Building Materials,* vol. 372, 2023, https://doi.org/10.1016/j.conbuildmat.2023.130821.

461. Amran, M.; Huang, S.S.; Onaizi, A.M.; Murali, G.; Abdelgader, H.S., "Fire spalling behavior of high-strength concrete: A critical review," *Construction and Building Materials,* vol. 341, 2022, https://doi.org/10.1016/j.conbuildmat.2022.127902.

462. Carlton, A.; Guo, Q.; Ma. S.; Quiel, S.E.; Naito, C.J., "Experimental assessment of explosive spalling in normal weight concrete panels under high intensity thermal exposure.," *Fire Safety Journal,* vol. 134, 2022, https://doi.org/10.1016/j.firesaf.2022.103677.

463. Ning, X.; Li, J.; Li, Y., "An Explorative Study into the Influence of Different Fibers on the Spalling Resistance and Mechanical Properties of Self-compacting Concrete after Exposure to Elevated Temperatures," *Applied Science,* vol. 12, 2022, https://doi.org/10.3390/app122412779.

464. Liu, J.C.; Zhang, Y., "A Simplified Model to Predict Thermo-Hygral Behaviour and Explosive Spalling of Concrete," *Journal of Advanced Concrete Technology,* vol. 17, no. 7, pp. 419-433, 2019, https://doi.org/10.3151/jact.17.419.

465. Kalifa, P.; Menneteau, F.D.; Quenard, D., "Spalling and pore pressure in HPC at high temperatures," *Cement and Concrete Research,* vol. 30, no. 12, pp. 1915-1927, 2000, https://doi.org/10.1016/S0008-8846(00)00384-7.

466. Zhao, J.; Zheng, J.J.; Peng, G.F.; Breugel, K.V., "Numerical analysis of heating rate effect on spalling of high-performance concrete under high temperature conditions," *Construction and Building Materials,* vol. 152, pp. 456-466, 2017, https://doi.org/10.1016/j.conbuildmat.2017.07.023.

467. Bensalem, H.; Djaknoun, S.; Ouedraogo, E.; Amrouche, R., "Analysis of thermal-induced spalling tests on high to ultra-high performance concrete subjected to standard fire," *Case Studies in Construction Materials,* vol. 15, 2021, https://doi.org/10.1016/j.cscm.2021.e00704.

468. von Greve-Dierfeld, S.; Lothenbach, B.; Vollpracht, A.; et al, "Understanding the carbonation of concrete with supplementary cementitious materials: a critical review by RILEM TC 281-CCC," *Materials and Structures,* vol. 53, 2020, https://doi.org/10.1617/s11527-020-01558-w.

469. Hwang, J.Y.; Kwak, H.G.; Shim, M., "Numerical approach for concrete carbonation considering moisture diffusion," *Materials and Structures,* vol. 53, 2020, https://doi.org/10.1617/s11527-020-01550-4.

470. Mahood, A.; Dehn, F.; Thissen, P, "Carbonation under Varying Humidity Conditions: A 3D Micro-Scale Kinetic Monte Carlo Approach," *Langmuir,* vol. 41, no. 4, pp. 2259-2268, 2025, https://doi.org/10.1021/acs.langmuir.4c03811.

471. Xie, Q.; Zhang, L.; Yin, S.; Zhang, B.; Wu, Y., "Effects of High Temperatures on the Physical and Mechanical Properties of Carbonated Ordinary Concrete," *Advances in Materials Science and Engineering,* 2019, https://doi.org/10.1155/2019/5753232.

472. Alhakim, A.; chen, S.E.; Braxtan, N.L.; Tempest, B.; Sun, Q.; Alamakhadmeh, W.; Zhang, Y., "Burnt Building Material Carbonation Evaluation Using Primary Color Analysis," *CivilEng,* vol. 6, no. 2, 2025, https://doi.org/10.3390/civileng6020029.

473. Leemann, A.; Moro, F., "Carbonation of concrete: the role of CO2 concentration, relative humidity and CO2 buffer capacity," *Materials and Structures,* vol. 50, 2016, https://doi.org/10.1617/s11527-016-0917-2.

474. Chen, Y.; Liu, P.; Yu, Z., "Effects of Environmental Factors on Concrete Carbonation Depth and Compressive Strength," *Materials,* vol. 11, no. 11, 2018, https://doi.org/10.3390/ma11112167.

475. Thiel, C.; Kratzer, J.; Grimm, B.; Krankel, T.; Gehlen, C., "Effect of Internal Moisture and Outer Relative Humidity on Concrete Carbonation," *CivilEng,* vol. 3, no. 4, 2022, https://doi.org/10.3390/civileng3040058.

476. Drouet, E.; Poyet, S.; Bescop, P.L.; Torrenti, J.M.; Bourbon, X., "Carbonation of hardened cement pastes: Influence of temperature," *Cement and Concrete Research,* vol. 115, pp. 445-459, 2019, https://doi.org/10.1016/j.cemconres.2018.09.019.

477. Liu, P.; Yu, Z.; Chen, Y., "Carbonation depth model and carbonated acceleration rate of concrete under different environment," *Cement and Concrete Composites,* vol. 114, 2020, https://doi.org/10.1016/j.cemconcomp.2020.103736.

478. Vollpracht, A.; Gluth, G.J.G.; Rogiers, B.; et al, "Report of RILEM TC 281-CCC: insights into factors affecting the carbonation rate of concrete with SCMs revealed from data mining and machine learning approaches," *Materials and Sturctures,* vol. 57, 2024, https://doi.org/10.1617/s11527-024-02465-0.

479. Ruan, S.; Unluer, C., "Influence of mix design on the carbonation, mechanical properties and microstructure of reactive MgO cement-based concrete," *Cement and Concrete Composites,* vol. 80, pp. 104-114, 2017, https://doi.org/10.1016/j.cemconcomp.2017.03.004.

480. Alshaeer, H.A.Y.; Irwan, J.M.; alshalif, A.F.; Al-Fakiah, A.; Ewais, D.Y.Z.; Salmi, A.; Alhokabi, A.A., "Review on Carbonation Study of Reinforcement Concrete Incorporating with Bacteria as Self-Healing Approach," *Materials,* vol. 15, 2022, https://doi.org/10.3390/ma15165543.

481. Medvedev, V.; Pustovgar, A., "A Review of Concrete Carbonation and Approaches to Its Research under Irradiation," *Buildings,* vol. 13, 2023, https://doi.org/10.3390/buildings13081998.

482. Fuhaid, A.F.A.; Niaz, A., "Carbonation and Corrosion Problems in Reinforced Concrete Structures," *Buildings,* vol. 12, 2022, https://doi.org/10.3390/buildings12050586.

483. Angst, U.; Moro, F.; Geiker, M.; et al, "Corrosion of steel in carbonated concrete: mechanisms, practical experience, and research priorities - a critical review by RILEM TC 281-CCC," *RILEM Technical Letters,* vol. 5, pp. 85-100, 2020, https://doi.org/10.21809/rilemtechlett.2020.127.

484. Daungwilailuk, T.; Kitagawa, T.; Bui, P.T.; Ogawa, Y.; Kawai, K., "Penetration of Moisture, CO2, and Cl Ions in Concrete after Exposure to High Temperature," *Journal of Advanced Concrete Technology,* vol. 17, no. 1, 2019.

485. Oliveira, J.dA.; Ribeiro, J.C.L.; Pedroti, L.G.; de Faria, C.S.; Nalon, G.H.; de Oliveira Junior, A.L., "Durability of Concrete After Fire Through Accelerated Carbonation Tests," *SciFLO,* vol. 22, no. 1, 2019, https://doi.org/10.1590/1980-5373-MR-2019-0049.

486. Gerasimidis, S.; Civjan, S.; Menz, N., "Post-Fire Damage Inspection of Concrete Structures: Final Report," Massachusetts Department of Transportation Office of Transportation Planning, Boston, Massachusetts, 2021, https://rosap.ntl.bts.gov/view/dot/59901/dot_59901_DS1.pdf.

487. Albrektsson, J.; Flansbjer, M.; Lindqvist, J.E.; Jansson, R., "Assessment of concrete structures after fire," SP Technical Research Insititute of Sweden, Boras, Sweden, 2011.

488. Jovanovic, B.; Caspeele, R.; Reynders, E.; Lombaert, G.; Coile, R.V., "Bayesian Updating Methodology for the Post-fire Evaluation of the Maximum Temperature Profile Inside Concrete Elements," *Fire Technology,* vol. 60, pp. 2155-2175, 2024, https://doi.org/10.1007/s10694-024-01564-2.

489. Tunc, E.T., "Relationship Between Schmidt Hammer Rebound Hardness Test and Concrete Strength Tests for Limestone Aggregate Concrete Based on Experimental and Statistical Studey," *Materials,* vol. 18, 2025, https://doi.org/10.3390/ma18061388.

490. Pahade, C.; Parmar, U.; Salaam, A.; Rao, D.S.N.M.; Manjunatha; Singla, A.; Rambabu, G.V., "Comparative Study of Non-Destructive test with different methods in various curing days," *E3S Web Conferences,* vol. 552, 2024, https://doi.org/10.1051/e3sconf/202455201090.

491. Kazemi, M; de Brito, J., "Compressive strength assessment of recycled aggregate concrete using Schmidt rebound hammer and core testing," *Construction and Building Materials,* vol. 224, pp. 630-638, 2019, https://doi.org/10.1016/j.conbuildmat.2019.07.110.

492. Hong, S.; Yoon, S.; Kim, J.; Lee, C.; Kim, S.; Lee, Y., "Evolution of Condition of Concrete Structures Using Ultrasonic Pulse Velocity Method," *Applied Sciences,* vol. 10, 2020, http://dx.doi.org/10.3390/app10020706.

493. Karaiskos, G.; Deraemaeker, A.; Aggelis, D.G.; Hemelrijck, D.V., "Monitoring of concrete structures using the ultrasonic pulse velocity method," *Smart Materials and Structures,* vol. 24, 2015, https://doi.org/10.1088/0964-1726/24/11/113001.

494. Jedidi, M., "Evaluation of Concrete by Non-destructive Ultrasonic Pulse Velocity Method," *Civil Engineering and Architecture,* vol. 10, no. 4, 2022, https://doi.org/10.13189/cea.2022.100431.

495. Kairu, W.M.; Mumenya, S.W.; Njoroge, K.D.; Kaniu, I.M., "Application of schmidt hammer and ultrasonic pulse velocity for structural integrity assessment in water dams," *Journal of Infrastructure Preservation and Resilience,* vol. 6, 2025, https://doi.org/10.1186/s43065-025-00123-5.

496. Tosti, F.; Ferrante, C., "Using Ground Penetrating Radar Methods to Investigate Reinforced Concrete Structures," *Surveys in Geophysics,* vol. 41, pp. 485-530, 2019, https://doi.org/10.1007/s10712-019-09565-5.

497. Gastineau, A.; Johnson, T.; Schultz, A., "Bridge Health Monitoring and Inspections – A Survey of Methods," Minnesota Department of Transportation, St. Paul, Minnesota, 2009, http://www.lrrb.org/pdf/200929.pdf.

498. Zhang, J.K.; Yan, W.; Cui, D.M., "Concrete Condition Assessment Using Impact-Echo Method and Extreme Learning Machines," *Sensors,* vol. 16, no. 4, 2016, https://doi.org/10.3390/s16040447.

499. Dvorak, R.; Topolar, L., "Effect of Hammer Type on Generated Mechanical Signals in Impact-Echo Testing," *Materials,* vol. 14, no. 3, 2021, https://doi.org/10.3390/ma14030606.

500. Kirchhof, L.D.; de Lima, R.C.A.; Neto, A.B.D. S.; Quispe, A.C.; Filho, L.C.P.D.S., "Effect of Moisure Content on the Behavior of High Strength Concrete at High Temperatures," *Revista Materia,* vol. 25, no. 01, 2020, https://doi.org/10.1590/S1517-707620200001.0898.

501. Shakraki, M.; Hua, N.; Elhami-Khorasani, N.; Tessari, A.; Garlock, M., "Residual compressive strength of concrete after exposure to high temperatures: A review and probabilistic models," *Fire Safety Journal,* vol. 135, 2023, https://doi.org/10.1016/j.firesaf.2022.103698.

502. Bao, J.; Zheng, R.; Zhang, P.; Cui, Y.; Zue, S.; Song, Q.; Ma, Y., "Thermal resistance, water absorption and microstructure of high-strength self-compacting lightweight aggregate concrete (HSSC-LWAC) after exposure to elevated temperatures," *Construction and Building Materials,* vol. 365, 2023, https://doi.org/10.1016/j.conbuildmat.2022.130071.

503. Zhao, H.; Liu, F.; Yang, H., "Residual compressive response of concrete produced with both coarse and fine recycled concrete aggregates after thermal exposure," *Construction and Building Materials,* vol. 244, 2020, https://doi.org/10.1016/j.conbuildmat.2020.118397.

504. Jedidi, M., "Evaluation of the Quality of Concrete Structures by the Rebound Hammer Method," *Current Trends in Civil & Structural Engineering,* vol. 5, 2020, http://dx.doi.org/10.33552/CTCSE.2020.05.000621.

505. Kumavat, H.R.; Chandak, N.R.; Patil, I.T., "Factors influencing the performance of rebound hammer used for non-destructive testing of concrete members: A review," *Case Studies in Construction Materials,* vol. 14, 2021, https://doi.org/10.1016/j.cscm.2021.e00491.

506. El-Mir, A.; El-Zahab, S.; Sbartai, Z.M.; Homsi, F.; Saliba, J.; El-Hassan, H., "Machine learning prediction of concrete compressive strength using rebound hammer test," *Journal of Building Engineering,* vol. 64, 2023, https://doi.org/10.1016/j.jobe.2022.105538.

507. Brencich, A.; Bovolenta, R.; Ghiggi, V.; Pera, D.; Redaelli, P., "Rebound Hammer Test: An Investigation into Its Reliability inApplications on Concrete Structures," *Advances in Materials Science and Engineering,* no. 1, 2020, https://doi.org/10.1155/2020/6450183.

508. Revilla-Cuesta, V.; Skaf, M.; Serrano-Lopez, R.; Ortega-Lopez, V., "Models for compressive strength estimation through non-destructive testing of highly self-compacting concrete containing recycled concrete aggregate and slag-based binder," *Construction and Building Materials,* vol. 280, 2021, https://doi.org/10.1016/j.conbuildmat.2021.122454.

509. Dungi, J.K.; Rao, K.S., "Quality Grading of Heated RC Columns by NDT Methods," *International Journal of Engineering and Technology,* vol. 11, no. 4, pp. 793-769, 2019, https://doi.org/10.21817/ijet/2019/v11i4/191104010.

510. Awoyera, P.O.; Olalusi, O.B., "Modeling Temperature of Fire-Damaged Reinforced Concrete Buildings Based on Nondestructive Testing and Gene Algorithm Techniques," *Fire Technology,* vol. 58, pp. 941-957, 2021, https://doi.org/10.1007/s10694-021-01182-2.

511. Araujo, R.C.D.; da Silva, W.M.; Pires, T.A.D.; Silva, J.J.D., "Compressive strength assessment of high strength concrete after fire using ultrasonic," *Research, Society, and Development,* vol. 11, no. 11, 2022, http://dx.doi.org/10.33448/rsd-v11i11.32719.

512. Almasaeid, H., "Ultrasonic pulse velocity and artificial neural network prediction of high-temperature damaged concrete splitting strength," *Discover Applied Sciences,* 2024, https://doi.org/10.1007/s42452-024-05645-3.

513. Ndagi,A.; Umar, A.A.; Hejazi, F.; Jaafar, M.S., "Non-destructive assessment of concrete deterioration by ultrasonic pulse velocity: A review," in *Sustainalbe Civil and Construction Engineering Conference*, Seattle, Washington, 2019, https://doi.org/10.1088/1755-1315/357/1/012015?urlappend=%3Futm_source%3Dresearchgate.

514. Wroblewski, R.; Stawiski, B., "Ultrasonic Assessment of the Concrete Residual Strength after a Real Fire Exposure," *Buildings,* vol. 10, no. 154, 2020, http://dx.doi.org/10.3390/buildings10090154.

515. Mpalaskas, A.C.; Kytinou, V.K.; Zapris, A.G.; Matikas, T., "Optimizing Building Rehabilitation through Nondestructive Evaluation of Fire-Damaged Steel-Fiber-Reinforced Concrete," *Sensors,* vol. 24, no. 17, 2024, https://doi.org/10.3390/s24175668.